86-02709/

NATIONAL AERONAUTICAL ESTABLISHMENT

SCIENTIFIC AND TECHNICAL PUBLICATIONS

AERONAUTICAL REPORTS:

Aeronautical Reports (LR): Scientific and technical information pertaining to aeronautics considered important, complete, and a lasting contribution to existing knowledge.

Mechanical Engineering Reports (MS): Scientific and technical information pertaining to investigations outside aeronautics considered important, complete, and a lasting contribution to existing knowledge.

AERONAUTICAL NOTES (AN): Information less broad in scope but nevertheless of importance as a contribution to existing knowledge.

LABORATORY TECHNICAL REPORTS (LTR): Information receiving limited distribution because of preliminary data, security classification, proprietary, or other reasons.

Details on the availability of these publications may be obtained from:

Publications Section,
National Research Council Canada,
National Aeronautical Establishment,
Bldg. M-16, Room 204,
Montreal Road,
Ottawa, Ontario
K1A 0R6

ÉTABLISSEMENT AÉRONAUTIQUE NATIONAL

PUBLICATIONS SCIENTIFIQUES ET TECHNIQUES

RAPPORTS D'AÉRONAUTIQUE

Rapports d'aéronautique (LR): Informations scientifiques et techniques touchant l'aéronautique jugées importantes, complètes et durables en termes de contribution aux connaissances actuelles.

Rapports de génie mécanique (MS). Informations scientifiques et techniques sur la recherche externe à l'aéronautique jugées importantes, complètes et durables en termes de contribution aux connaissances actuelles.

CAHIERS D'AÉRONAUTIQUE (AN): Informations de moindre portée mais importantes en termes d'accroissement des connaissances.

RAPPORTS TECHNIQUES DE LABORATOIRE (LTR): Informations peu disséminées pour des raisons d'usage secret, de droit de propriété ou autres ou parce qu'elles constituent des données préliminaires.

Les publications ci-dessus peuvent être obtenues à l'adresse suivante:

Section des publications
Conseil national de recherches Canada
Établissement aéronautique national
Im. M-16, pièce 204
Chemin de Montréal
Ottawa (Ontario)
K1A 0R6

UNLIMITED
UNCLASSIFIED

UNSTEADY PRESSURE AND FORCE MEASUREMENTS ASSOCIATED WITH TRANSONIC BUFFETING OF A TWO-DIMENSIONAL SUPERCRITICAL AIRFOIL

MESURES DE PRESSION ET DE FORCE INSTATIONNAIRES DUES AU BUFFETING TRANSSONIQUE D'UN PROFIL AÉRODYNAMIQUE SURCRITIQUE BIDIMENSIONNEL

by/par

B.H.K. Lee and L.H. Ohman

National Aeronautical Establishment

AERONAUTICAL NOTE
NAE-AN-14
NRC NO. 22448

OTTAWA
JUNE 1983

L.H. Ohman, Head/Chef
High Speed Aerodynamics Laboratory/
Laboratoire d'aérodynamique à hautes vitesses

G.M. Lindberg
Director/Directeur

SUMMARY

Buffet characteristics of the BGK No. 1 shockless airfoil have been investigated. Fluctuating pressure measurements along the airfoil chord and unsteady force balance data have been obtained in various regions inside the buffet régime close to the onset boundary curve. The Mach number range where buffet intensity reaches high values is determined from balance measurements. The rms values of the fluctuating pressure show generally monotonic increase downstream of the shock to the trailing-edge in this speed range. Statistical data from pressure and normal force measurements have been processed and the appearance of distinct frequency peaks in the power spectral density curves has been detected in the speed range $0.7 \leq M_\infty \leq 0.78$. The coherence between pressure signals and pressure and force signals has also been investigated.

RÉSUMÉ

Les caractéristiques de buffeting du profil sans shoc BGK No. 1 ont été étudiées. Des mesures de pression instationnaire le long de la corde du profil et des forces instationnaires de la balance ont été établies dans différentes zones de la domaine de buffeting au voisinage de la courbe seuil. La gamme de nombres de Mach dans laquelle le buffeting devient intense est établie à partir des mesures des forces de la balance. Les valeurs rms de la pression instationnaire présentent une augmentation presque monotone en aval du front de choc jusqu'au bord de fuite dans cette gamme de vitesses. Des données statistiques découlant des mesures de pression et de force normale ont été analysées et révèlent des pics de fréquence distincts dans les courbes spectrales, dans la gamme des vitesses $0,7 \leq M_\infty \leq 0,78$. On a aussi examiné la correspondance entre les mesures de pression et celles de force.

CONTENTS

		Page
	SUMMARY	(iii)
	SYMBOLS	(vii)
1.0	INTRODUCTION	1
2.0	MODEL AND INSTRUMENTATION	1
3.0	TEST FACILITY	2
4.0	TEST PROGRAM	2
5.0	DATA REDUCTION	2
6.0	PRESENTATION OF RESULTS	3
7.0	DISCUSSION OF RESULTS	4
8.0	CONCLUSIONS	5
9.0	REFERENCES	5

TABLE

Table		Page
1	Summary of Wind Tunnel Runs at 19.3% Wall Porosity	7

ILLUSTRATIONS

Figure		Page
1	BGK No. 1 Airfoil Model with Pressure Hole Locations	9
2	Mounting Arrangement for Transducers for Buffet Studies	10
3	South Side Wing Pressure Connector Showing Ports Connected to Transducers for Buffet Studies	11
4	Location of Pressure Ports for Fluctuating Pressure Measurements	11
5	Typical Output from a Step-Pause Incidence Test	12
6	Variation of the Fluctuating Normal Force Coefficient C'_{N_2} with Mach Number and Steady State Lift Coefficient	13
7	Variation of Fluctuating Pressure Coefficient Along Airfoil Chord	14

ILLUSTRATIONS (Cont'd)

Figure		Page
8a	Power Spectral Density for $M_\infty = 0.501$, $C_L = 1.124$, $Q = 17.7$ psi	17
8b	Auto Correlation Functions for $M_\infty = 0.501$, $C_L = 1.124$, $Q = 17.7$ psi	17
8c	Cross Correlation Functions for $M_\infty = 0.501$, $C_L = 1.124$, $Q = 17.7$ psi	18
8d	Cross Power Spectral Density for $M_\infty = 0.501$, $C_L = 1.124$, $Q = 17.7$ psi	19
8e	Coherence Functions for $M_\infty = 0.501$, $C_L = 1.124$, $Q = 17.7$ psi.	21
8f	Cross Power Spectral Density and Coherence Function Between Pressure and Normal Force N_2 for $M_\infty = 0.501$, $C_L = 1.124$, $Q = 17.7$ psi	22
8g	Steady State Pressure Distribution	24
9a	Power Spectral Density for $M_\infty = 0.703$, $C_L = 1.069$, $Q = 23.8$ psi	25
9b	Auto Correlation Functions for $M_\infty = 0.703$, $C_L = 1.069$, $Q = 23.8$ psi	25
9c	Cross Correlation Functions for $M_\infty = 0.703$, $C_L = 1.069$, $Q = 23.8$ psi	26
9d	Cross Power Spectral Density for $M_\infty = 0.703$, $C_L = 1.069$, $Q = 23.8$ psi	27
9e	Coherence Functions for $M_\infty = 0.703$, $C_L = 1.069$, $Q = 23.8$ psi.	29
9f	Cross Power Spectral Density and Coherence Function Between Pressure and Normal Force N_2 for $M_\infty = 0.703$, $C_L = 1.069$, $Q = 23.8$ psi	30
9g	Steady State Pressure Distribution	32
10a	Power Spectral Density for $M_\infty = 0.753$, $C_L = 0.945$, $Q = 24.5$ psi	33
10b	Auto Correlation Functions for $M_\infty = 0.753$, $C_L = 0.945$, $Q = 24.5$ psi	33
10c	Cross Correlation Functions for $M_\infty = 0.753$, $C_L = 0.945$, $Q = 24.5$ psi	34
10d	Cross Power Spectral Density for $M_\infty = 0.753$, $C_L = 0.945$, $Q = 24.5$ psi	35
10e	Coherence Functions for $M_\infty = 0.753$, $C_L = 0.945$, $Q = 24.5$ psi.	38
10f	Cross Power Spectral Density and Coherence Function Between Pressure and Normal Force N_2 for $M_\infty = 0.753$, $C_L = 0.945$, $Q = 24.5$ psi	39
10g	Steady State Pressure Distribution	41
11a	Power Spectral Density for $M_\infty = 0.775$, $C_L = 0.868$, $Q = 18.3$ psi	42
11b	Auto Correlation Functions for $M_\infty = 0.775$, $C_L = 0.868$, $Q = 18.3$ psi	42

ILLUSTRATIONS (Cont'd)

Figure		Page
11c	Cross Correlation Functions for $M_\infty = 0.775$, $C_L = 0.868$, Q = 18.3 psi	43
11d	Cross Power Spectral Density for $M_\infty = 0.775$, $C_L = 0.868$, Q = 18.3 psi	44
11e	Coherence Functions for $M_\infty = 0.775$, $C_L = 0.868$, Q = 18.3 psi.	46
11f	Cross Power Spectral Density and Coherence Function Between Pressure and Normal Force N_2 for $M_\infty = 0.775$, $C_L = 0.868$, Q = 18.3 psi	47
11g	Steady State Pressure Distribution	49
12a	Power Spectral Density for $M_\infty = 0.784$, $C_L = 0.806$, Q = 25.1 psi.	50
12b	Auto Correlation Functions for $M_\infty = 0.784$, $C_L = 0.806$, Q = 25.1 psi	50
12c	Cross Correlation Functions for $M_\infty = 0.784$, $C_L = 0.806$, Q = 25.1 psi	51
12d	Cross Power Spectral Density for $M_\infty = 0.784$, $C_L = 0.806$, Q = 25.1 psi	52
12e	Coherence Functions for $M_\infty = 0.784$, $C_L = 0.806$, Q = 25.1 psi.	54
12f	Cross Power Spectral Density and Coherence Function Between Pressure and Normal Force N_2 for $M_\infty = 0.784$, $C_L = 0.806$, Q = 25.1 psi	55
12g	Steady State Pressure Distribution	57
13a	Power Spectral Density for $M_\infty = 0.775$, $C_L = 0.762$, Q = 18.3 psi.	58
13b	Auto Correlation Functions for $M_\infty = 0.775$, $C_L = 0.762$, Q = 18.3 psi	58
13c	Cross Correlation Functions for $M_\infty = 0.775$, $C_L = 0.762$, Q = 18.3 psi	59
13d	Cross Power Spectral Density for $M_\infty = 0.775$, $C_L = 0.762$, Q = 18.3 psi	60
13e	Coherence Functions for $M_\infty = 0.775$, $C_L = 0.762$, Q = 18.3 psi.	62
13f	Steady State Pressure Distribution	63
14a	Power Spectral Density for $M_\infty = 0.805$, $C_L = 0.727$, Q = 25.5 psi.	64
14b	Auto Correlation Functions for $M_\infty = 0.805$, $C_L = 0.727$, Q = 25.5 psi	64
14c	Cross Correlation Functions for $M_\infty = 0.805$, $C_L = 0.727$, Q = 25.5 psi	65
14d	Cross Power Spectral Density for $M_\infty = 0.805$, $C_L = 0.727$, Q = 25.5 psi	66
14e	Coherence Functions for $M_\infty = 0.805$, $C_L = 0.727$, Q = 25.5 psi.	69

ILLUSTRATIONS (Cont'd)

Figure		Page
14f	Cross Power Spectral Density and Coherence Function Between Pressure and Normal Force N_2 for $M_\infty = 0.805$, $C_L = 0.727$, Q = 25.5 psi	70
14g	Steady State Pressure Distribution	72
15a	Power Spectral Density for $M_\infty = 0.805$, $C_L = 0.314$, Q = 25.5 psi	73
15b	Auto Correlation Functions for $M_\infty = 0.805$, $C_L = 0.314$, Q = 25.5 psi	73
15c	Cross Correlation Functions for $M_\infty = 0.805$, $C_L = 0.314$, Q = 25.5 psi	74
15d	Cross Power Spectral Density for $M_\infty = 0.805$, $C_L = 0.314$, Q = 25.5 psi	75
15e	Coherence Functions for $M_\infty = 0.805$, $C_L = 0.314$, Q = 25.5 psi.	77
15f	Cross Power Spectral Density and Coherence Function Between Pressure and Normal Force N_2 for $M_\infty = 0.805$, $C_L = 0.314$, Q = 25.5 psi	78
15g	Steady State Pressure Distribution	80

SYMBOLS

Symbol	Definition
b	model span
c	model chord
f	frequency
M_∞	free stream Mach number
N_2	force balance component
p	model local static pressure
p_∞	free stream static pressure
Q, q_∞	free stream dynamic pressure
Re	Reynolds number based on chord
$R_x(\tau)$	auto correlation function of x(t)
$R_{xy}(\tau)$	cross correlation function of x(t) and y(t)
$S_x(f)$	power spectral density of x(t)
$S_{xy}(f)$	cross power spectral density of x(t) and y(t)

SYMBOLS (Cont'd)

Symbol	Definition
t, T	time
x	distance measured along chord from the leading edge
x(t)	random signal
y(t)	random signal
α_g	geometric angle of attack, i.e. angle between airfoil chord at midspan and wind tunnel centreline
γ^2_{xy}	coherence function of x(t) and y(t)
τ	delay
C_p	pressure coefficient
C_L	lift coefficient
C_N	normal force coefficient
C_p'	fluctuating pressure coefficient
C_{N_2}'	fluctuating normal force coefficient for balance component N_2

Subscripts

A, B, . . . F	pressure transducer locations on airfoil
G	force balance component N_2
45R	refers to reference pressure port 45R located 81″ upstream of balance centreline

UNSTEADY PRESSURE AND FORCE MEASUREMENTS ASSOCIATED WITH TRANSONIC BUFFETING OF A TWO-DIMENSIONAL SUPERCRITICAL AIRFOIL

1.0 INTRODUCTION

Buffeting is a dynamic behaviour of an aircraft due to aerodynamic excitation arising from random loading when flow separations on the wing are encountered. In recent years increased attention has been given to the investigation of buffet characteristics in order to meet the design requirements of future aircraft. This arose from the demand for greater maneuverability and gust requirements in the transonic flight régime. Methods for predicting buffet characteristics based on wind tunnel rigid model testing are extremly useful and much needed in aircraft design.

Supercritical airfoils have been found to have favourable buffet characteristics compared with classical airfoils, at least that is the case for airfoils investigated in the NAE high Reynolds number 2D test facility (Ref. 1). The BGK No. 1 airfoil was the first supercritical airfoil to be investigated at NAE and its buffet boundary, or rather buffet onset boundary, is reported by Kacprzynski in Reference 2. His results were found to be in good agreement with theoretical predictions by Redeker and Proksch (Ref. 3) using Thomas (Ref. 4) buffet onset criterion. The method used for determining buffet onset was to osberve the analog signal from a force element of one of the sidewall balances supporting the model, and to note the onset of oscillations. Other common methods used in determining buffet onset is to detect the divergence of the trailing edge pressure or the so-called break in the lift curve slope. In either case buffet onset is fairly easy to determine experimentally, requiring little sophistication in instrumentation.

In order to gain more insight into the aerodynamic aspects of buffet, and not just buffet onset, detailed investigations of surface pressure signatures are necessary. Such an investigation was carried out at NAE with the BGK No. 1 airfoil. A number of pressure orifices on the upper surface of the airfoil model were connected to fast response miniature transducers and the signals recorded on FM tape for further analysis. The investigation was carried out in the Mach number range 0.5 to 0.8 at chord Reynolds numbers of 15 to 21 $\times 10^6$. Both constant incidence and step-pause incidence runs were performed. The constant incidence runs were of sufficiently long duration so that spectral, correlation and coherence functions for force and pressure data could be obtained. The step-pause runs were only processed to give rms values of the force and pressure fluctuations.

The wind tunnel tests were carried out in conjunction with a series of other investigations in the NAE 2D test facility involving the BGK No. 1 airfoil and reported on in Reference 5. This report gives a brief description of the experimental arrangements and the procedure for data processing. The main emphasis in the report is in the presentation of the statistical data of the investigation and a discussion of them. It should be noted that convection effects and spatial decay are not treated but will be the subject of an ensuing report.

2.0 MODEL AND INSTRUMENTATION

The model (Fig. 1) was the same as that used by Kacprzynski (Ref. 2). Six Kulite TQ 360 25 psid transducers were closely coupled to six ports in the 'south' pressure connector on the model (Figs. 2 and 3). When these transducers were connected, the normal south male pressure connector was disconnected and left open to plenum pressure. The transducers were connected with the 'reference' side to the wing and the 'measuring' side to the plenum. (The reference side has a considerably smaller volume than the measuring side for these transducers.) The frequency response of the installed transducers was calibrated and established to be flat up to approximately 200 Hz. The location of the pressure ports connected to the transducers is shown in Figure 4. The normal pressure scanning system was inhibited for this investigation. The force balance fluctuating signal was obtained from the 'north' downstream flexure N_2 located at 0.725 chord, which was close to the expected centre of the buffet force. All unsteady signals were recorded on FM tape for subsequent analysis.

3.0 TEST FACILITY

The test facility is described in Reference 6. Those aspects of the facility and instrumentation relevant to the present investigation that differ since Reference 6 was published, are reported in Reference 5. The porosity of the top and bottom walls in these tests was 19.3%.

4.0 TEST PROGRAM

The wind tunnel tests were carried out in December 1978 and constituted phase 'C' of 'Supplementary Investigation of BGK No. 1 Airfoil' (Ref. 5). The tests covered the following ranges in Mach number, angle of incidence and Reynolds number:

Mach number range:	$0.501 \leqslant M_\infty \leqslant 0.805$
Incidence range:	$-0.36 \leqslant \alpha_g \leqslant 11.74$
Reynolds number range:	$15 \leqslant Rex10^{-6} \leqslant 21$

Table 1 shows a summary of the wind tunnel runs for fluctuating pressure and force measurements. Corresponding to each Mach number and angle of incidence, a steady state pressure scan for the airfoil was obtained separately and reported in Reference 5.

5.0 DATA REDUCTION

The free stream quantities M_∞, q_∞ and p_∞ were determined from the measured reference quantities P_o and $P_o - P_{45R}$ and applying appropriate corrections between the 45R static pressure reference station and the test section in accordance with empty tunnel calibration results.

The geometric incidence α_g is that of the midspan section of the model. It is derived from the readings of the 'north' and 'south' balance potentiometers and allowing for the twist of the model; the 'south' balance does not react to any moment. Thus

$$\alpha_g = \alpha_N - (\alpha_N - \alpha_S) \cdot \frac{3}{4}$$

The transducer and the normal force balance component N_2 analog signals were recorded on FM tapes. These were later digitized and sampled at 1 kHz. The data were further filtered using a four-pole low pass active filter with roll-off at approximately 300 Hz.

A computer interactive program was developed to select the portion of the signals to be analysed. A Genisco 1000 graphics terminal was used to display the raw data on the screen of the terminal. The intervals, where analyses were to be carried out, were determined by the motion of the 'joystick' and a dataset was prepared for statistical analyses. For all cases requiring statistical processing 8192 data points were used, which corresponded approximately to eight seconds of recorded data.

The six Kulite pressure transducers and the force balance component N_2 signals were processed and statistical data such as spectra, auto correlation, cross spectra, cross correlation and coherence were obtained from computer programs written by Rabine, Schafer and Dlugos (Ref. 7) and Carter and Ferrie (Ref. 8). The rms values for the pressures and normal force were expressed in coefficents as follows:

$$C_p' = \frac{p_{rms}}{q_\infty}$$

$$C_N' = \frac{N_{2_{rms}}}{q_\infty \, b \, c}$$

For completeness in presentation, the definitions for the statistical properties of two time function x(t) and y(t) are given as follows:

Auto correlation function

$$R_x(\tau) = \lim_{T \to \infty} \frac{1}{T} \int_0^T x(t)\, x(t+\tau)\, dt$$

Power spectral density

$$S_x(f) = 2 \int_{-\infty}^{\infty} R_x(\tau)\, e^{-i2\pi f\tau}\, d\tau$$

$$= 4 \int_0^{\infty} R_x(\tau) \cos 2\pi f\tau d\tau$$

Cross correlation function

$$R_{xy}(\tau) = \lim_{T \to \infty} \frac{1}{T} \int_0^T x(t)\, y(t+\tau)\, dt$$

Cross power spectral density

$$S_{xy}(f) = 2 \int_{-\infty}^{\infty} R_{xy}(\tau)\, e^{-i2\pi f\tau}\, d\tau$$

Coherence function

$$\gamma_{xy}^2 = \frac{\left| S_{xy(f)} \right|^2}{S_x(f)\, S_y(f)}$$

Note that all data presented here are uncorrected for wall interference effects. The statistical results are unaffected by wall effects, but the free stream flow conditions are slightly influenced. The corrections to Mach number and angle of attack, if required, can be obtained from equivalent 'steady' run results presented in Reference 5.

6.0 PRESENTATION OF RESULTS

All results are presented in graphical form. In Table 1, runs marked with + indicate force balance component N_2 measurements are not available. Statistical data are only given for those runs marked by an asterisk, since they are of sufficiently long duration to make the analysis meaningful. For runs No. 20937 — 20939, which are at constant incidence, statistical data have been processed but are not included in this report, except for the fluctuating pressure coefficients C_p'. Upon inspection the statistical data for these runs were found to be nearly identical to those for runs 20949, which are included.

All pressure transducers are labelled from 'A' to 'F' as shown in Figure 4. The force balance element N_2 is labelled 'G'.

7.0 DISCUSSION OF RESULTS

Figure 5 shows a typical output of the transducer signals 'B', 'C' and 'D' together with the angle of incidence versus time for a step-pause incidence run. To analyse the data for any angle of incidence, the interactive computer program was used to prepare a dataset at the desired incidence for analysis.

Figure 6 shows the fluctuating normal force coefficient C'_{N_2} plotted versus M_∞ and C_L. Redeker's and Proksch's (Ref. 3) theoretical buffet onset prediction and Kacprzynski's (Ref. 2) experimental results for the BGK No. 1 airfoil are included to show the various regions in the vicinity of the buffet onset boundary where the present tests were conducted. It is of interest to note that the buffet intensities, as indicated by the fluctuations from the normal force balance, are most severe in the Mach number range $0.7 - 0.78$ for C_L between $0.8 - 1.1$. In this transonic Mach number range observations of the steady state C_p plots in Figures 11(g) to 17(g) indicate fairly strong shocks and flow separations extending from the shock to the trailing-edge.

The variations of C'_p versus x/c are shown in Figure 7. Also shown are the approximate shock locations inferred from steady state pressure data included in Figures 8 to 15. The large C'_p from transducer 'A' for run No. 20944 is most certainly due to shock oscillation. The steady state C_p plot for this run condition is available from unpublished data, Figure 10(g), and shows the location of the shock to be just over or very close to the transducer measuring station. The relatively small values of C'_p at 'A' for runs 20937, 20953 and 20954 are consistent with the shock being too far downstream of the 'A' position to have any significant effect on the fluctuating pressure, or the absence of a shock (20954).

Corresponding to those runs in Figure 6 where the buffet intensity if fairly large (i.e. in the range $0.7 \leq M_\infty \leq 0.78$, $0.8 \leq C_L \leq 1.1$), C'_p in Figure 7 also shows relatively larger values than those outside this range in M_∞ and C_L. Another point to be observed is that C'_p for these runs increases downstream from the shock and attains a maximum value at the transducer closest to the trailing-edge which is x/c = 0.95 for these tests. Note also that for runs 20937 and 20940, where the shock is close to the 'B' station (60% chord), the C'_p values are markedly higher than for the next station (70% chord).

Figures 8 to 15 show the statistical properties for representative runs in various regions inside the buffet régime close to the buffet boundary. The symbol 'Y' represents the function (spectrum, auto correlation, etc.) and the following single letter or double letter indicate basic or joint properties respectively. The units for pressure and force are in psi and lbs respectively. Hence the spectra are in psi^2/Hz or lb^2/Hz for pressure and force measurements respectively and they are expressed in db. For cross spectra between pressure transducer and force balance, the units are in psi-lb/Hz. The cross correlation functions are plotted for all delays τ positive. To convert to the more conventional positive and negative τ form, simply set the time scale for $\tau = 0$ at 0.512 seconds and all delays are then measured in positive and negative time directions from that point. For light buffeting (runs 20948, 20940, 20953 and 20954) outside the speed range of $0.7 \leq M \leq 0.78$, the power spectral density curves do not exhibit distinct frequency peaks. However, in the region of strong buffet distinct frequency peaks are observed. These peaks have a fundamental frequency, which increases with M_∞ along the buffet boundary (approx. 45 Hz for run 20946 at $M_\infty = 0.703$ to 70 Hz for run 20951 at $M_\infty = 0.784$). (The first harmonic is also detected in most cases.) This frequency is substantially lower than the model resonance frequency and flow studies of the wind tunnel do not reveal any oscillations in this frequency range. Unfortunately, the transducer A at x/c = 0.3402 malfunctioned in many of the runs. Experiments correlating the shock motion with the oscillations in the pressure measurements downstream will undoubtedly shed more light on the nature of the frequency peaks detected in the power spectral density curves.

Observations of the phase curves for the cross power spectral density plots indicate that for some transducer pairs at certain run conditions, a convection velocity is detected. The data will be analysed for convection effect and spatial decay, and will be reported at a later date.

The coherence functions between transducer pairs show similar characteristics in the Mach number range 0.7 to 0.78, that is, strong coherence in the frequency range where oscillation in the fluctuating pressure occur. Outside this speed range, the coherence functions resemble those for random fluctuations.

The correlation between individual transducers with the force balance output indicate that within the range $0.7 \leqslant M_\infty \leqslant 0.78$, the coherence between transducer and force balance measurements is strong in the frequency range where noticeable oscillations in the unsteady pressure field are detected. It is clear that the unsteady normal force is primarily due to pressure fluctuation in the separated flow region on the airfoil from the shock to the trailing-edge.

The C_p plots included at the end of Figures 8 to 15 are taken from Reference 5 except that for Figure 10 which is from unpublished data. These data are provided so that the present results can be related to the mean flow conditions over the airfoil, namely, shock position and flow separation. Even though these results were obtained from separate runs, the flow conditions were practically the same as those for the present test.

8.0 CONCLUSIONS

A study of the buffet characteristics of the BGK No. 1 airfoil was carried out by measuring the fluctuating pressures along the airfoil chord and the normal force balance outputs. The tests were performed in various regions inside the buffet régime. In the range $0.7 \leqslant M_\infty \leqslant 0.78$ and $0.8 \leqslant C_L \leqslant 1.1$, balance measurements show the buffet intensity to be fairly large relative to other regions, even though all the tests were performed very close to the onset boundary. Typical characteristics of the flow in the high intensity region are: a monotonic increase in the fluctuating pressure coefficient downstream of the shock to the trailing-edge, a significant increase in fluctuating pressure level when a shock wave is located close to a measuring station, and the appearance of distinct frequency peaks in the power spectral density curves. Also, a strong coherence is observed between the fluctuating pressures in the separated flow region and the force balance outputs. For some transducer pairs, a convection velocity is detected from the phase curves in the cross power spectral density measurements.

9.0 REFERENCES

1. Ohman, L.H. — *The Role of the NAE 5-ft × 5-ft Wind Tunnel in the Development of Modern Airfoil Sections.* American Institute of Aeronautics and Astronautics, Paper 75-959, August 1975.

2. Kacprzynski, J.J. — *An Experimental Analysis and Buffet Investigation of the Shockless Lifting Airfoil No. 1.* NAE, Laboratory Report LR-569, National Research Council Canada, August 1973.

3. Redeker, G.; Proksch, H.-J. — *The Prediction of Buffet Onset and Light Buffet by Means of Computational Methods.* North Atlantic Treaty Organization, Advisory Group for Aerospace and Development, AGARD-CP-204, 1977.

4. Thomas, F.

Die Ermittlung der Schüttelgrenzen von Tragflügeln im Transsonischen Geschwindigkeitsbereich.
Jahrb. WGLR 1966, pp. 126-144 (1967).
Translation by Aircraft Research Association (ARA) Bedford: "The Determination of the Buffet Boundaries of Aerofoils in the Transonic Régime." ARA Library Translation No. 19 (1969).

5. Ohman, L.H.

Supplementary Investigation of the BGK No. 1 Airfoil; Wall Interference Study, Part I.
NAE, Laboratory Technical Report LTR-HA-5X5/0127, National Research Council Canada, April 1981.

6. Ohman, L.H.

The NAE High Reynolds Number 15" X 60" Two-Dimensional Test Facility.
NAE, Laboratory Technical Report LTR-HA-4, Part 1, National Research Council Canada, April 1970.

7. Rabiner, L.R.
Schafer, R.W.
Dlugos, D.

Periodgram Method for Power Spectrum Estimation.
Programs for Digital Signal Processing Ed. by the Digital Signal Processing Committee, IEEE Acoustics, Speech, and Signal Processing Society, IEEE Press, 1979.

8. Carter, G.C.
Ferrie, J.F.

A Coherence and Cross Spectral Estimation Program.
Programs for Digital Signal Processing Ed. by the Digital Signal Processing Committee, IEEE Acoustics, Speech and Signal Processing Society, IEEE Press, 1979.

TABLE 1

SUMMARY OF WIND TUNNEL RUNS AT 19.3% WALL POROSITY

W/T Run	M_∞	P_o (psi a)	Q(psi)	$Re_c \times 10^{-6}$	α_g	C_L
20935+	0.775	64.9	18.3	15.3	- 0.29, 2.57, 3.56, 4.58, 5.60	0.306, 0.754, 0.845, 0.862, 0.873
20936+	0.775	64.9	18.3	15.3	- 0.31, 2.57, 2.89, 3.18, 3.56	0.302, 0.769, 0.814, 0.845, 0.858
20937+	0.774	64.8	18.3	15.3	3.57	0.859
20938+	0.774	64.8	18.3		4.60	0.865
20939+	0.774	64.8	18.3		4.60	0.865
*20940+	0.775	64.8	18.3	15.3	2.55	0.762
20941+	0.754	89.8	24.5	21.0	- 0.32, 2.61, 3.62, 4.64, 5.65	0.292, 0.723, 0.863, 0.945, 0.940
20943+	0.753	90.1	24.5	21.1	- 0.34, 2.62, 3.64, 4.64, 5.66	0.290, 0.733, 0.869, 0.951, 0.943
*20944	0.753	90.1	24.5	21.1	5.66	0.945
20945	0.703	95.8	23.8	21.3	- 0.31, 6.77, 8.71	0.278, 1.077, 1.020
*20946	0.703	95.6	23.8	21.3	6.77	1.069
20947	0.501	120.1	17.7	21.0	- 0.25, 8.76, 10.76, 11.73	0.248, 1.126, 1.151, 1.128
*20948	0.501	120.1	17.7	21.0	11.74	1.124
*20949	0.775	64.9	18.3	15.3	4.61	0.868
20950	0.783	87.8	25.1	21.0	- 0.34, 2.55, 3.55, 4.57, 5.60, 6.61	0.304, 0.756, 0.807, 0.820, 0.827, 0.840
*20951	0.784	87.8	25.1	21.0	3.56	0.806
20952	0.805	86.2	25.5	20.9	- 0.36, 2.01, 2.50, 3.00, 3.51, 4.02	0.313, 0.667, 0.694, 0.712, 0.728, 0.741
*20953	0.805	86.2	25.5	20.9	3.52	0.727
*20954	0.805	86.2	25.5	20.9	- 0.36	0.314

\+ Balance measurements not available.

* Statistical data for these runs are given in this report.

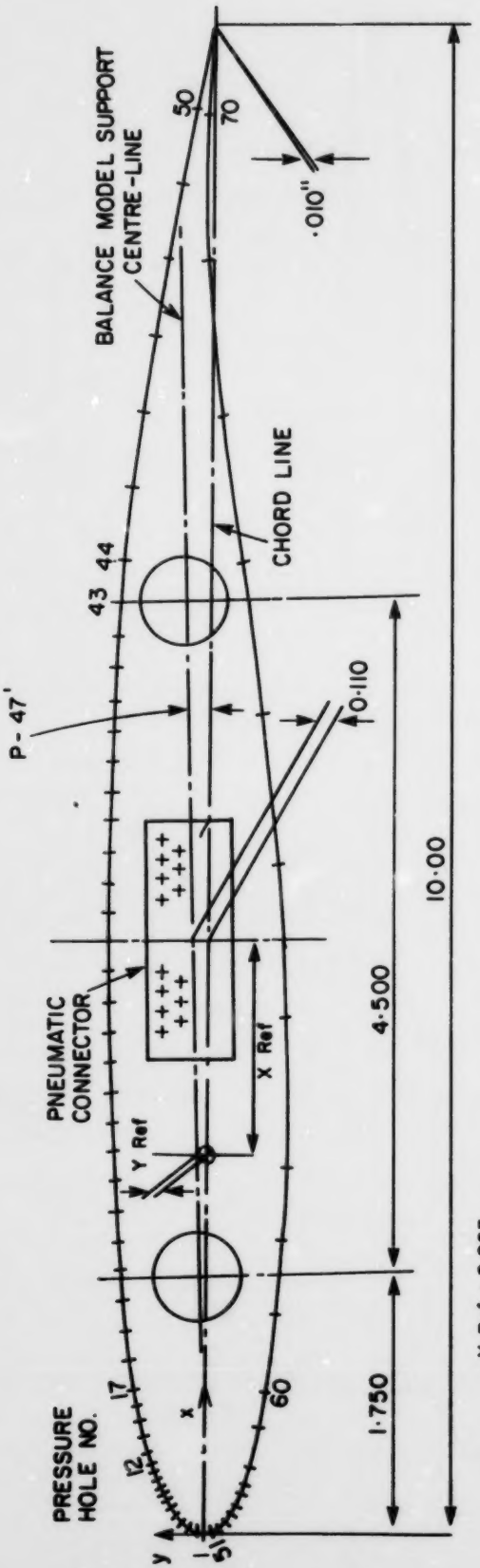

FIG. 1: BGK NO. 1 AIRFOIL MODEL WITH PRESSURE HOLE LOCATIONS

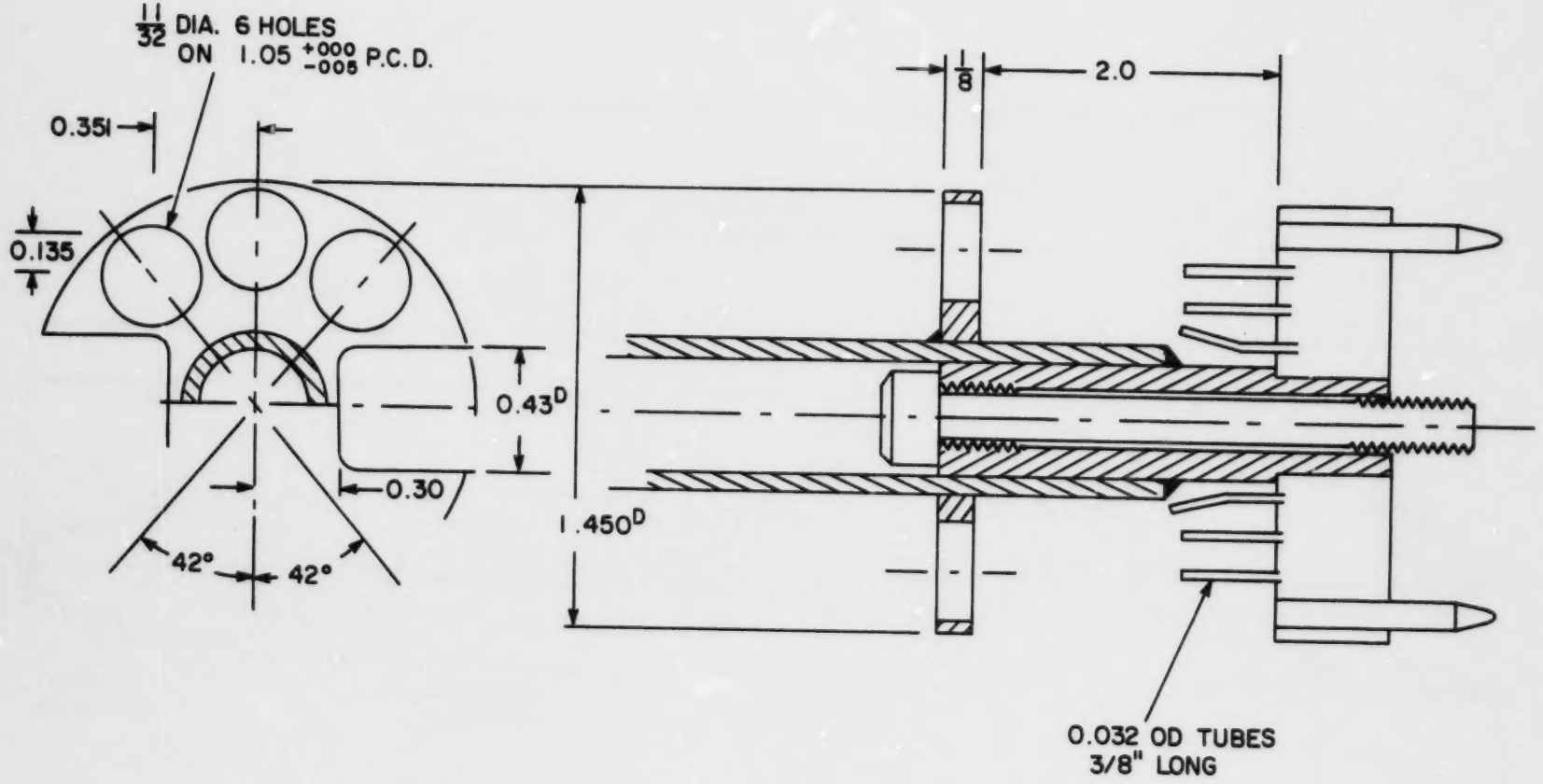

FIG. 2: MOUNTING ARRANGEMENT FOR TRANSDUCERS FOR BUFFET STUDIES

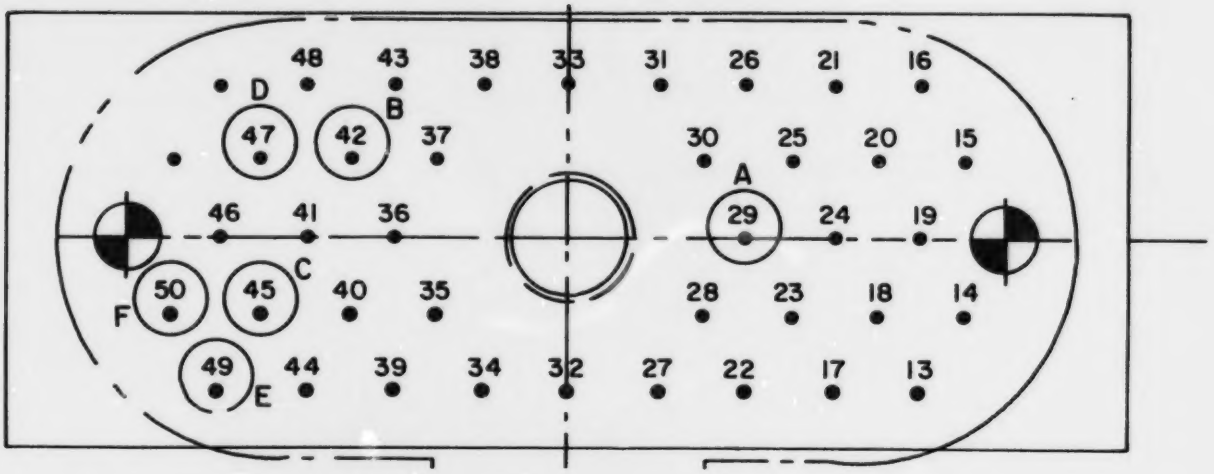

FIG. 3: SOUTH SIDE WING PRESSURE CONNECTOR SHOWING PORTS CONNECTED TO TRANSDUCERS FOR BUFFET STUDIES

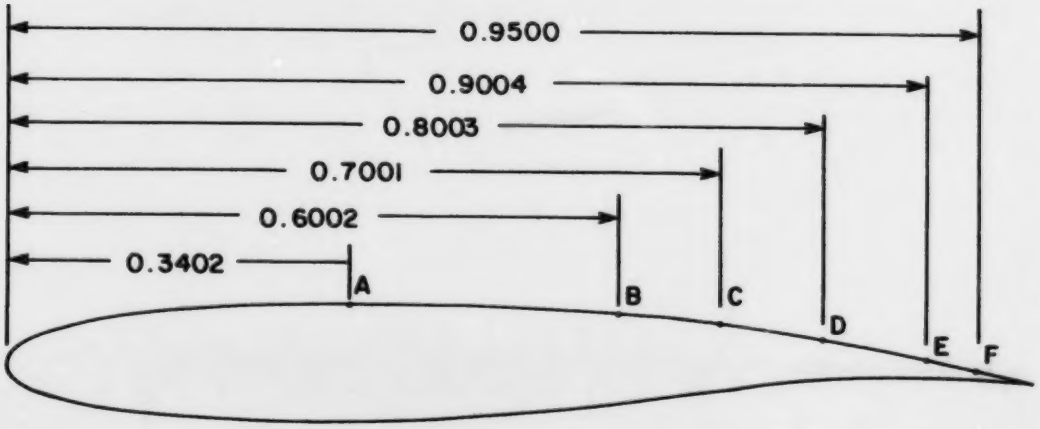

FIG. 4: LOCATION OF PRESSURE PORTS FOR FLUCTUATING PRESSURE MEASUREMENTS

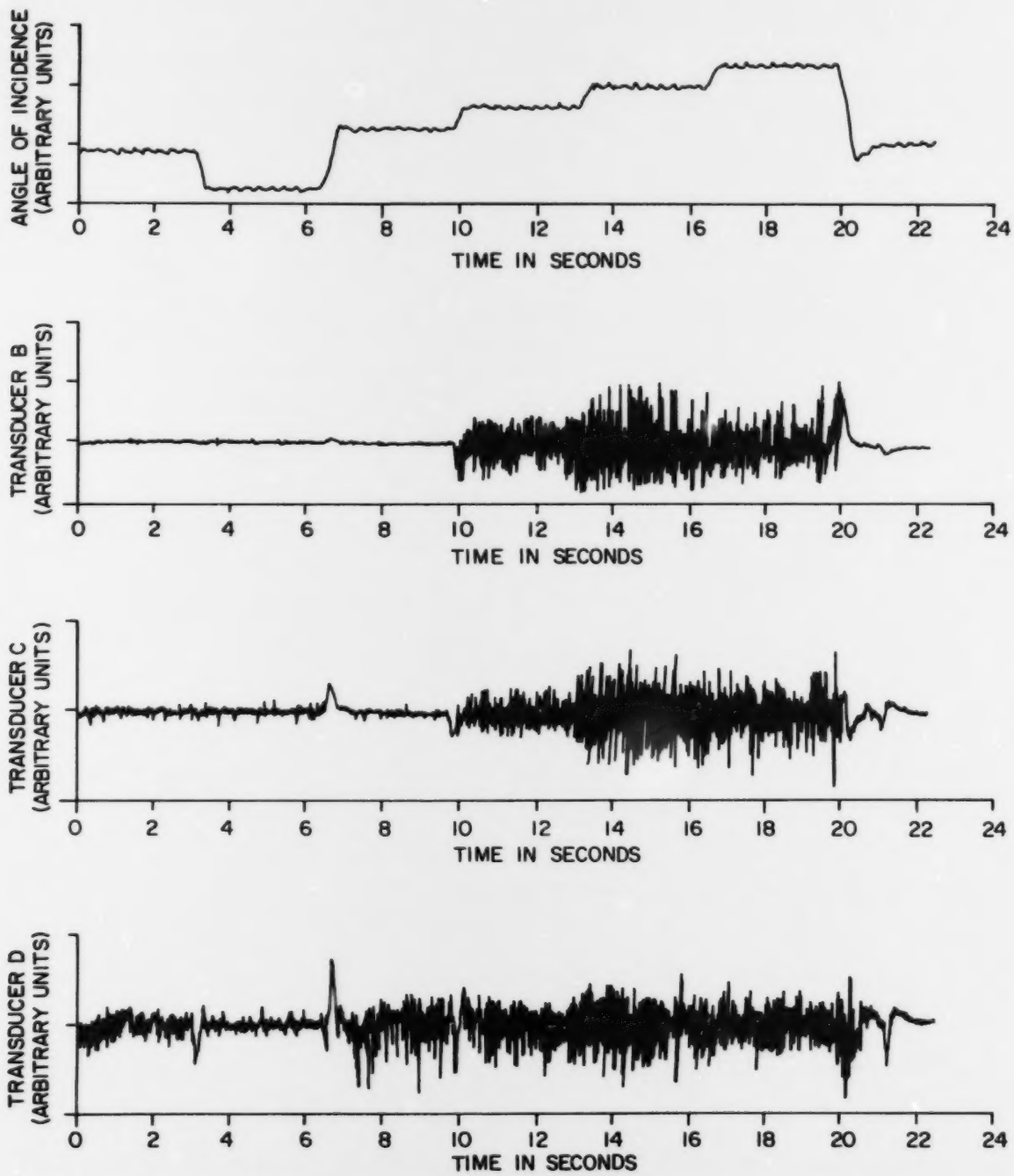
ANGLE OF INCIDENCE (ARBITRARY UNITS)
0 2 4 6 8 10 12 14 16 18 20 22 24
TIME IN SECONDS
TRANSDUCER B (ARBITRARY UNITS)
0 2 4 6 8 10 12 14 16 18 20 22 24
TIME IN SECONDS
TRANSDUCER C (ARBITRARY UNITS)
0 2 4 6 8 10 12 14 16 18 20 22 24
TIME IN SECONDS
TRANSDUCER D (ARBITRARY UNITS)
0 2 4 6 8 10 12 14 16 18 20 22 24
TIME IN SECONDS

FIG. 5: TYPICAL OUTPUT FROM A STEP-PAUSE INCIDENCE TEST

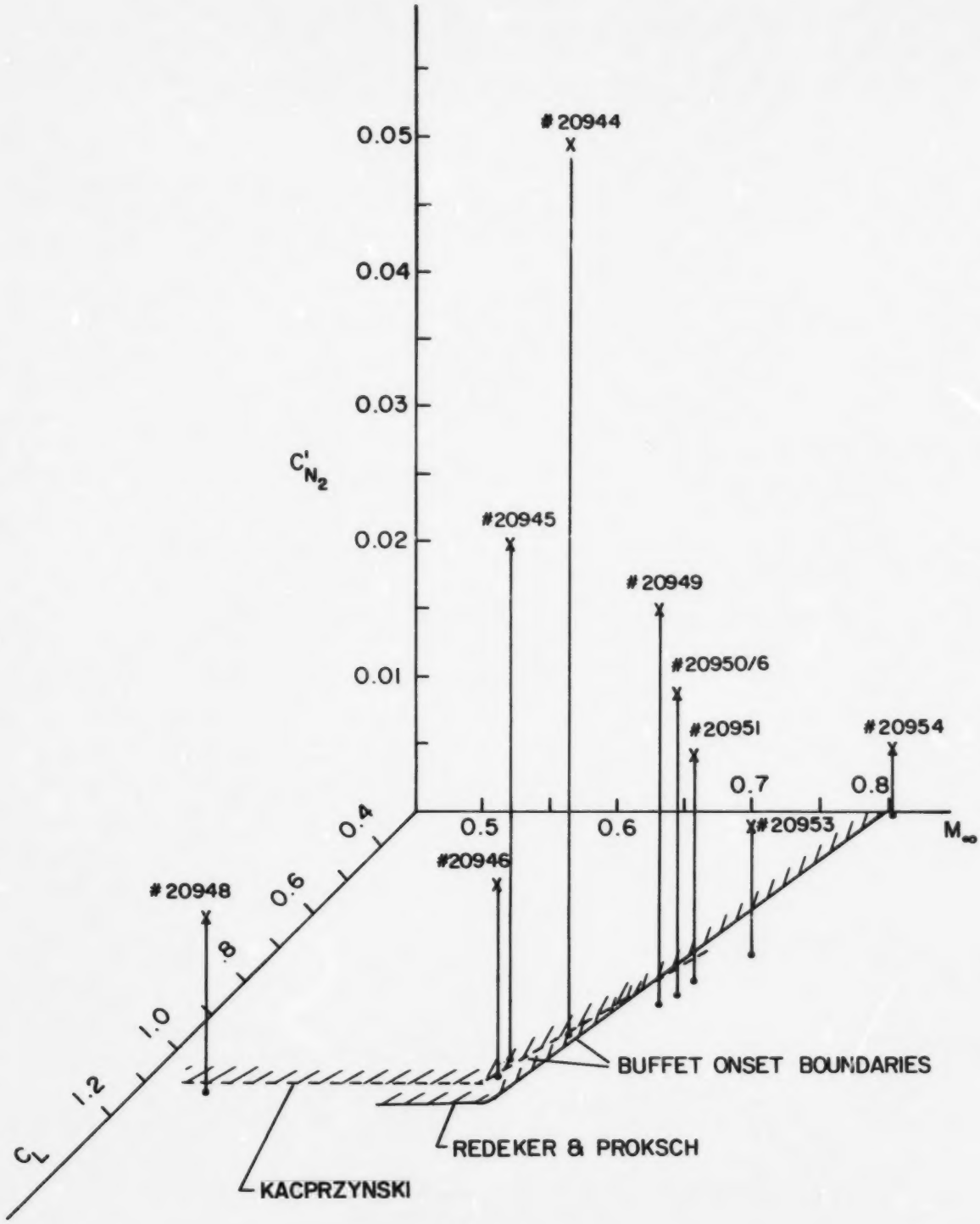

FIG. 6: VARIATION OF THE FLUCTUATING NORMAL FORCE COEFFICIENT C'_{N_2} WITH MACH NUMBER AND STEADY STATE LIFT COEFFICIENT

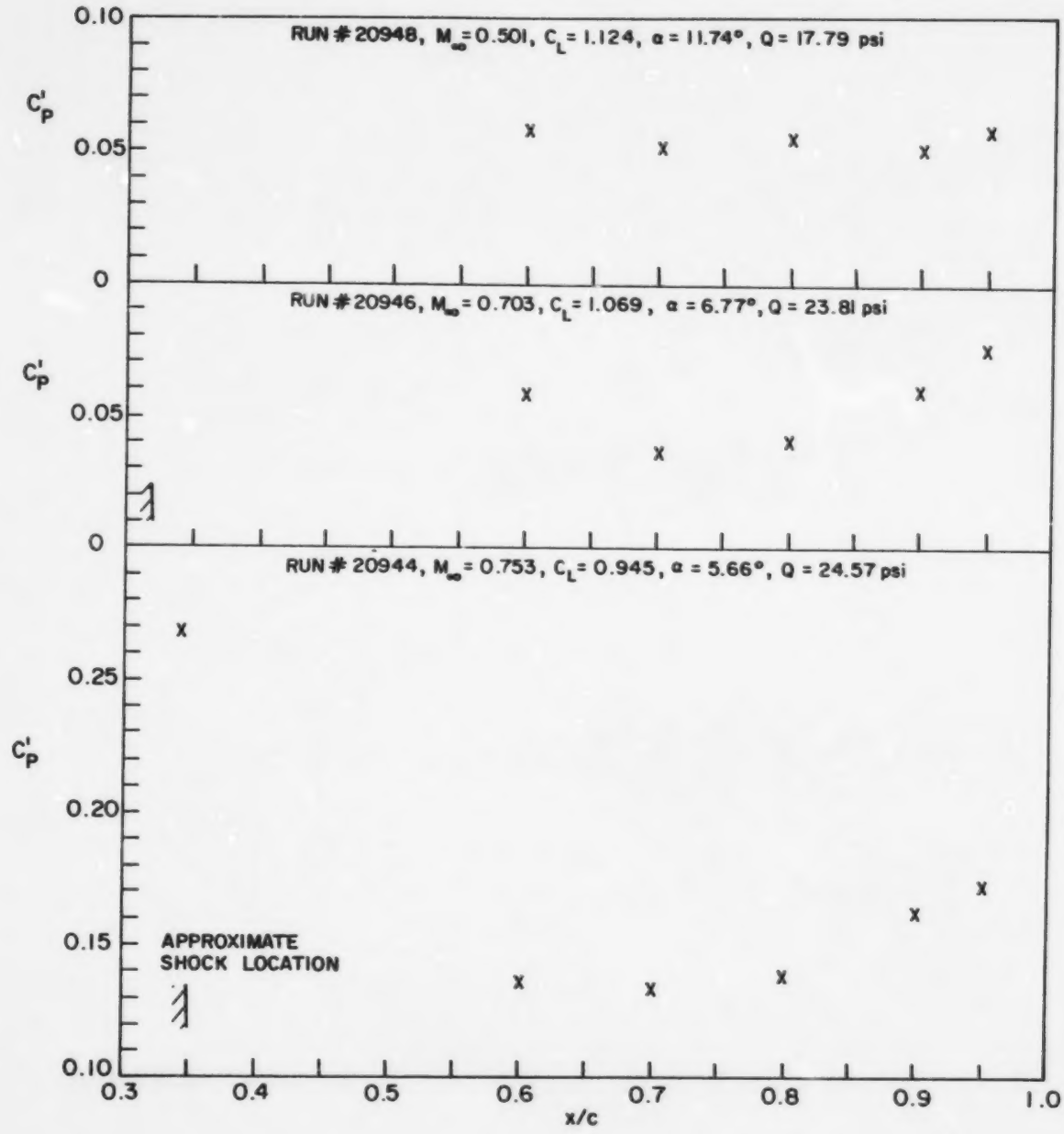

FIG. 7: VARIATION OF FLUCTUATING PRESSURE COEFFICIENT ALONG AIRFOIL CHORD

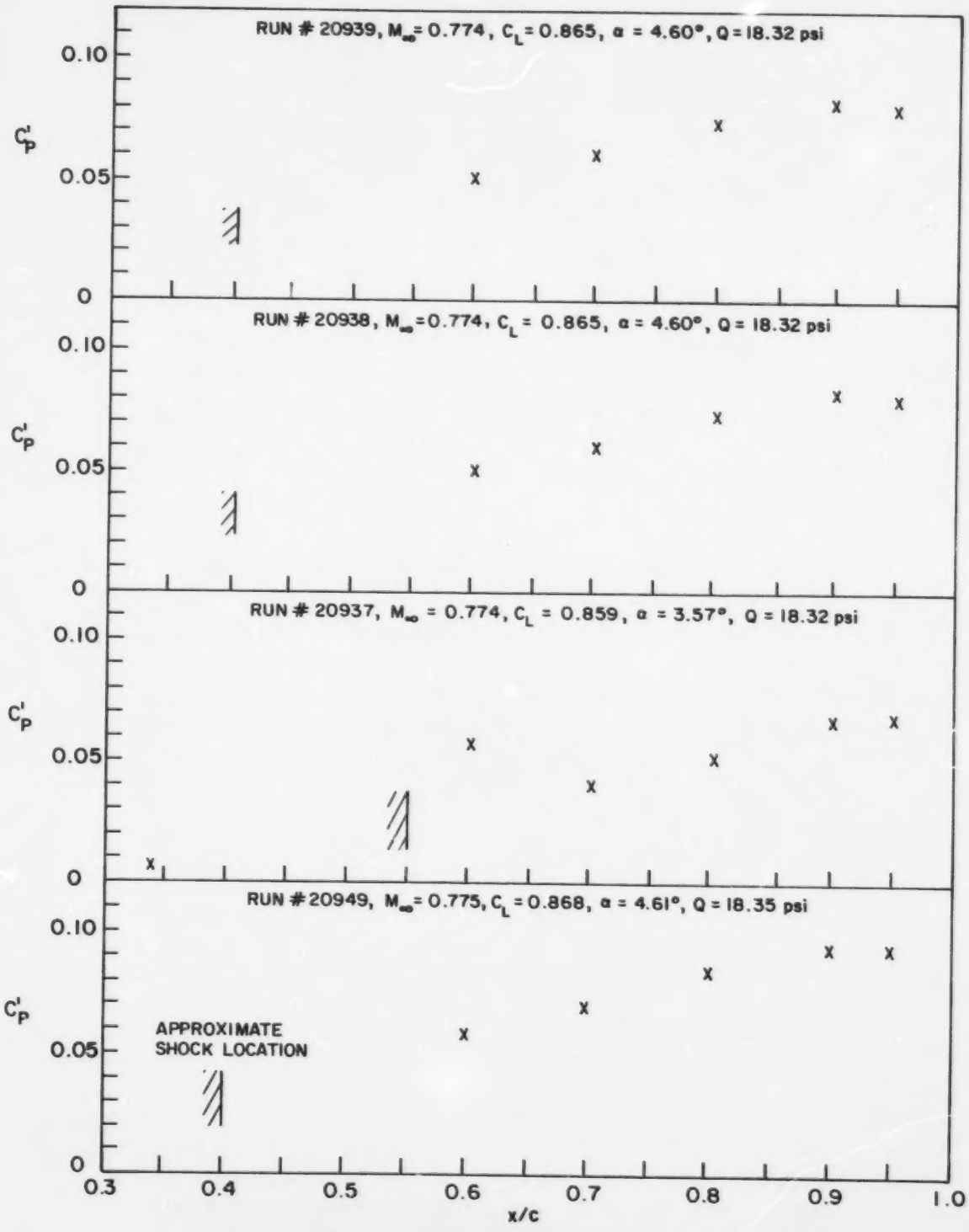

FIG. 7: VARIATION OF FLUCTUATING PRESSURE COEFFICIENT ALONG AIRFOIL CHORD (Cont'd)

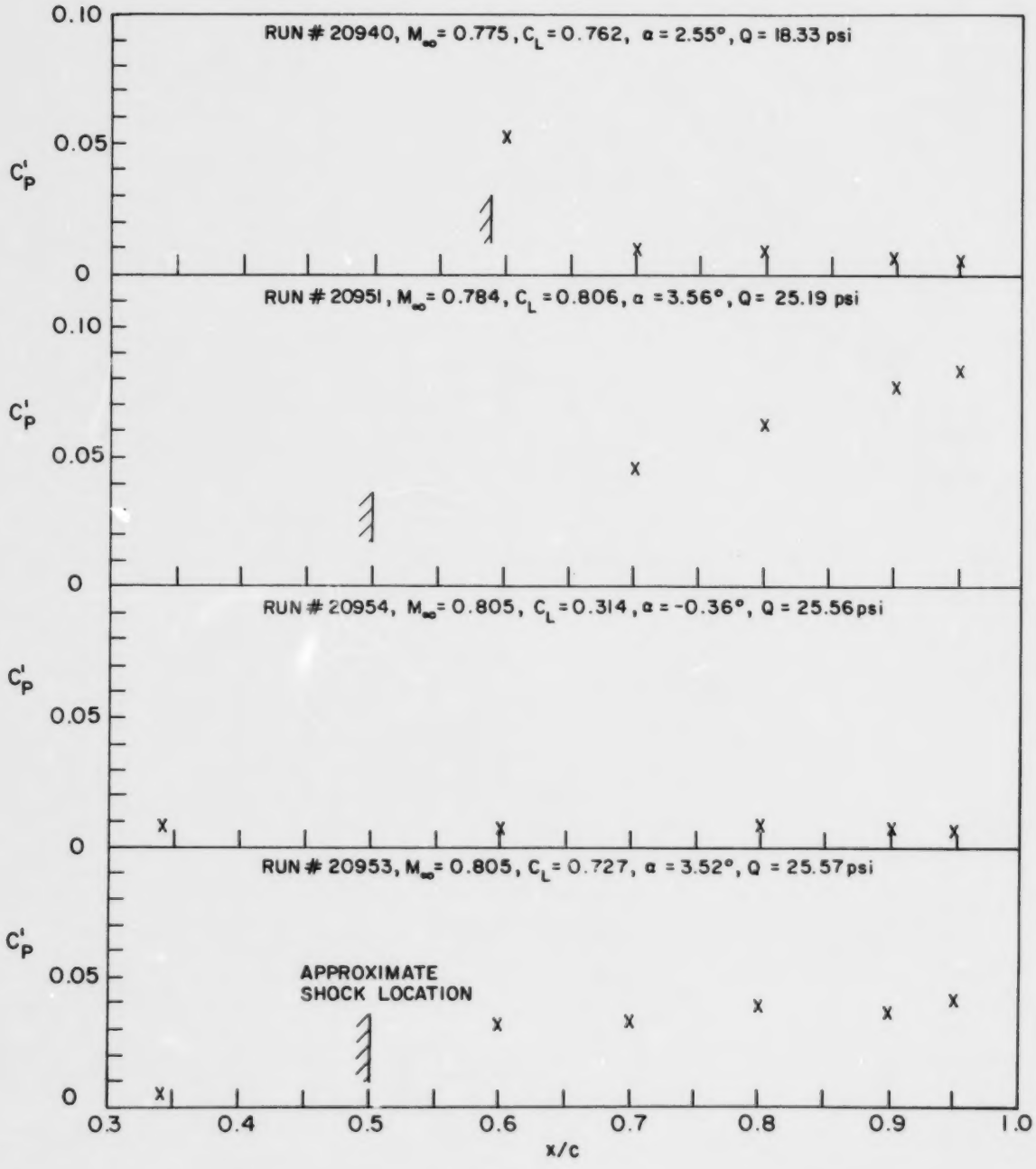

FIG. 7: VARIATION OF FLUCTUATING PRESSURE COEFFICIENT ALONG AIRFOIL CHORD (Cont'd)

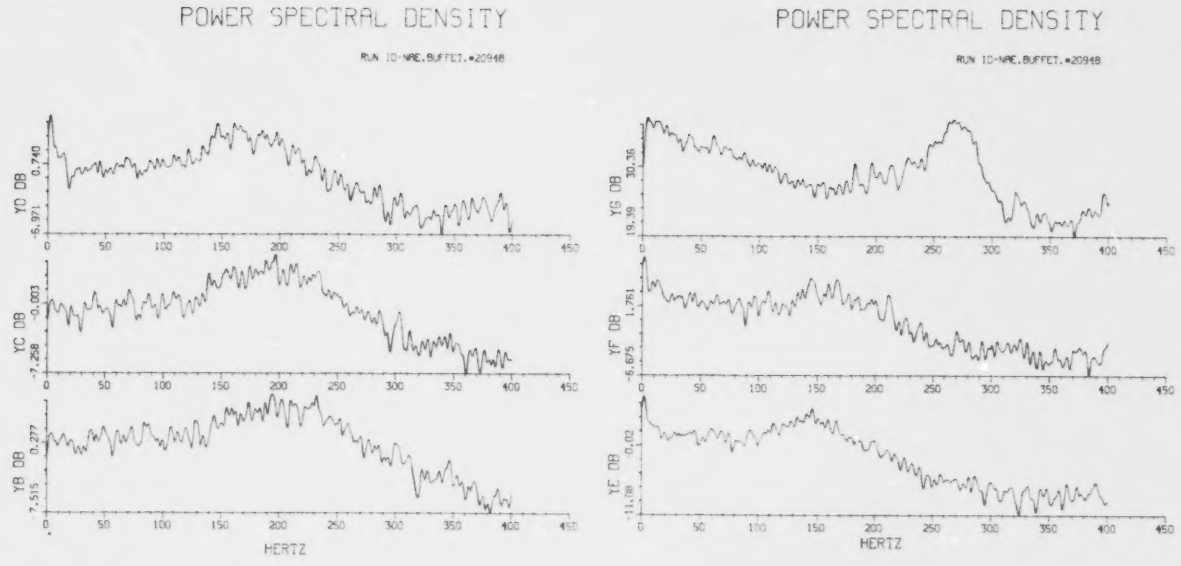

FIG. 8a: POWER SPECTRAL DENSITY FOR M_∞=0.501, C_L =1.124, Q =17.7 psi

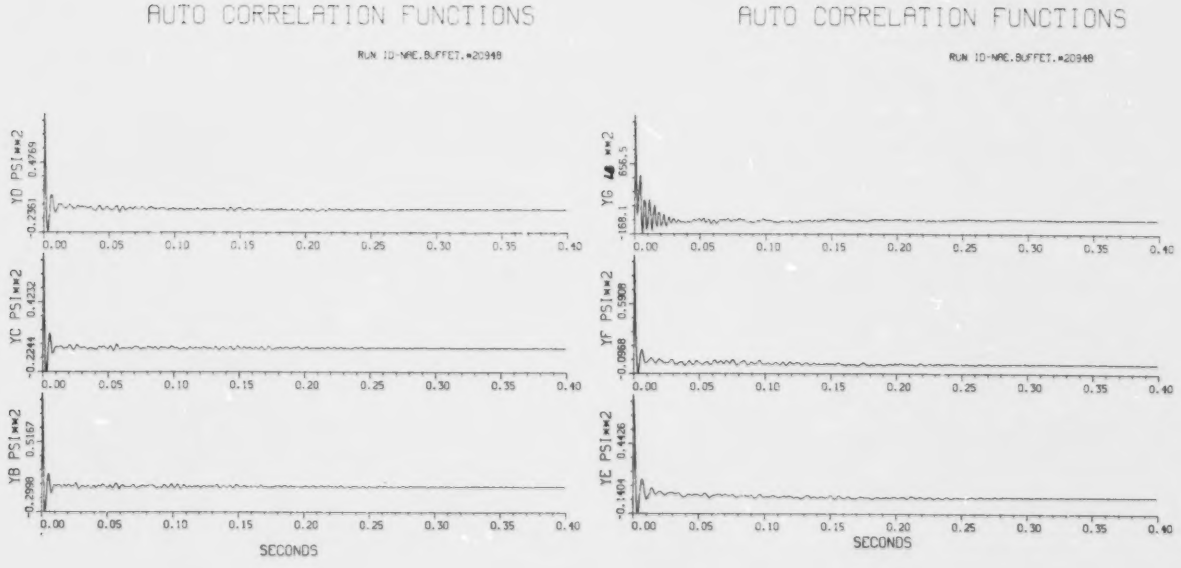

FIG. 8b: AUTO CORRELATION FUNCTIONS FOR M_∞=0.501, C_L =1.124, Q =17.7 psi

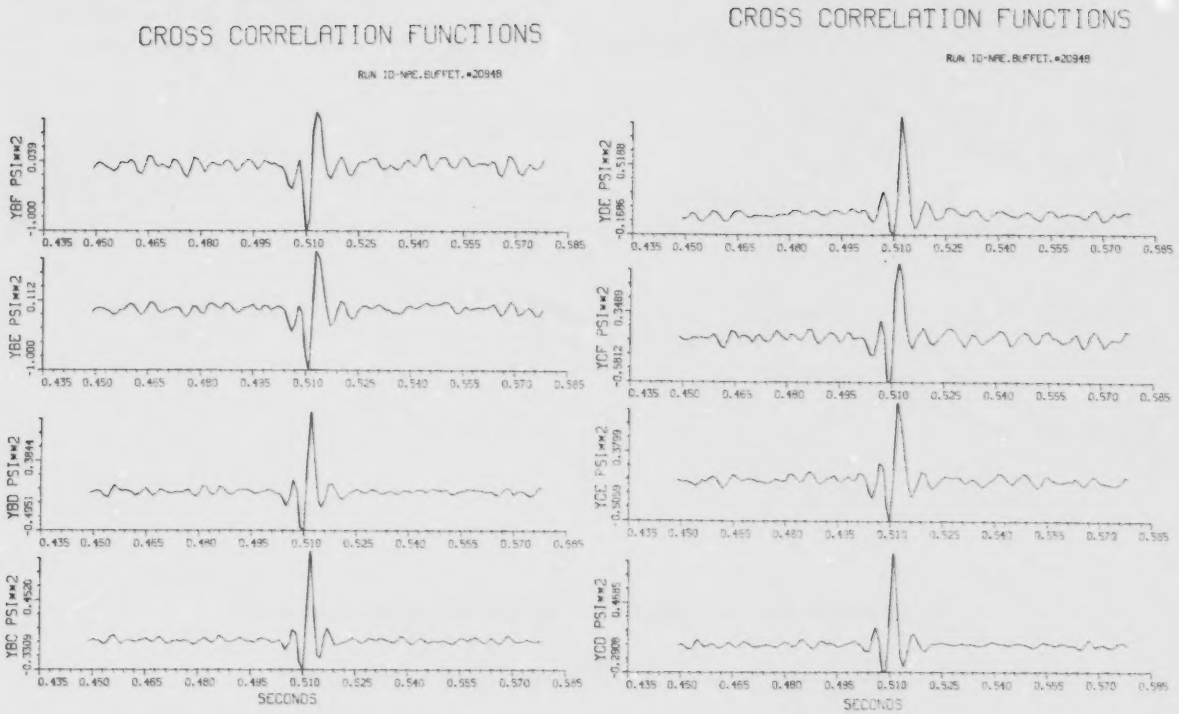

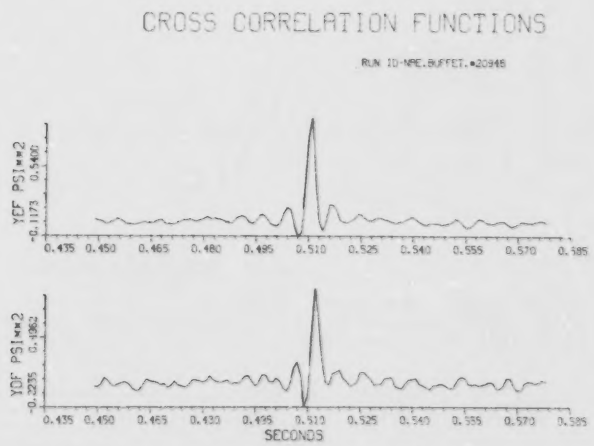

FIG. 8c: CROSS CORRELATION FUNCTIONS FOR M_∞=0.501, C_L = 1.124, Q =17.7 psi

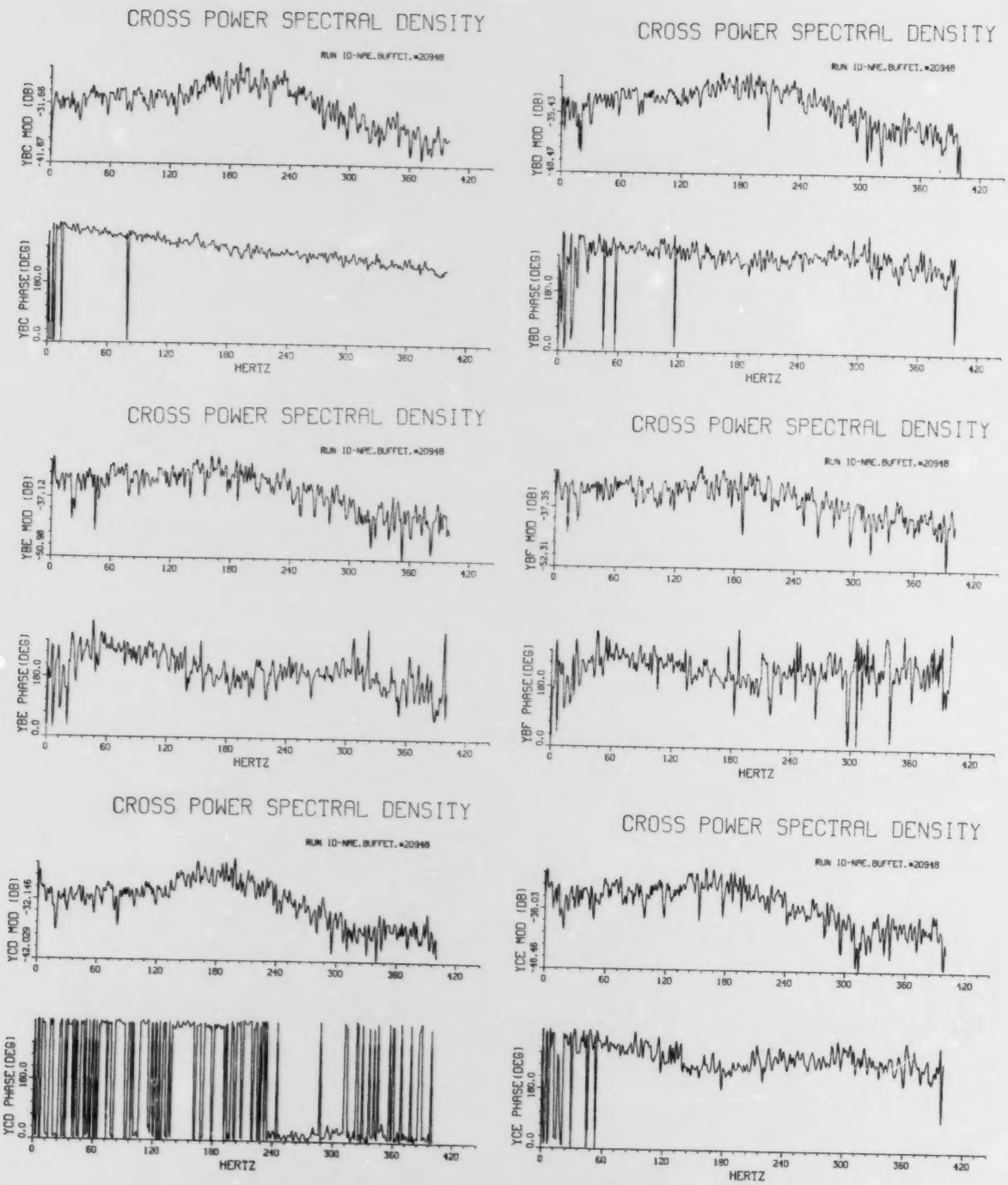

FIG. 8d: CROSS POWER SPECTRAL DENSITY FOR M_∞=0.501, C_l = 1.124, Q = 17.7 psi

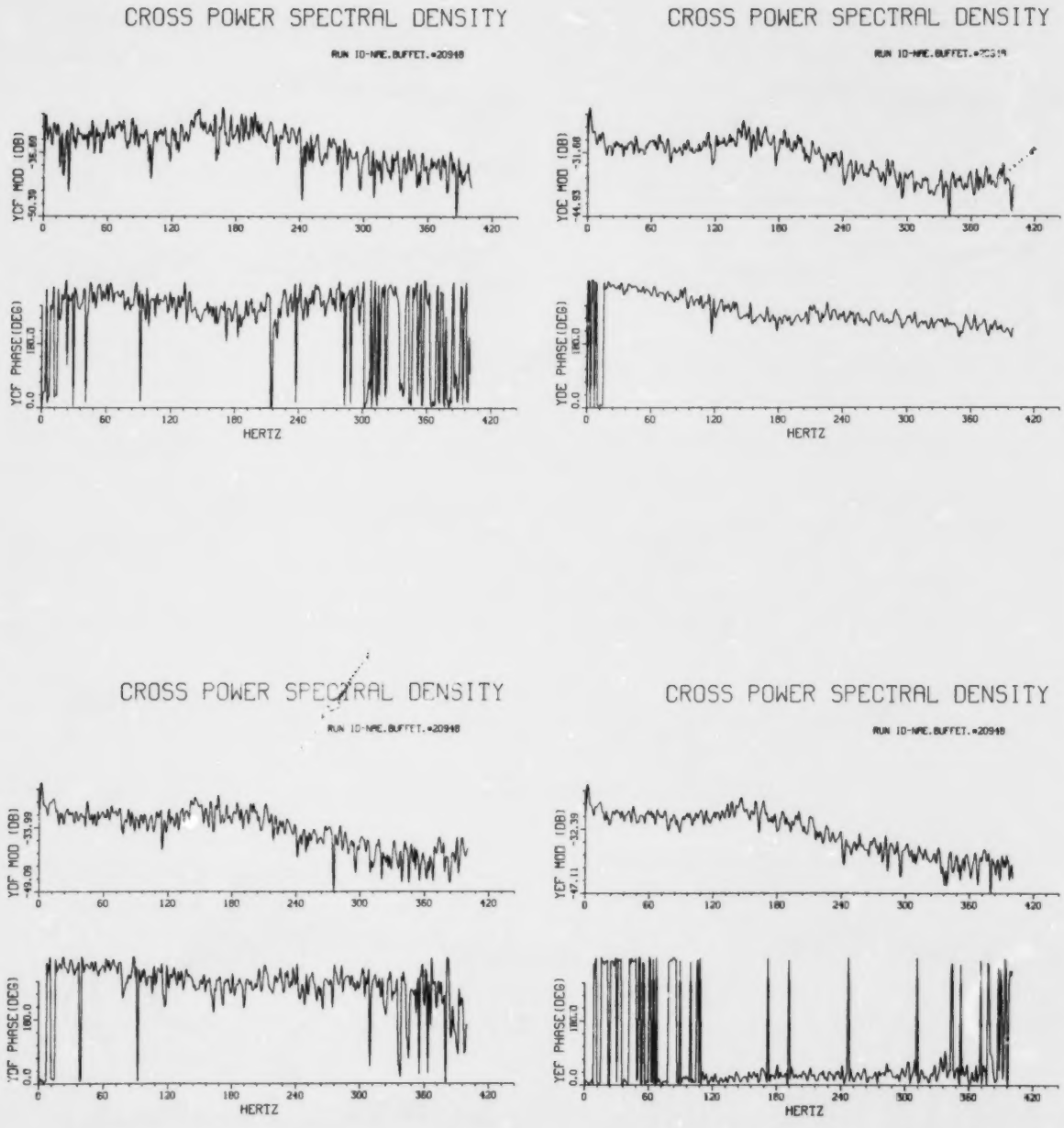

FIG. 8d: CROSS POWER SPECTRAL DENSITY FOR M_∞=0.501, C_L=1.124, Q =17.7 psi (Cont'd)

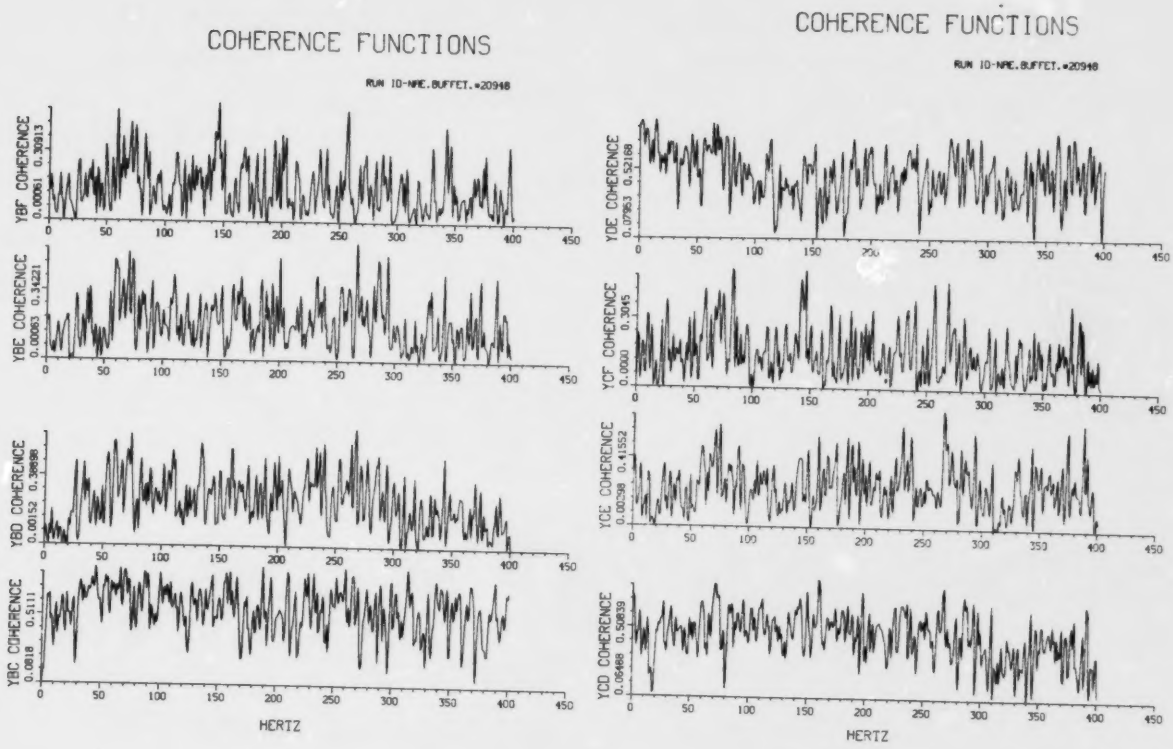

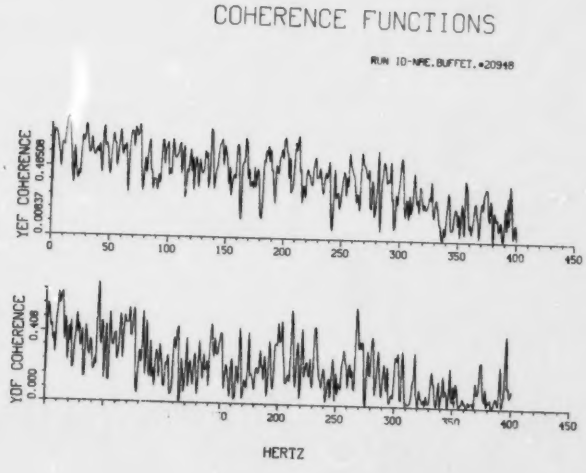

FIG. 8a: COHERENCE FUNCTIONS FOR M_∞=0.501, C_L=1.124, Q=17.7 psi

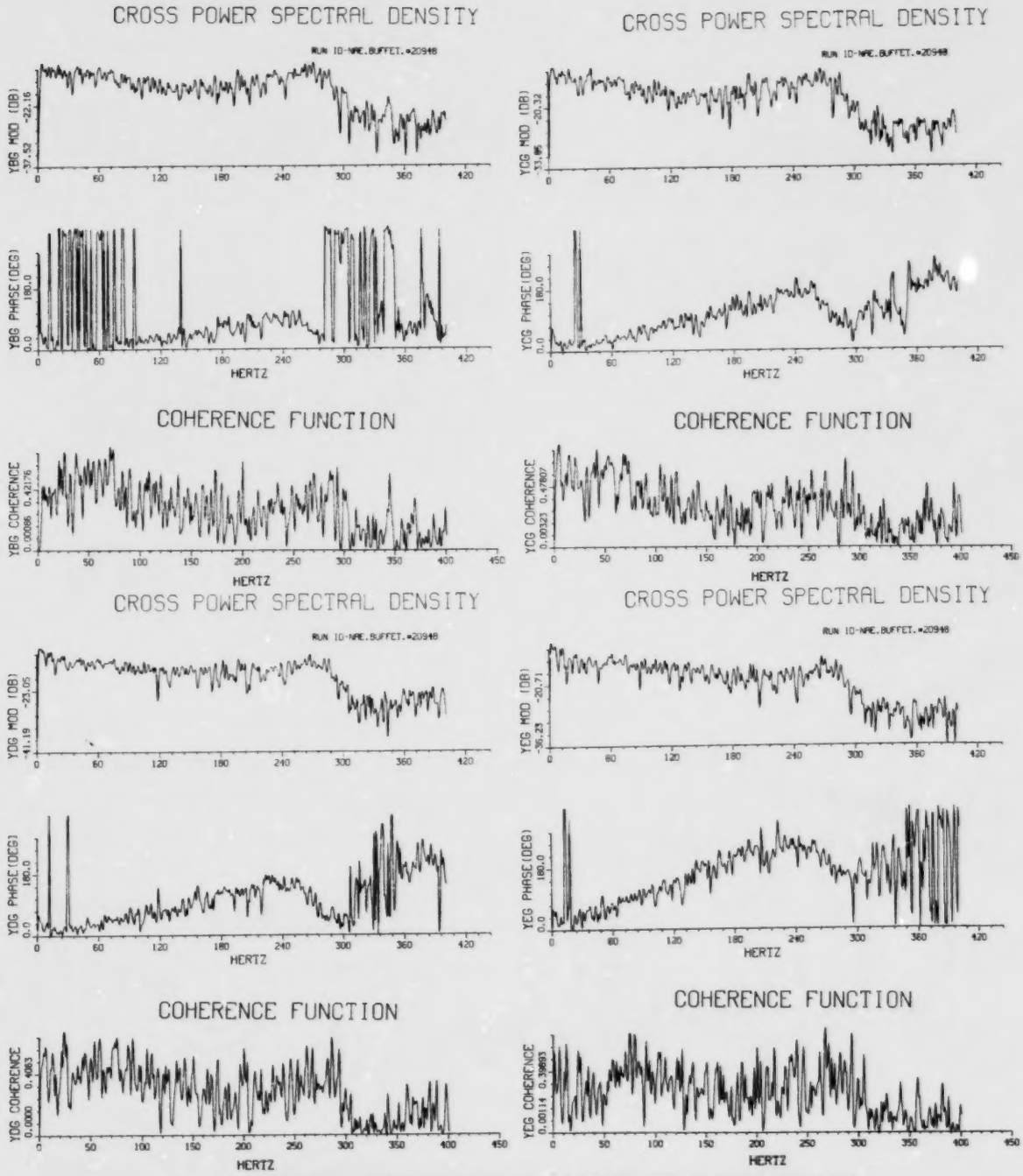

FIG. 81: CROSS POWER SPECTRAL DENSITY AND COHERENCE FUNCTION BETWEEN PRESSURE AND NORMAL FORCE N_2 FOR M_∞=0.501, C_l = 1.124, Q = 17.7 psi

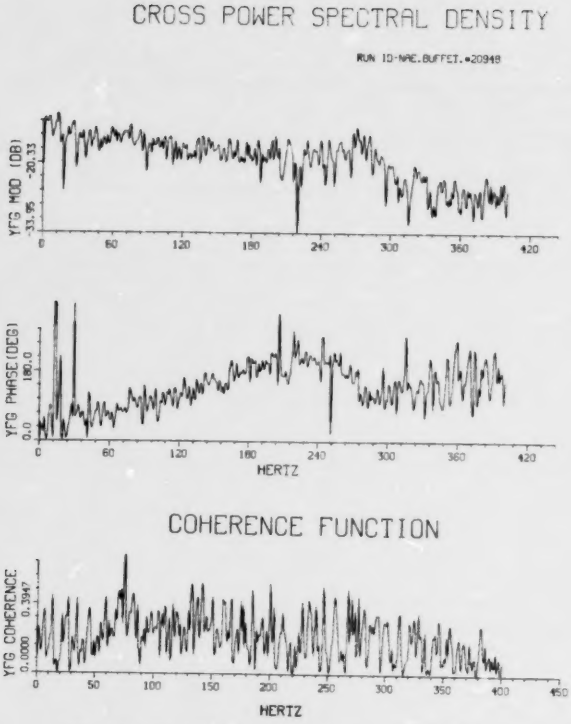

FIG. 8f: CROSS POWER SPECTRAL DENSITY AND COHERENCE FUNCTION BETWEEN PRESSURE AND NORMAL FORCE N_2 FOR M_∞=0.501, C_L =1.124, Q =17.7 psi (Cont'd)

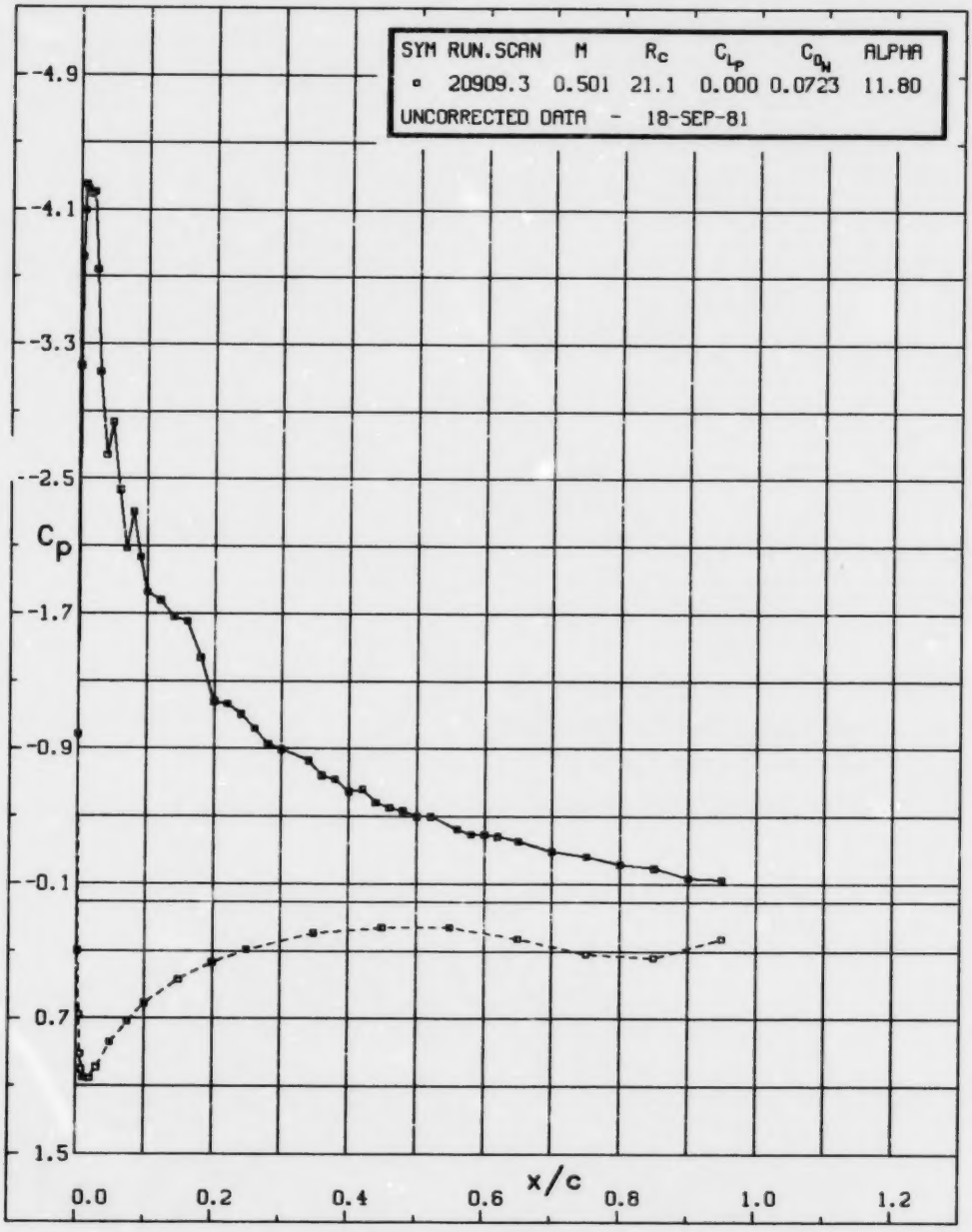

FIG. 8g: STEADY-STATE PRESSURE DISTRIBUTION

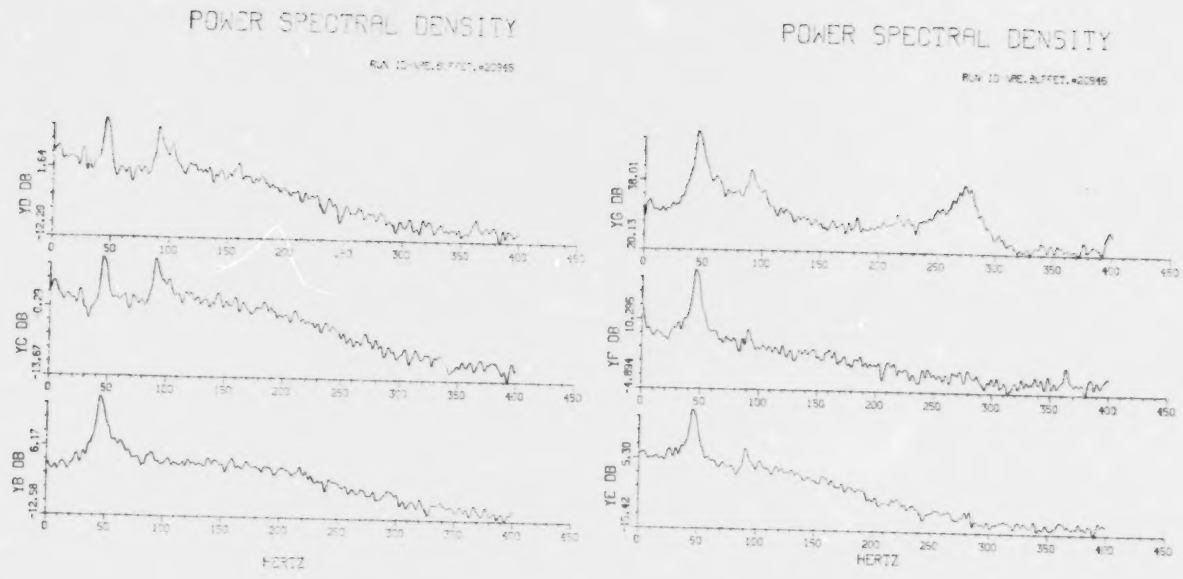

FIG. 9a: POWER SPECTRAL DENSITY FOR M_∞=0.703, C_L = 1.069, Q = 23.8 psi

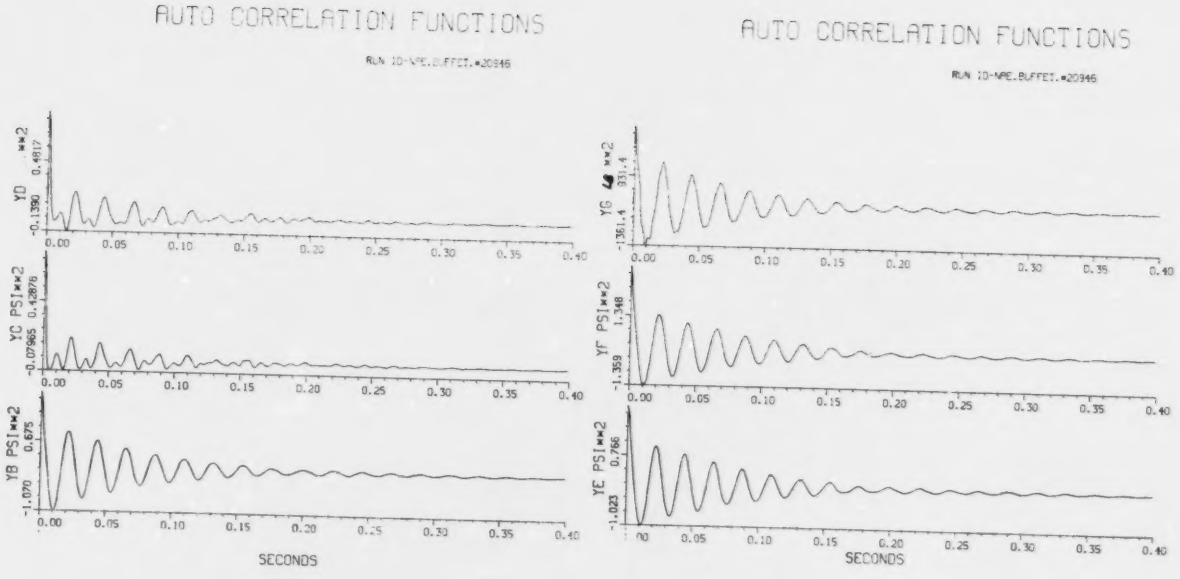

FIG. 9b: AUTO CORRELATION FUNCTIONS FOR M_∞=0.703, C_L = 1.069, Q = 23.8 psi

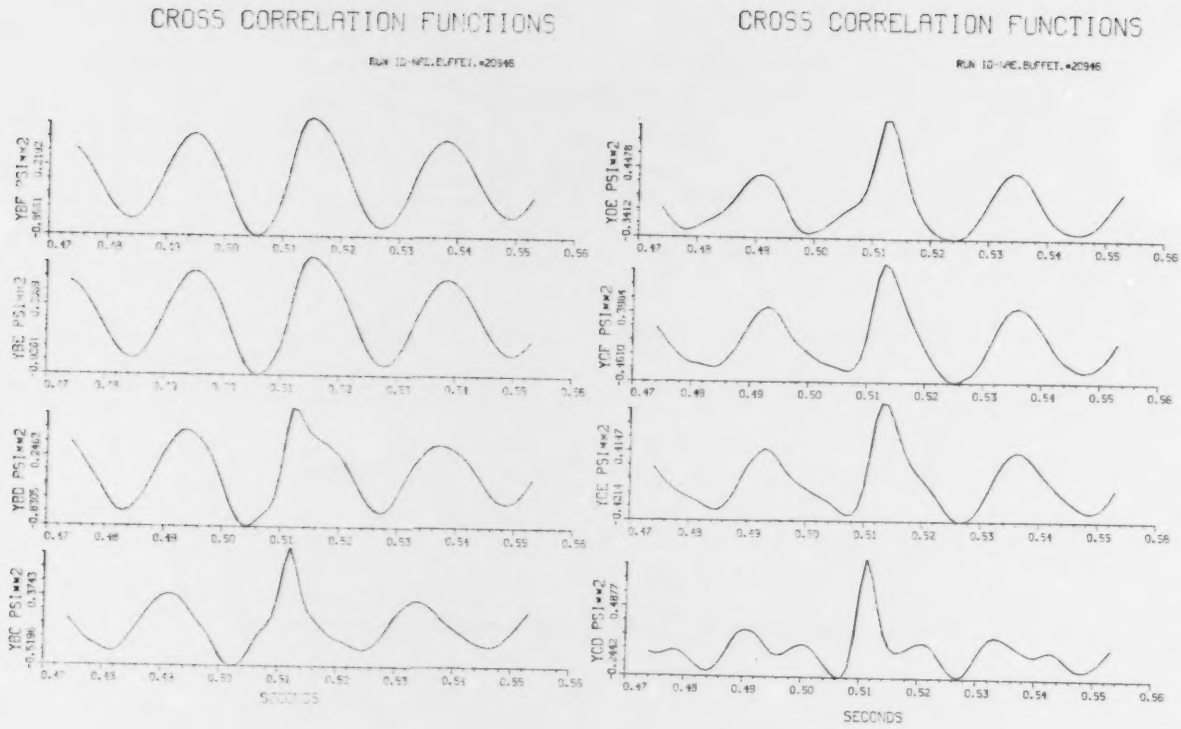

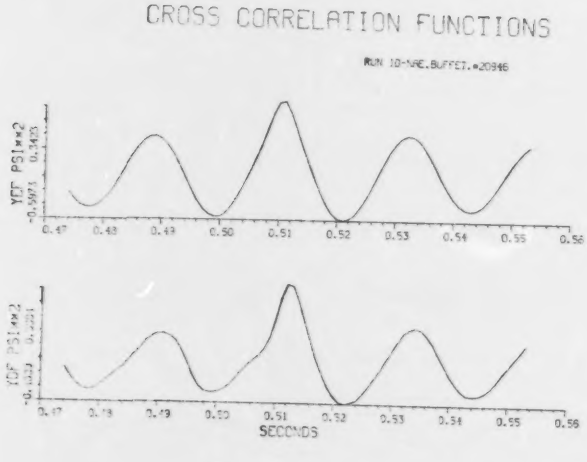

FIG. 9c: CROSS CORRELATION FUNCTIONS FOR M_∞=0.703, C_L=1.069, Q=23.8 psi

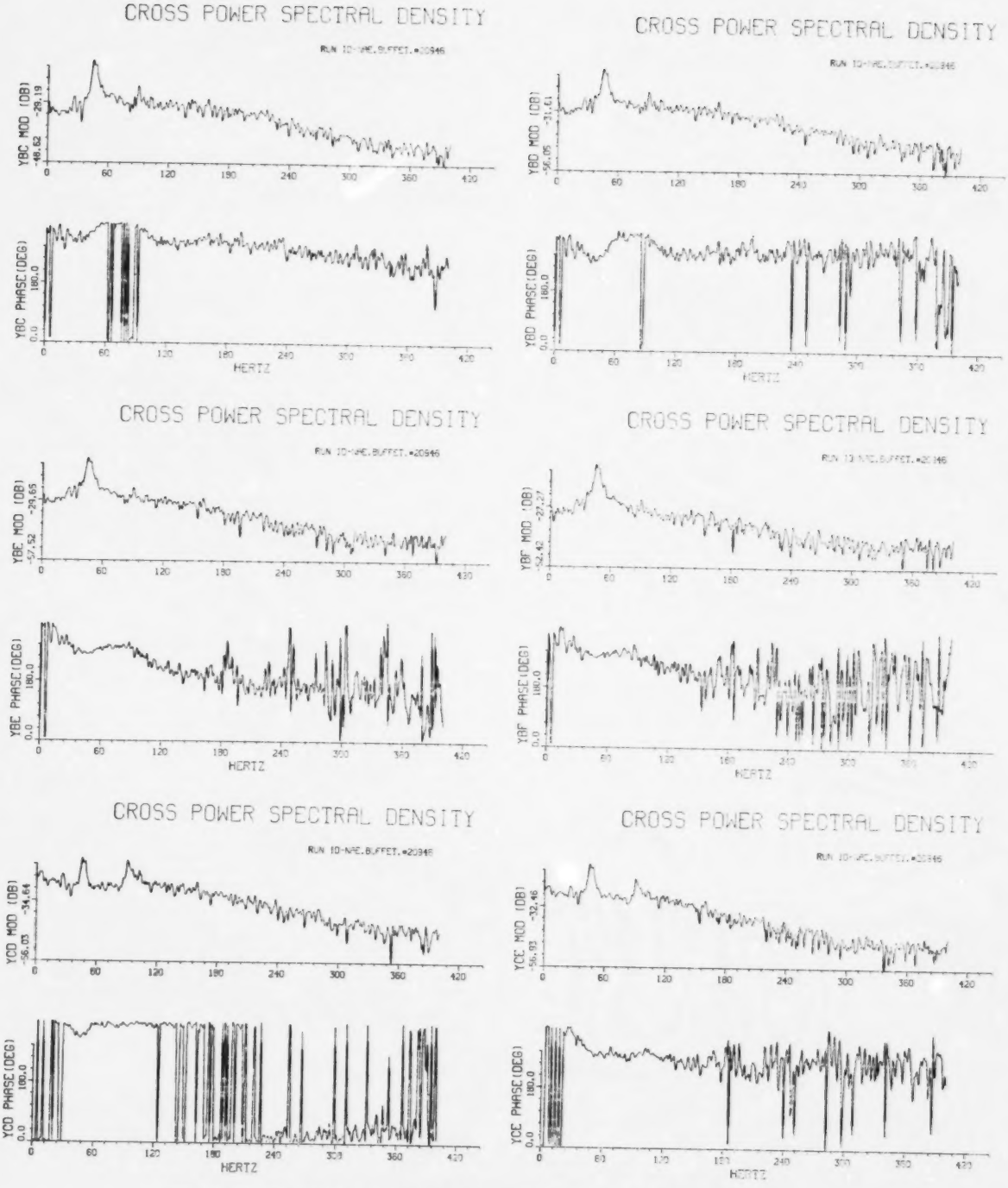

FIG. 9d: CROSS POWER SPECTRAL DENSITY FOR M_∞= 0.703, C_l = 1.069, Q = 23.8 psi

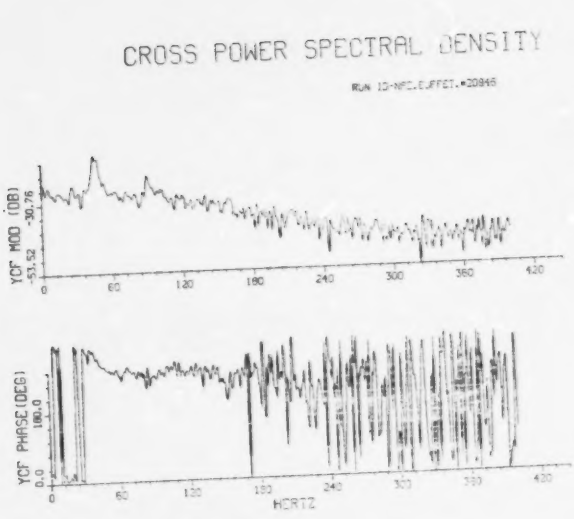

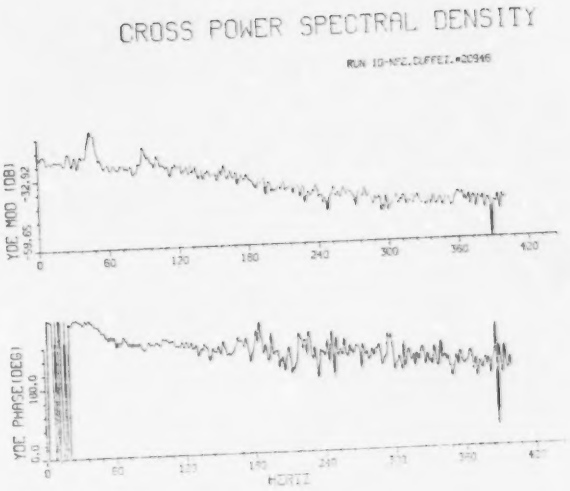

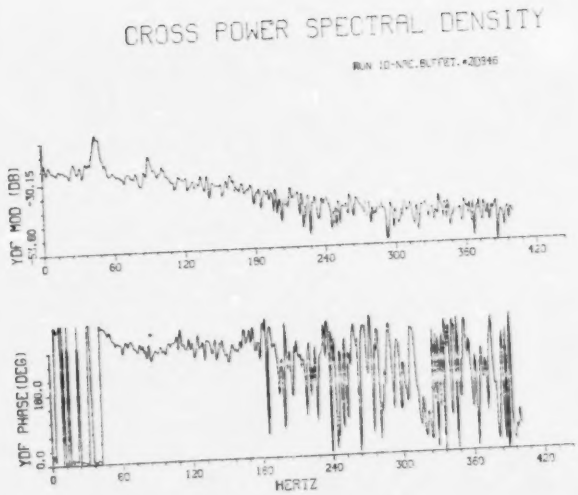

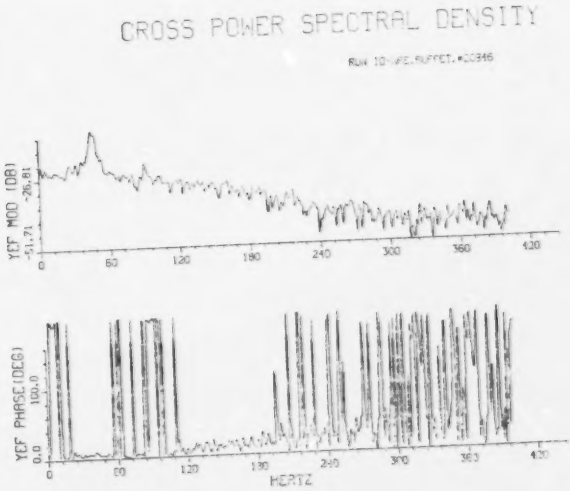

FIG. 9d: CROSS POWER SPECTRAL DENSITY FOR M_∞=0.703, C_L =1.089, Q =23.8 psi (Cont'd)

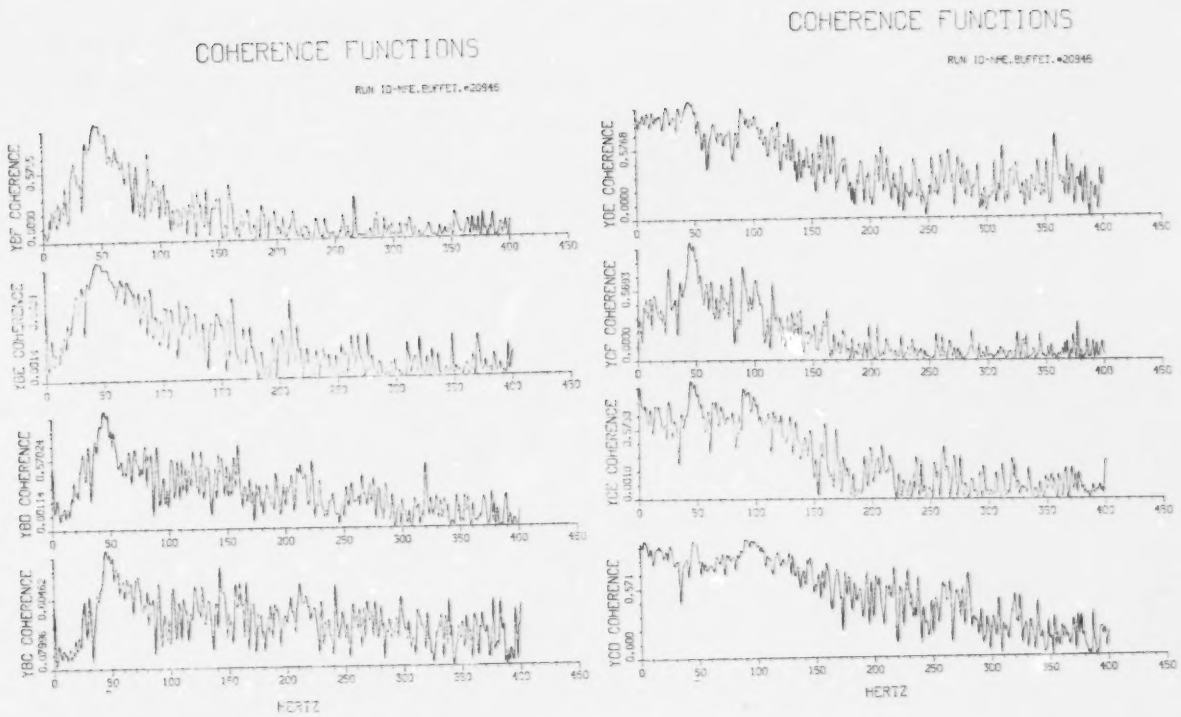

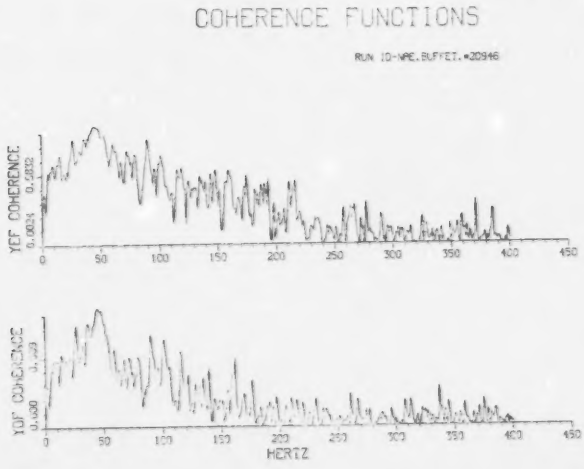

FIG. 9a: COHERENCE FUNCTIONS FOR M_∞=0.703, C_L = 1.069, Q = 23.8 psi

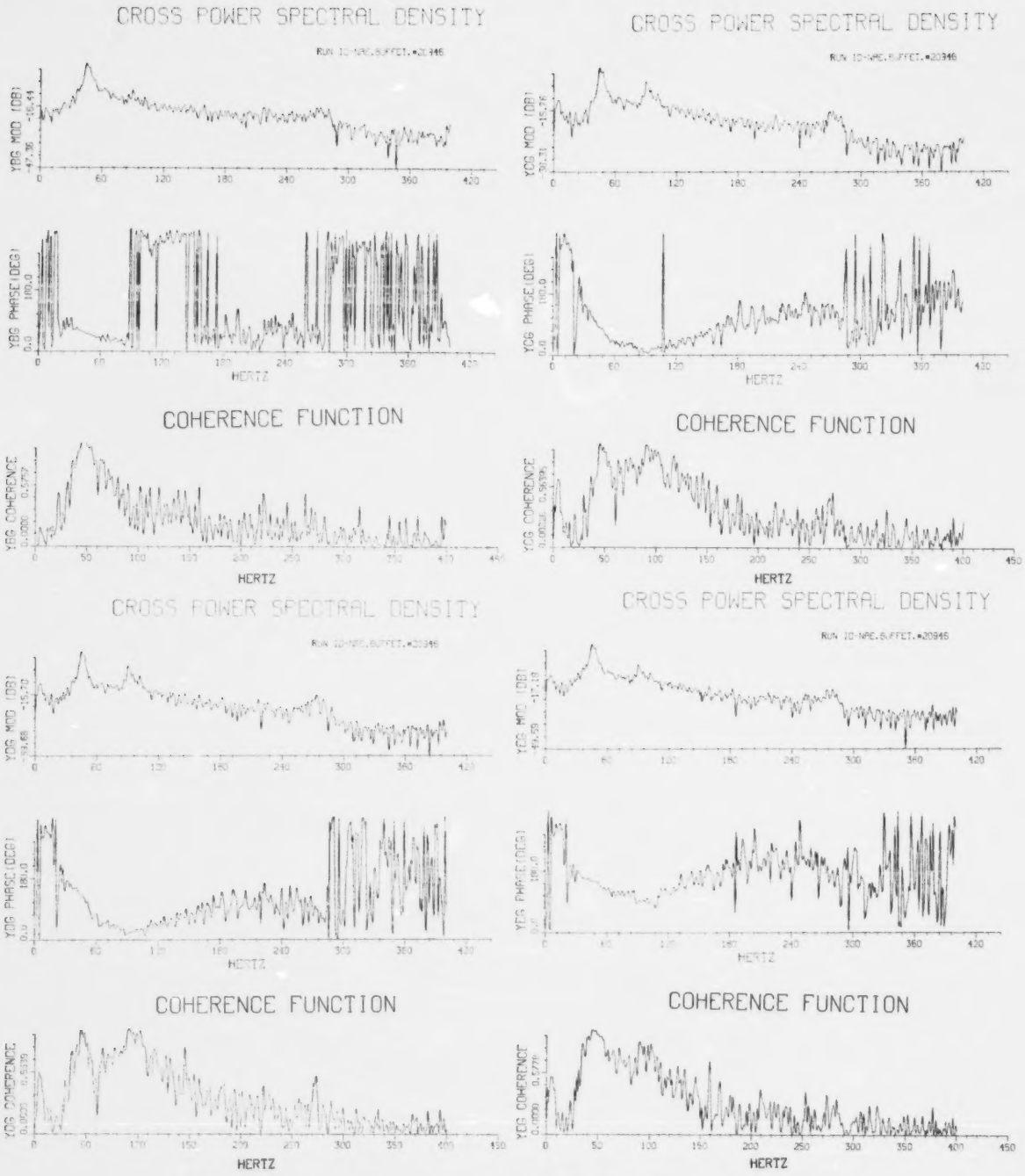

FIG. 9f: CROSS POWER SPECTRAL DENSITY AND COHERENCE FUNCTION BETWEEN PRESSURE AND NORMAL FORCE N_2 FOR M_∞=0.703, C_L = 1.069, Q = 23.8 psi

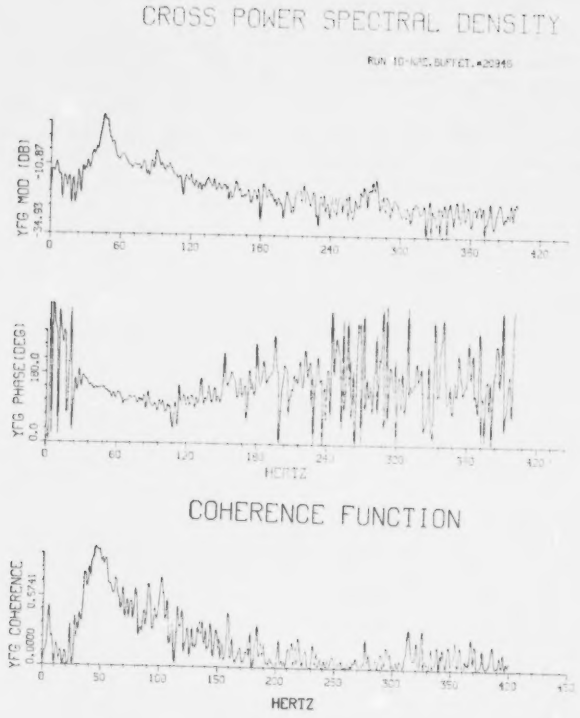

FIG. 9f: CROSS POWER SPECTRAL DENSITY AND COHERENCE FUNCTION BETWEEN PRESSURE AND NORMAL FORCE N_2 FOR M_∞=0.703, C_L = 1.069, Q = 23.8 psi (Cont'd)

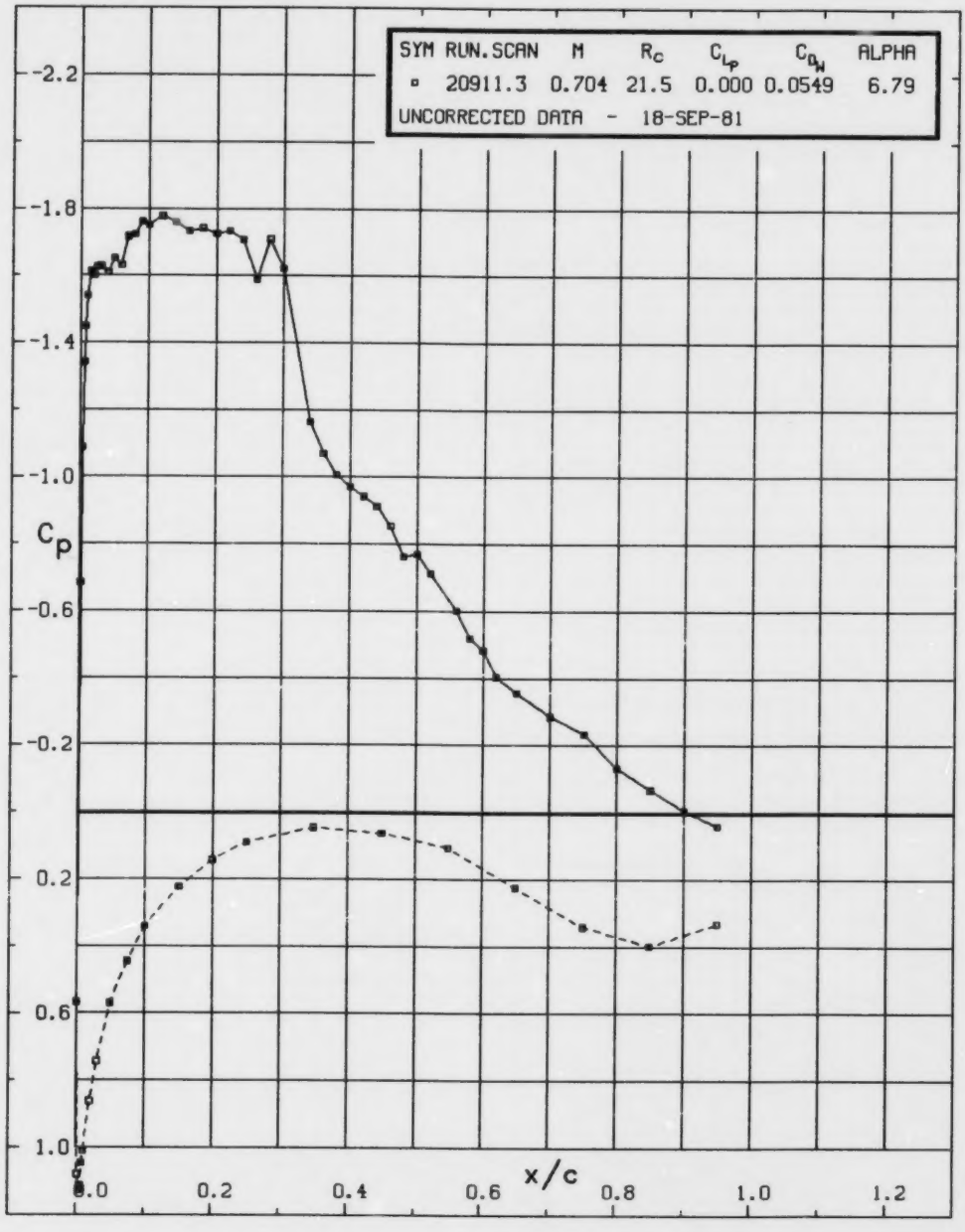

FIG. 9g: STEADY-STATE PRESSURE DISTRIBUTION

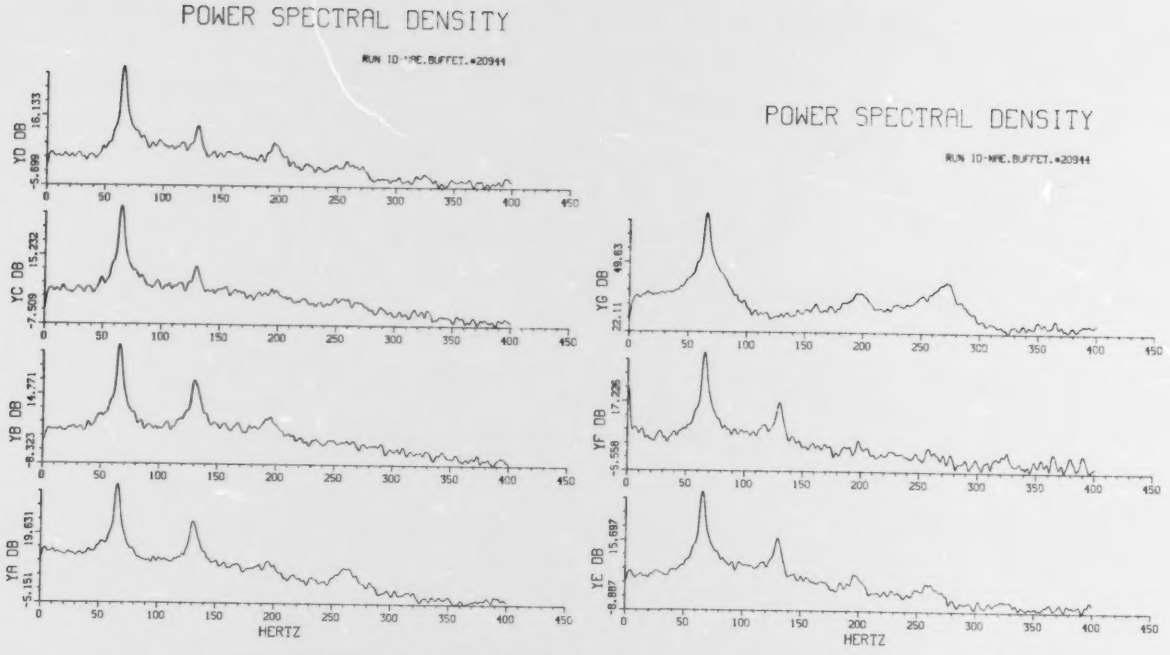

FIG. 10a: POWER SPECTRAL DENSITY FOR M_∞=0.753, C_L = 0.945, Q = 24.5 psi

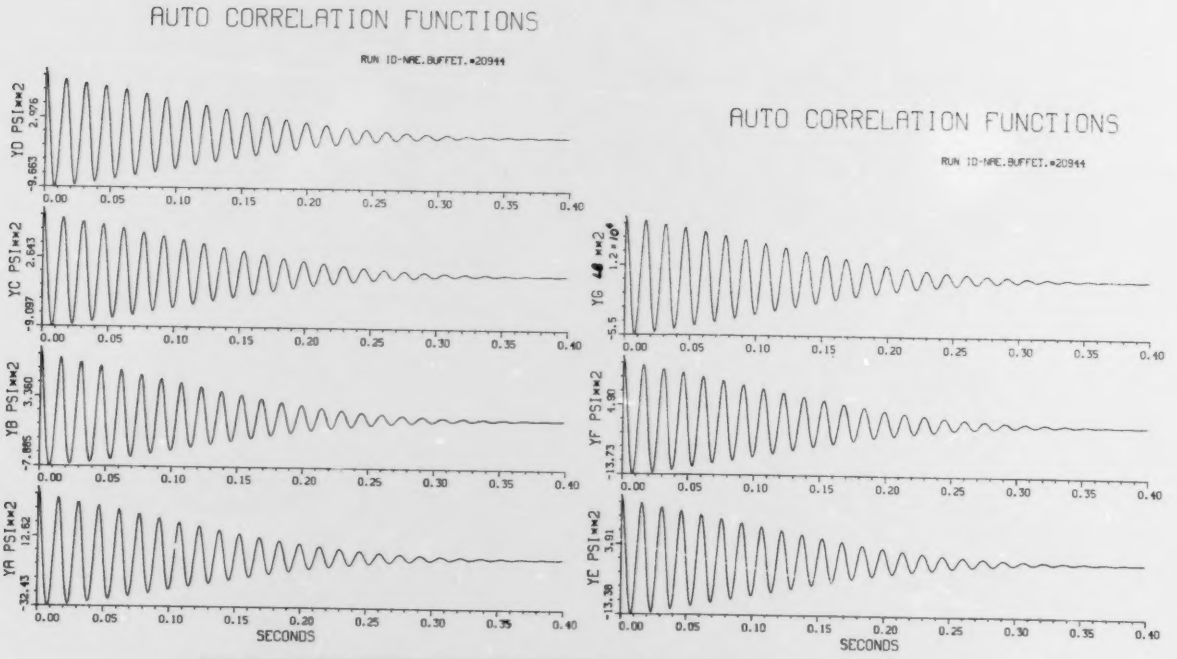

FIG. 10b: AUTO CORRELATION FUNCTIONS FOR M_∞=0.753, C_L = 0.945, Q = 24.5 psi

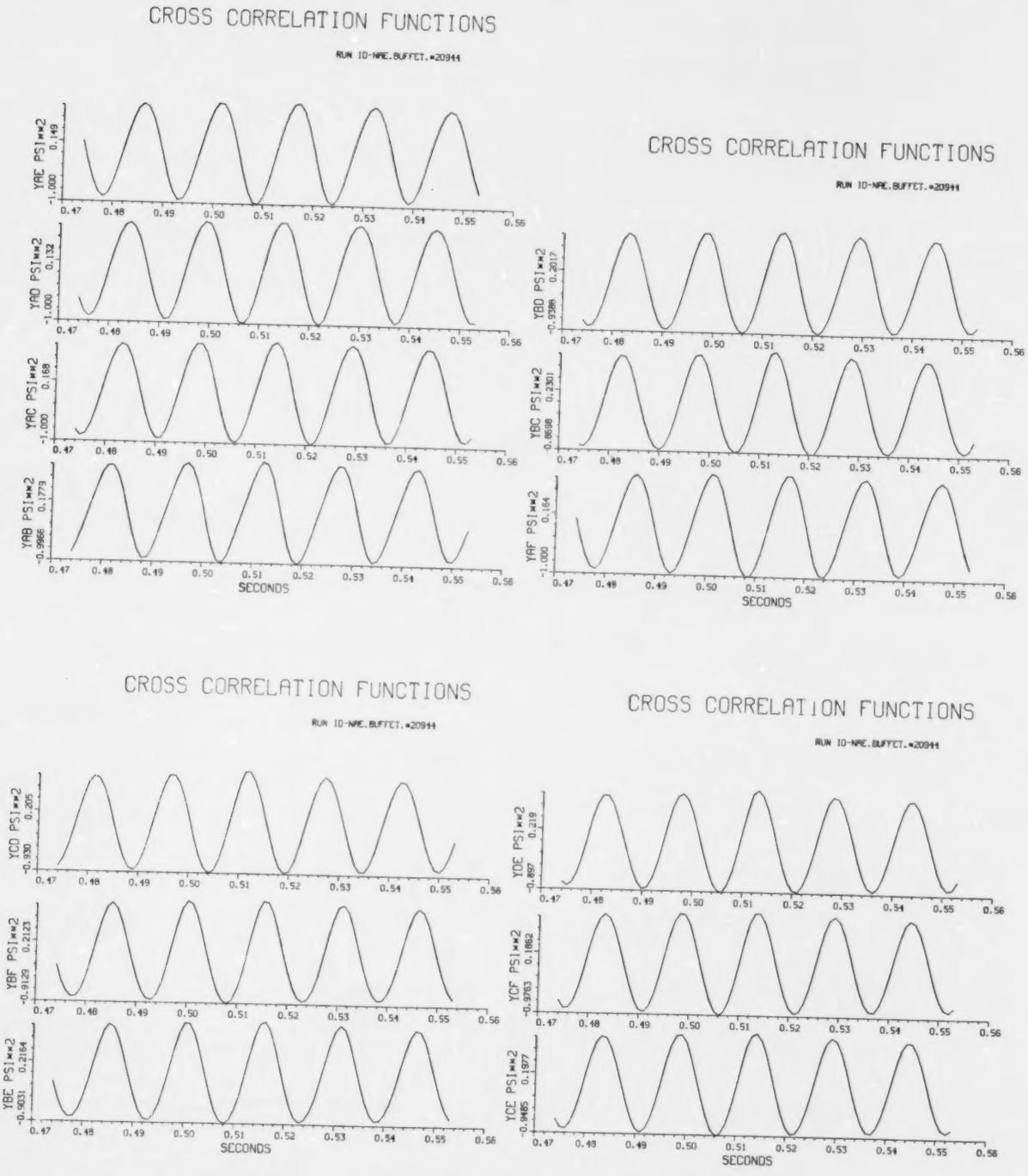

FIG. 10c: CROSS CORRELATION FUNCTIONS FOR M_∞=0.753, C_l = 0.945, Q = 24.5 psi

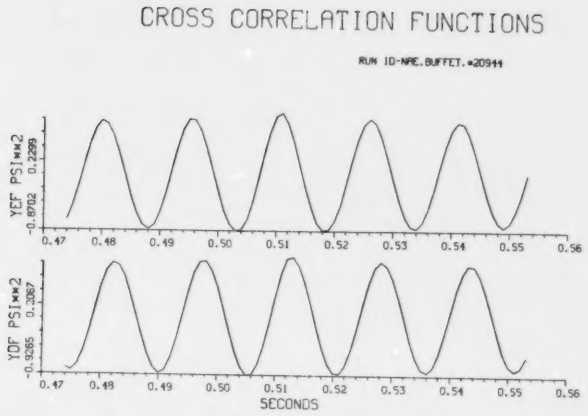

FIG. 10c: CROSS CORRELATION FUNCTIONS FOR M_∞=0.753, C_L = 0.945, Q = 24.5 psi (Cont'd)

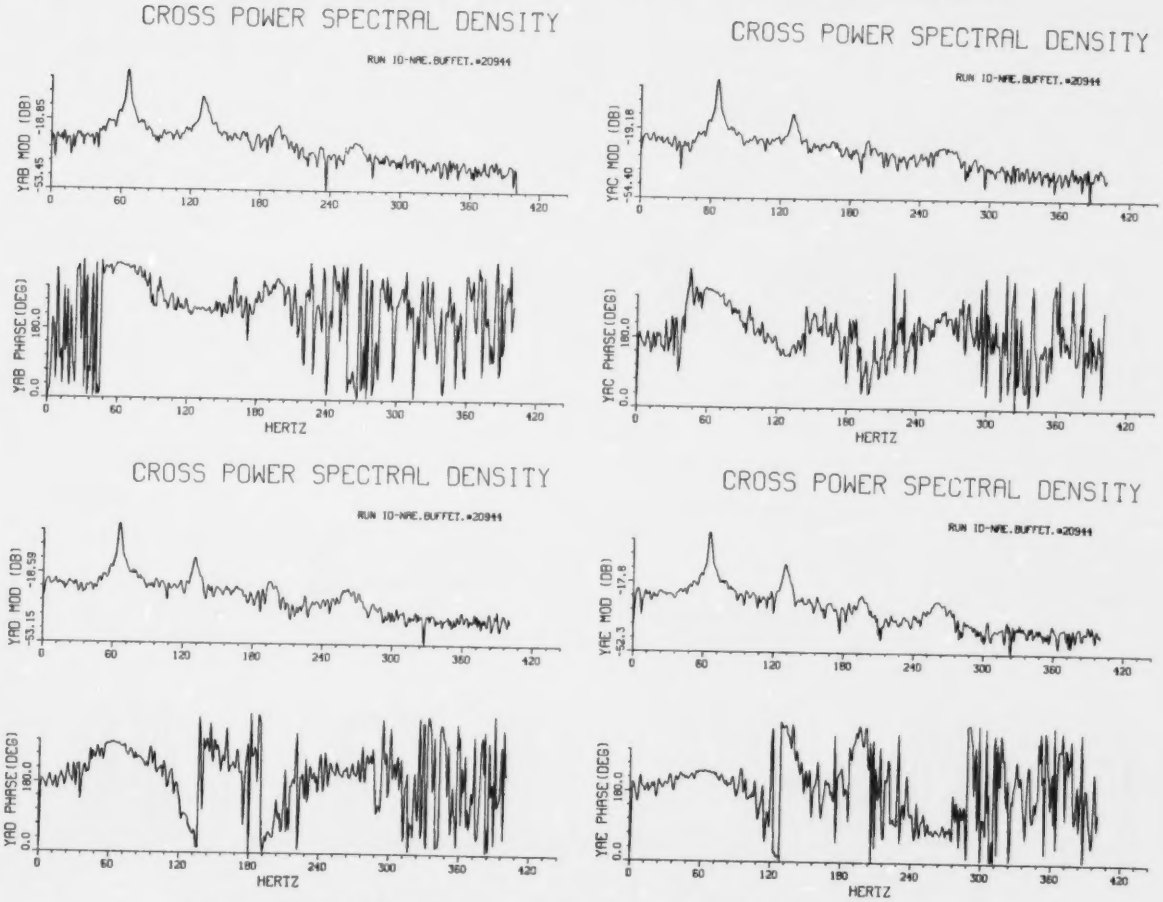

FIG. 10d: CROSS POWER SPECTRAL DENSITY FOR M_∞=0.753, C_L = 0.945, Q = 24.5 psi

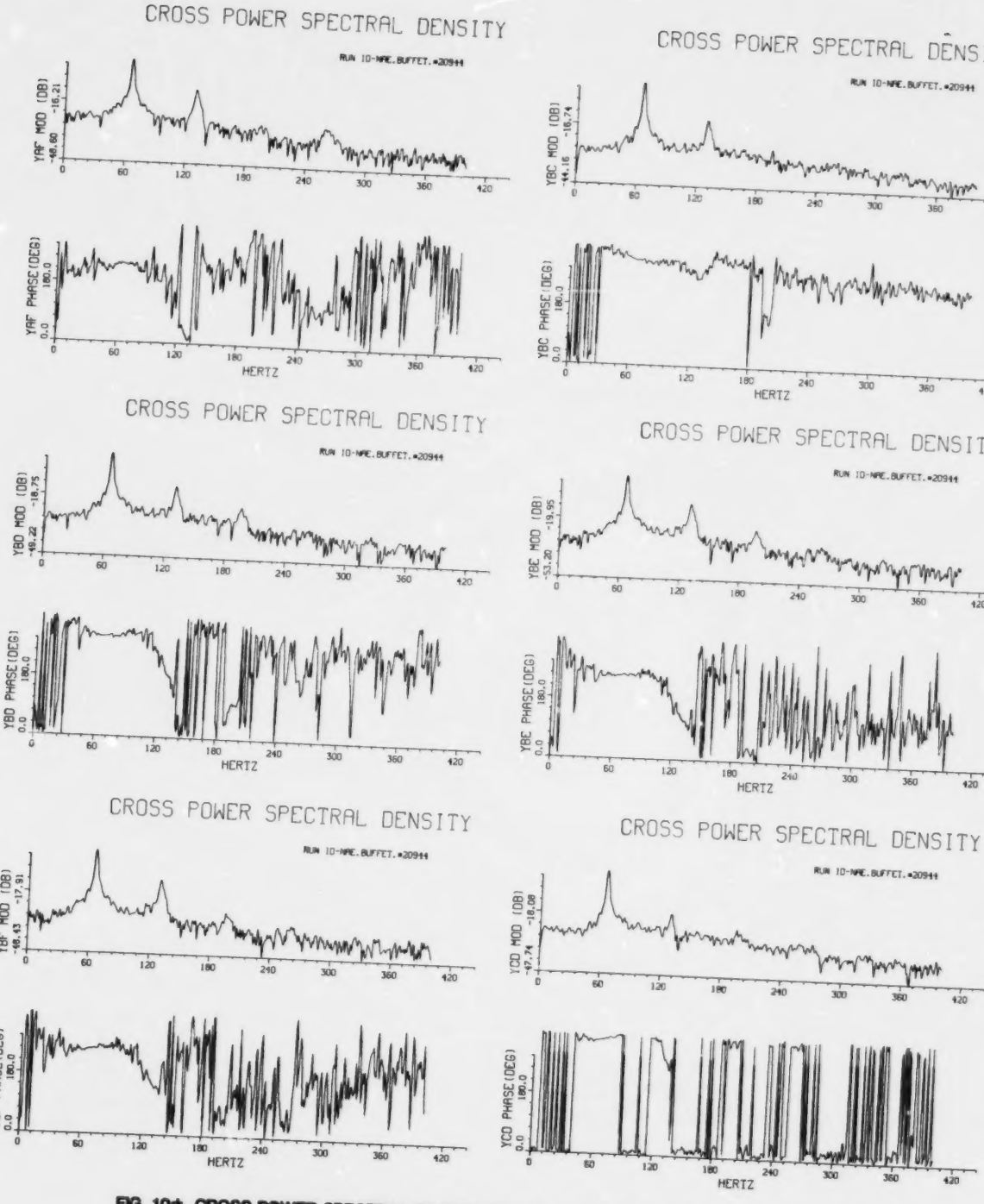

FIG. 10d: CROSS POWER SPECTRAL DENSITY FOR M_∞=0.753, C_L = 0.945, Q = 24.5 psi (Cont'd)

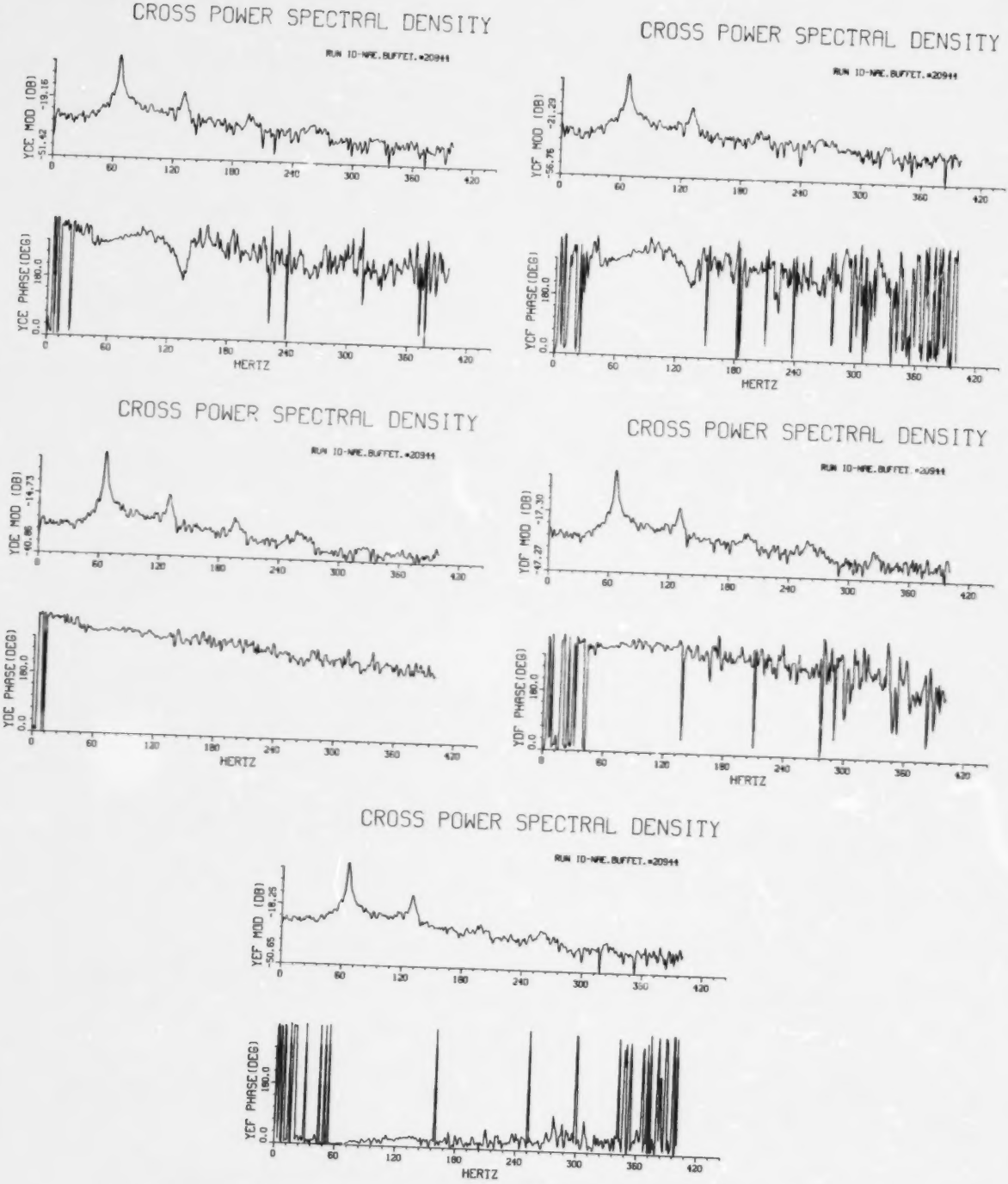

FIG. 10d CROSS POWER SPECTRAL DENSITY FOR M_∞=0.753, C_l = 0.245, Q = 24.5 psi (Cont'd)

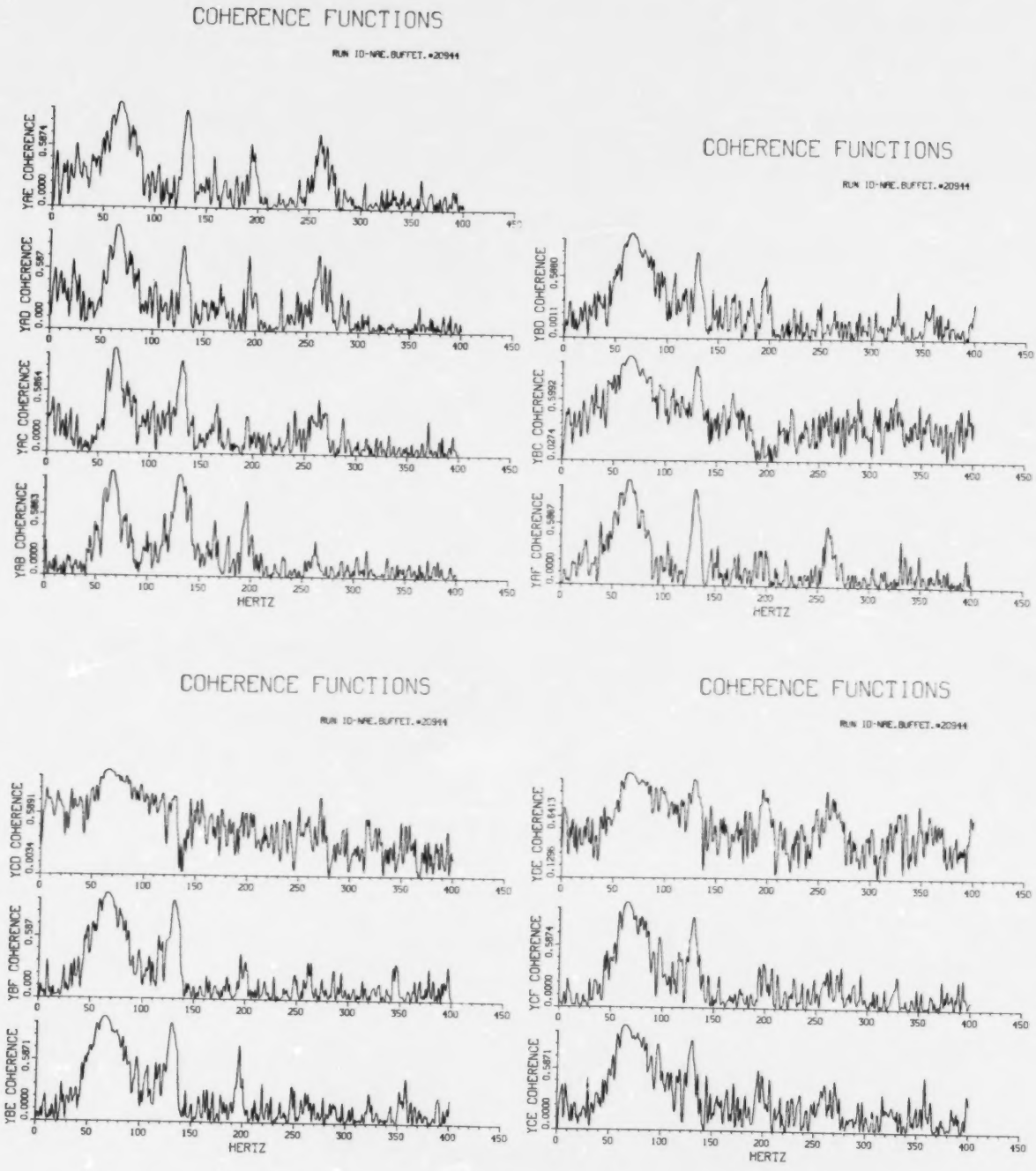

FIG. 10a: COHERENCE FUNCTIONS FOR M_∞=0.753, C_l = 0.945, Q = 24.5 psi

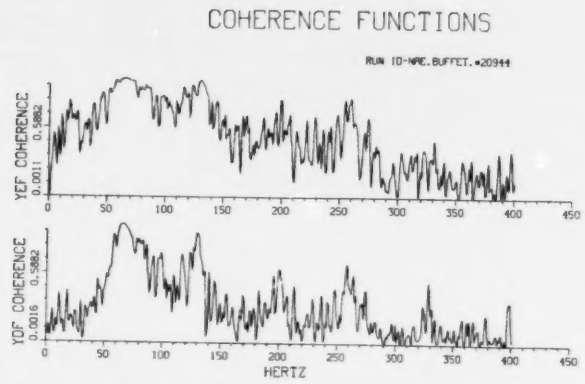

FIG. 10e: COHERENCE FUNCTIONS FOR M_∞=0.753, C_l = 0.945, Q = 24.5 psi (Cont'd)

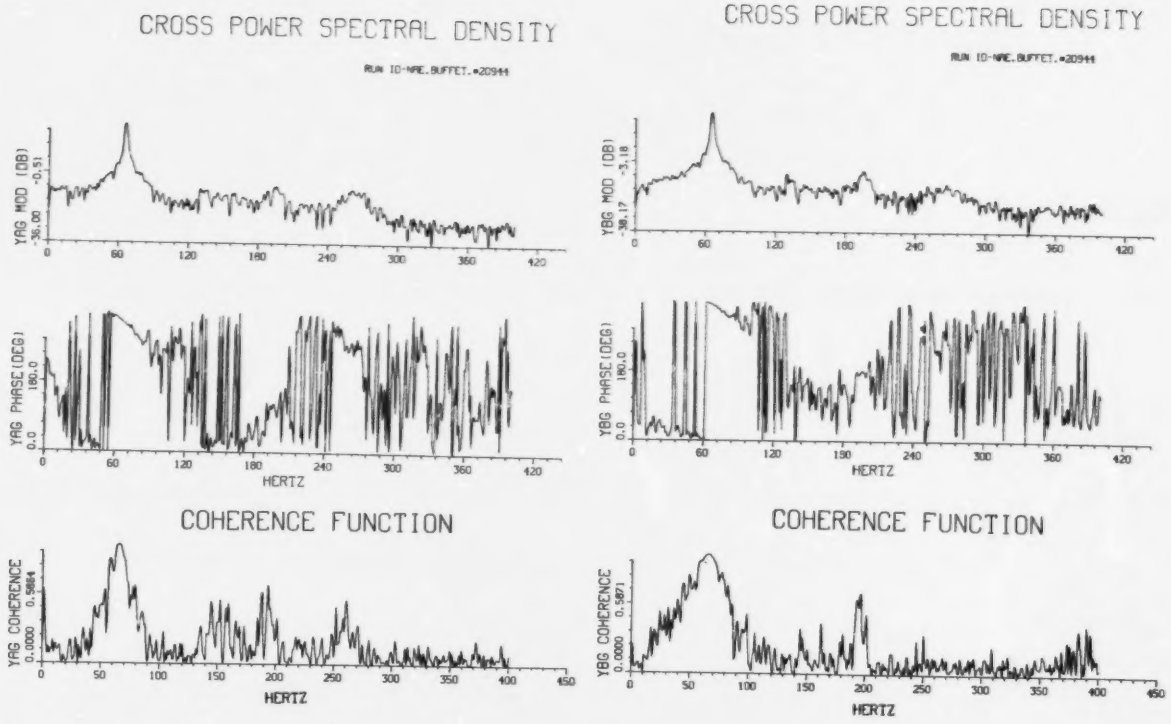

FIG. 10f: CROSS POWER SPECTRAL DENSITY AND COHERENCE FUNCTION BETWEEN PRESSURE AND NORMAL FORCE N_2 FOR M_∞=0.753, C_l = 0.945, Q = 24.5 psi

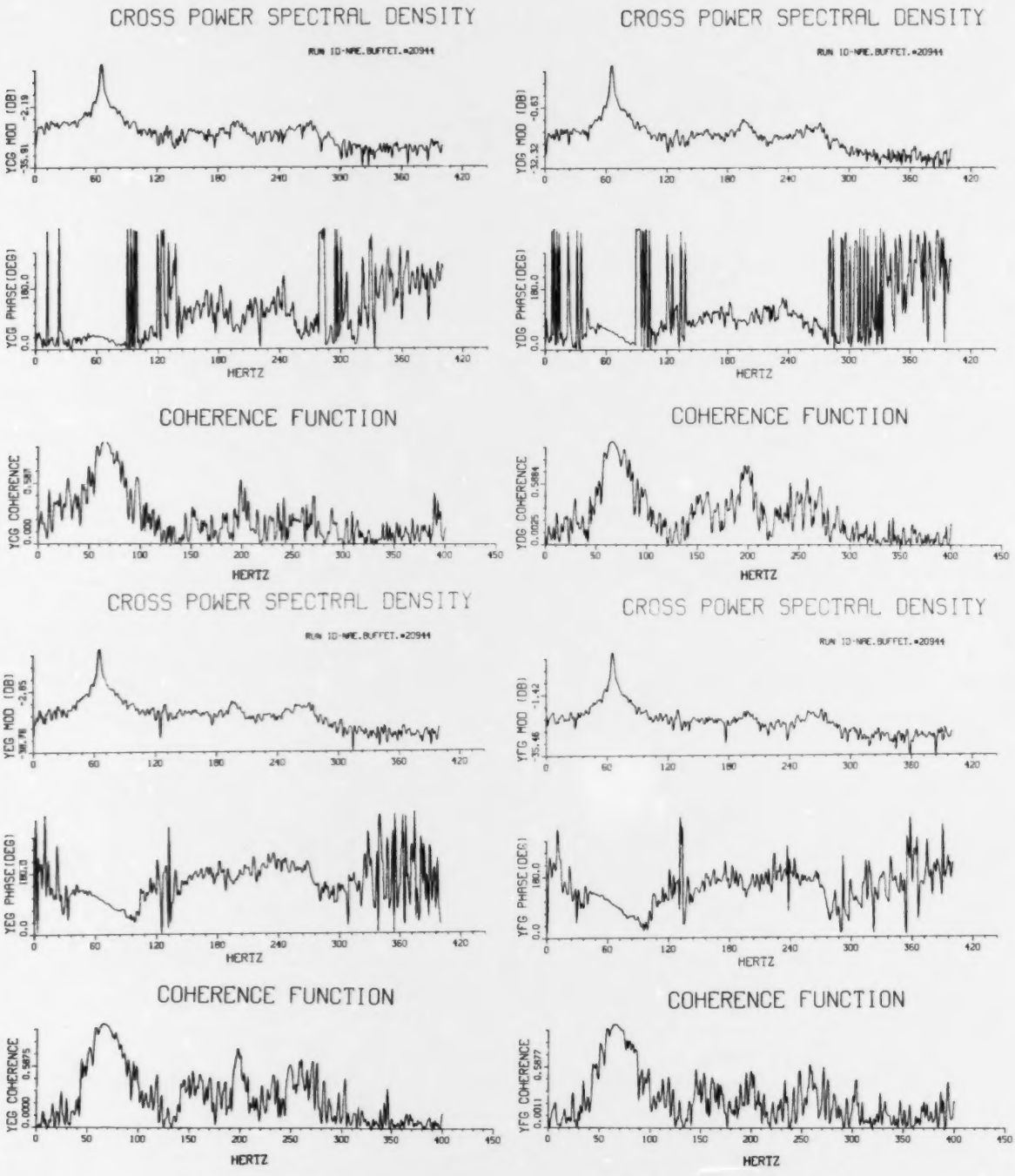

FIG. 10f: CROSS POWER SPECTRAL DENSITY AND COHERENCE FUNCTION BETWEEN PRESSURE AND NORMAL FORCE N_2 FOR M_∞=0.753, C_L = 0.945, Q = 24.5 psi (Cont'd)

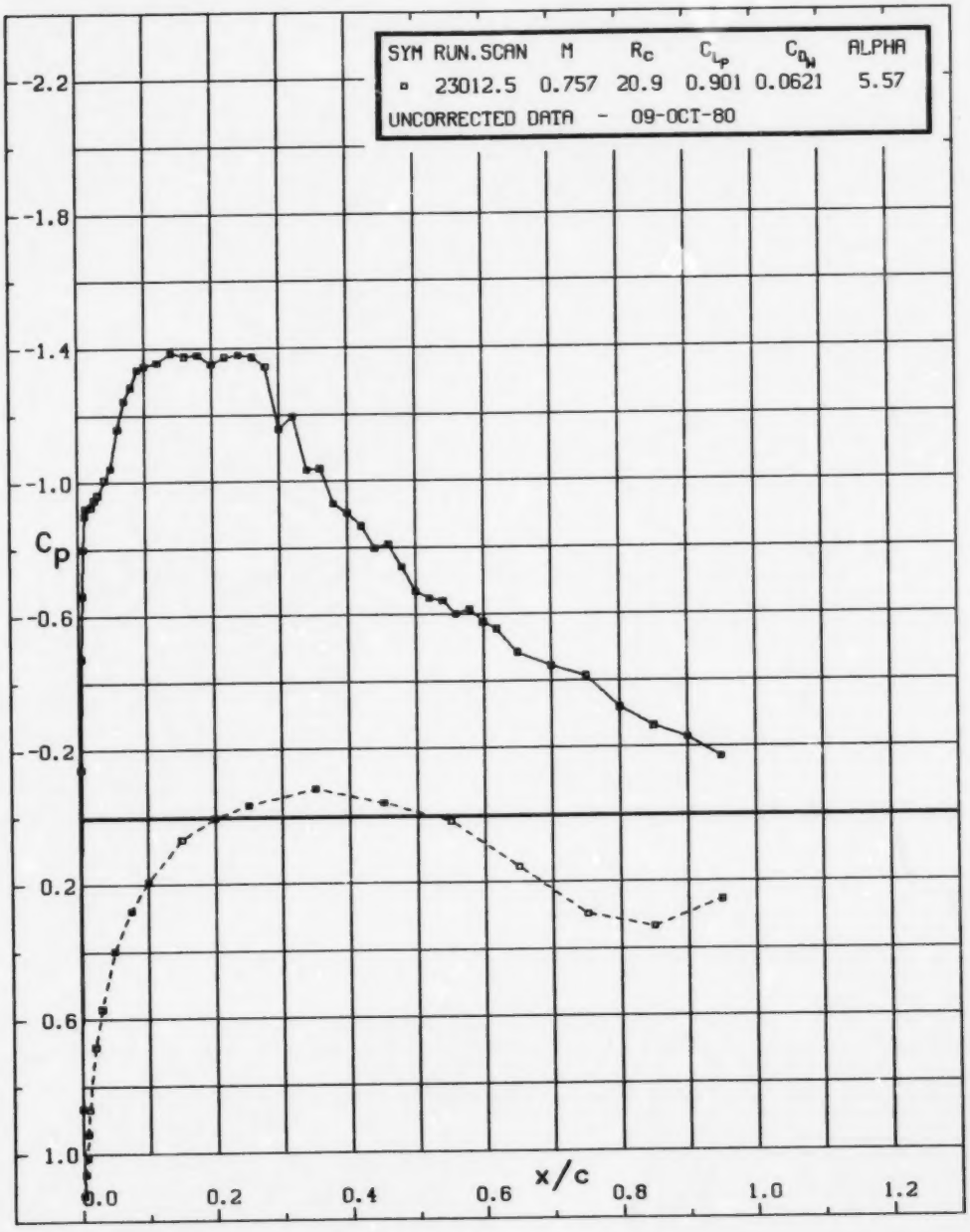

FIG. 10g: STEADY-STATE PRESSURE DISTRIBUTION

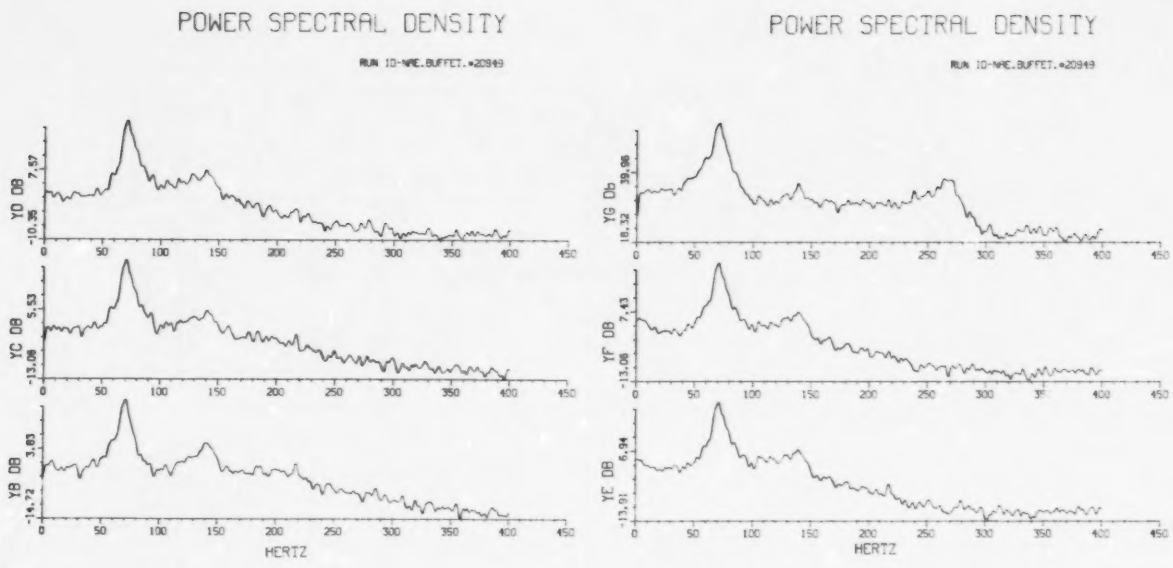

FIG. 11a: POWER SPECTRAL DENSITY FOR M_∞=0.775, C_L = 0.868, Q = 18.3 psi

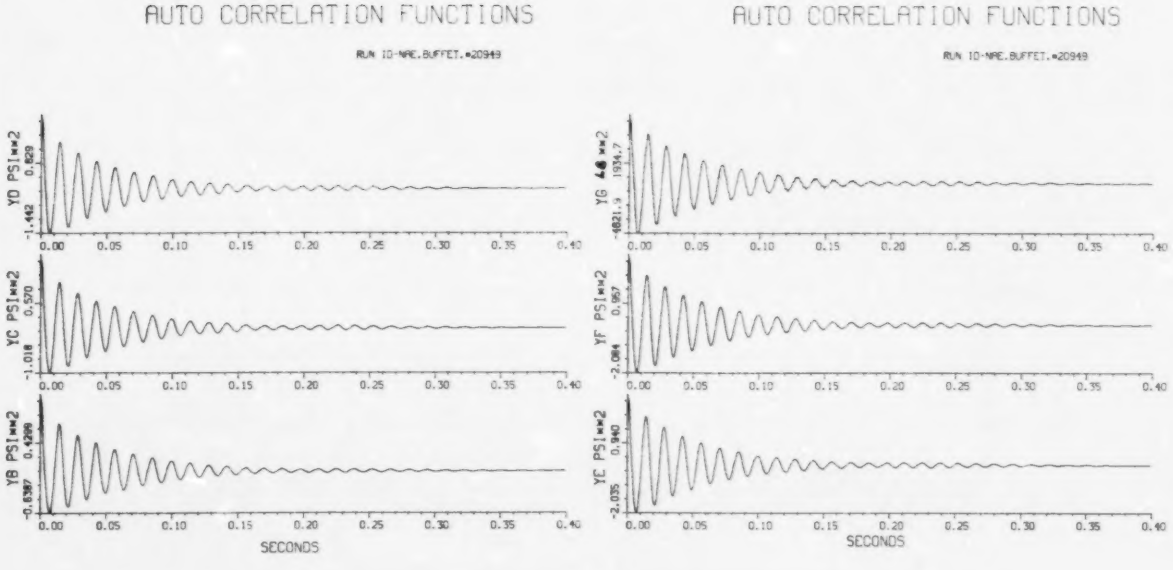

FIG. 11b: AUTO CORRELATION FUNCTIONS FOR M_∞=0.775, C_L = 0.868, Q = 18.3 psi

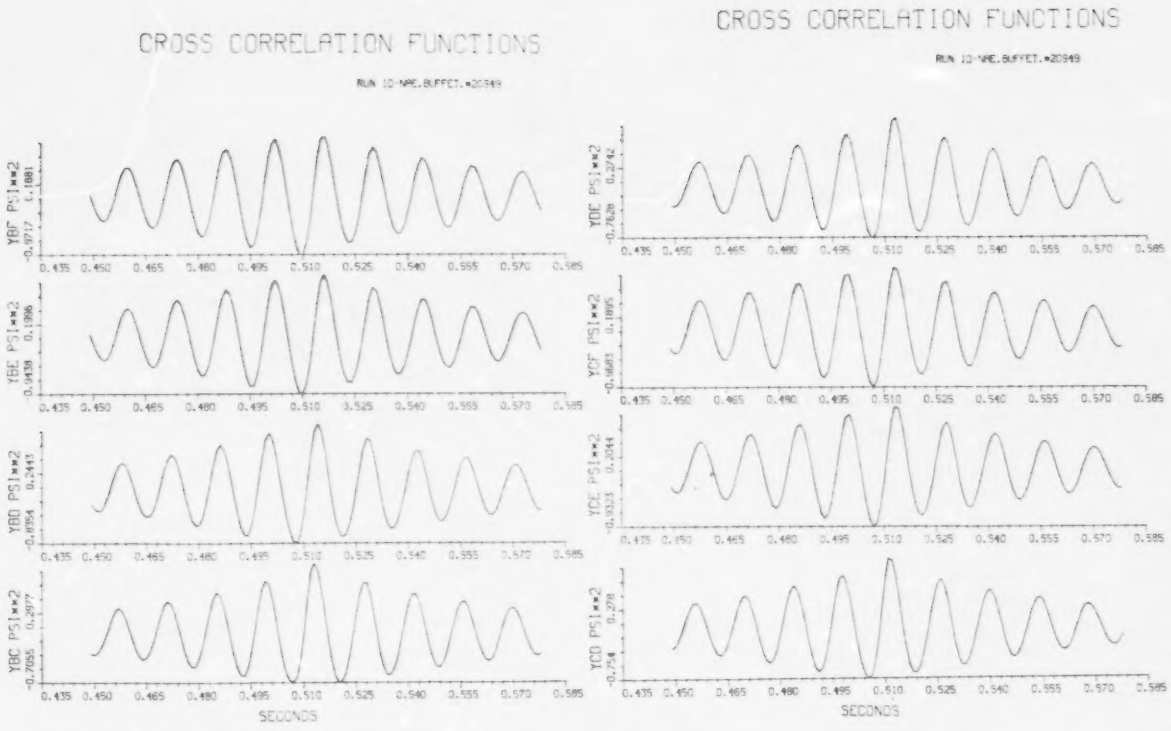

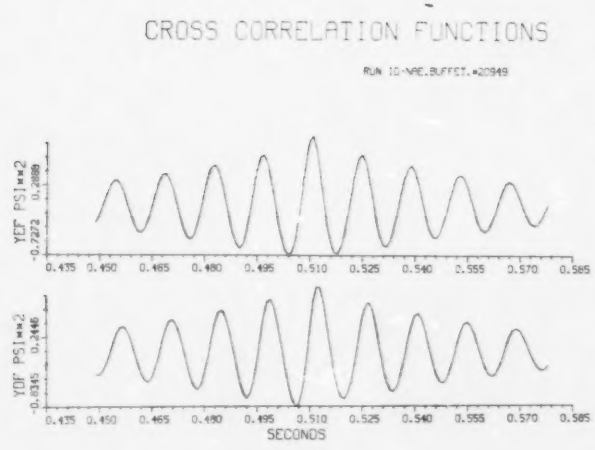

FIG. 11c: CROSS CORRELATION FUNCTIONS FOR M_∞=0.775, C_L= 0.868, Q = 18.3 psi

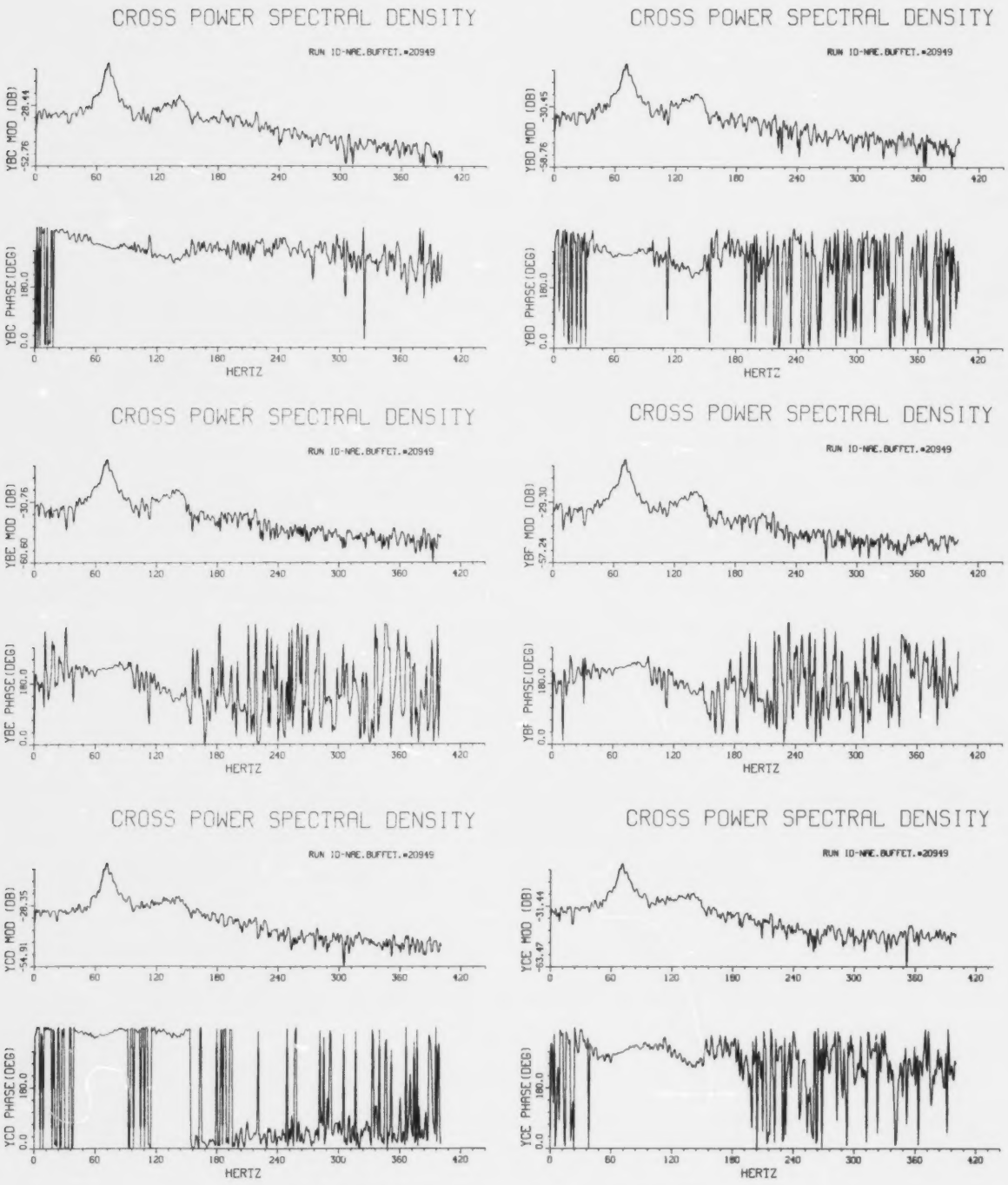

FIG. 11d: CROSS POWER SPECTRAL DENSITY FOR $M_\infty = 0.775$, $C_L = 0.888$, Q = 18.3 psi

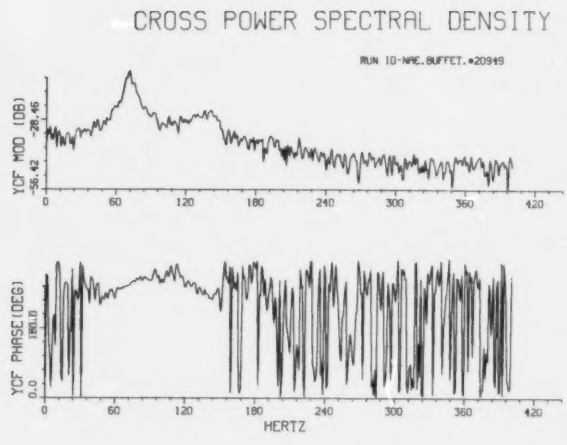

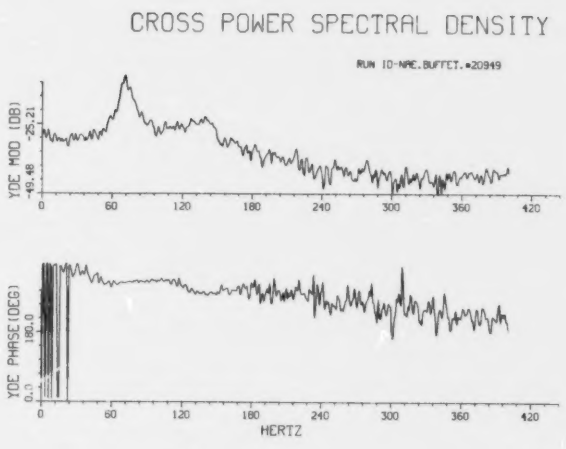

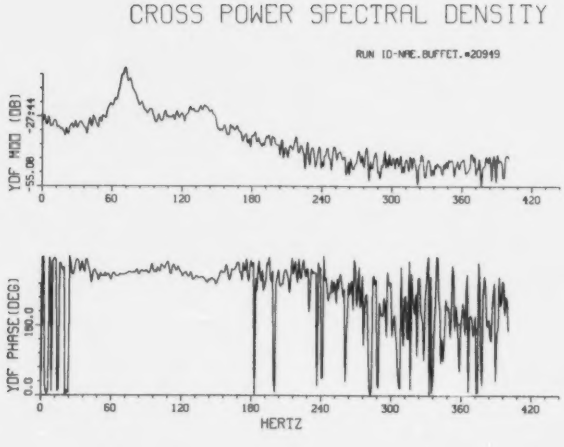

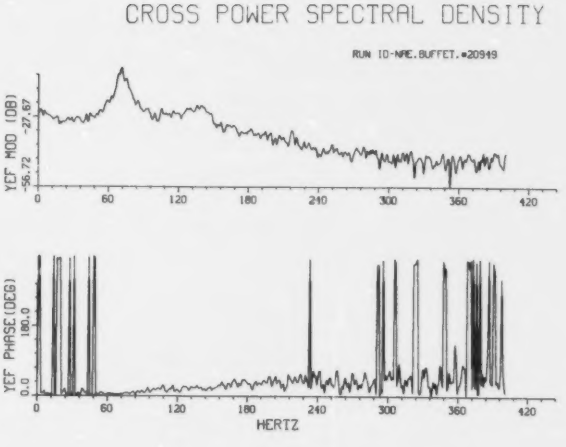

FIG. 11d: CROSS POWER SPECTRAL DENSITY FOR M_∞=0.775, C_L = 0.868, Q = 18.3 psi (Cont'd)

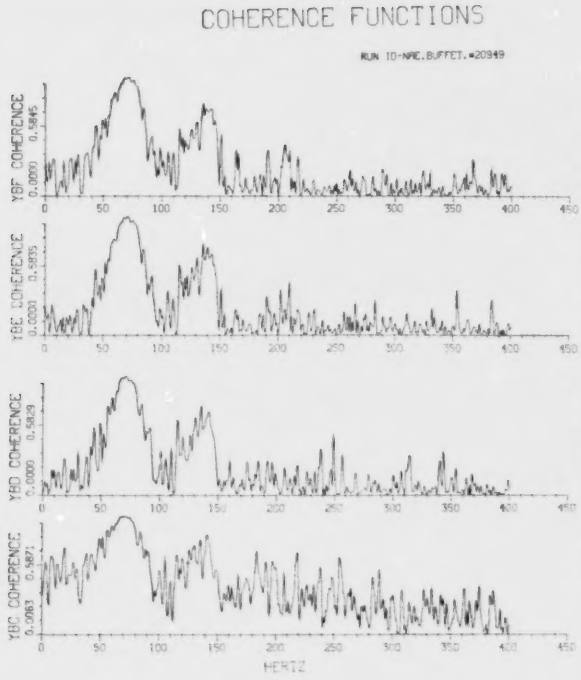

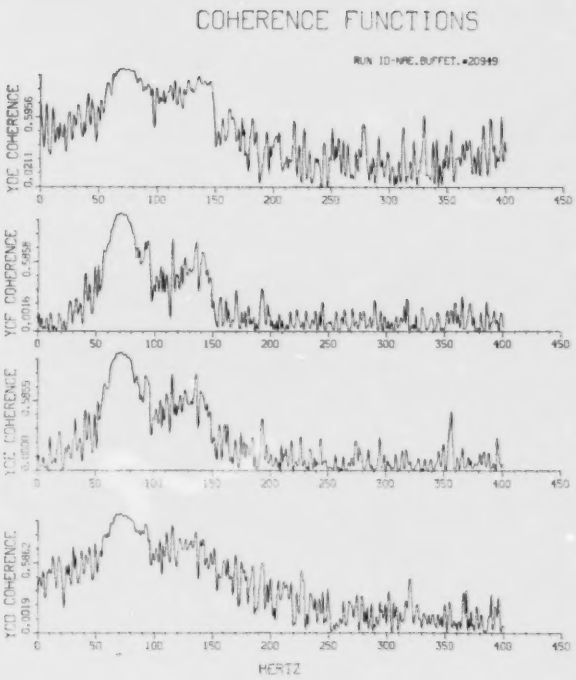

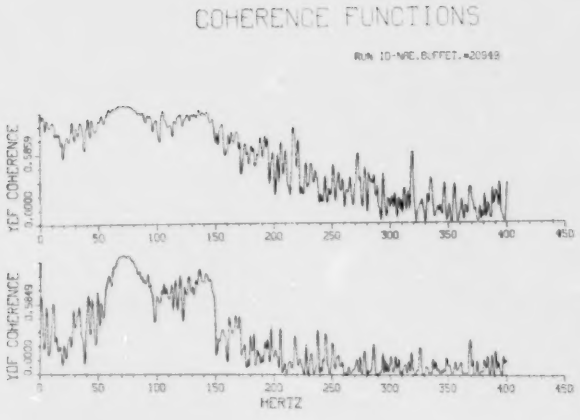

FIG. 11e: COHERENCE FUNCTIONS FOR M_∞=0.775, C_L = 0.868, Q = 18.3 psi

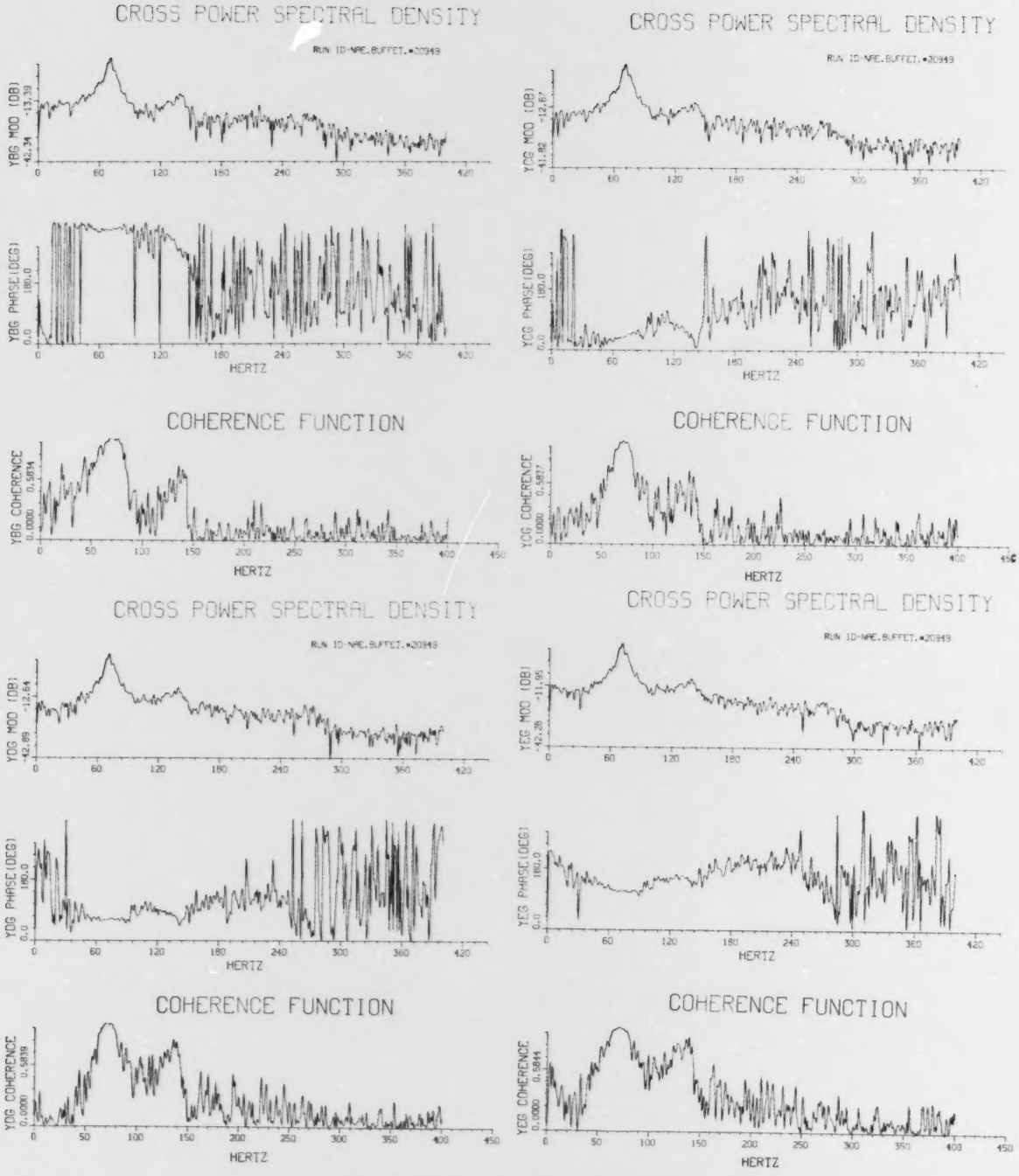

FIG. 11f: CROSS POWER SPECTRAL DENSITY AND COHERENCE FUNCTION BETWEEN PRESSURE AND NORMAL FORCE N FOR $M_\infty = 0.775$, $C_L = 0.868$, Q = 18.3 psi

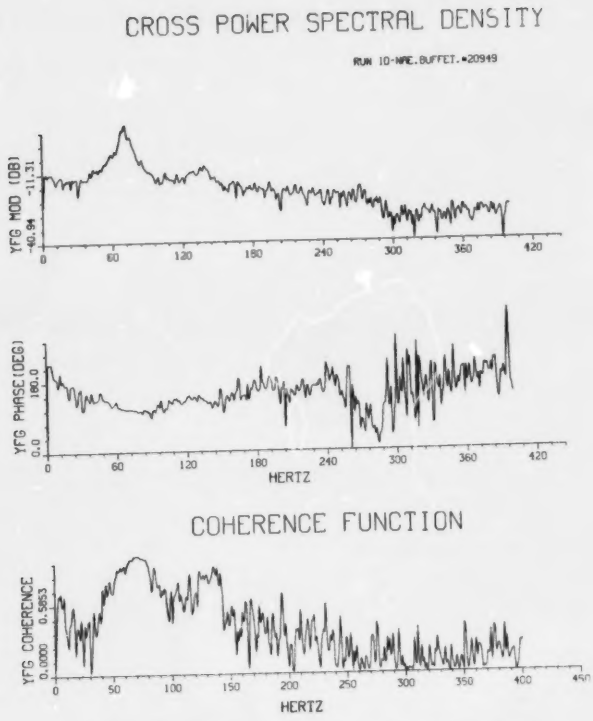

FIG. 11f: CROSS POWER SPECTRAL DENSITY AND COHERENCE FUNCTION BETWEEN PRESSURE AND NORMAL FORCE N_2 FOR M_∞=0.775, C_L = 0.868, Q = 18.3 psi (Cont'd)

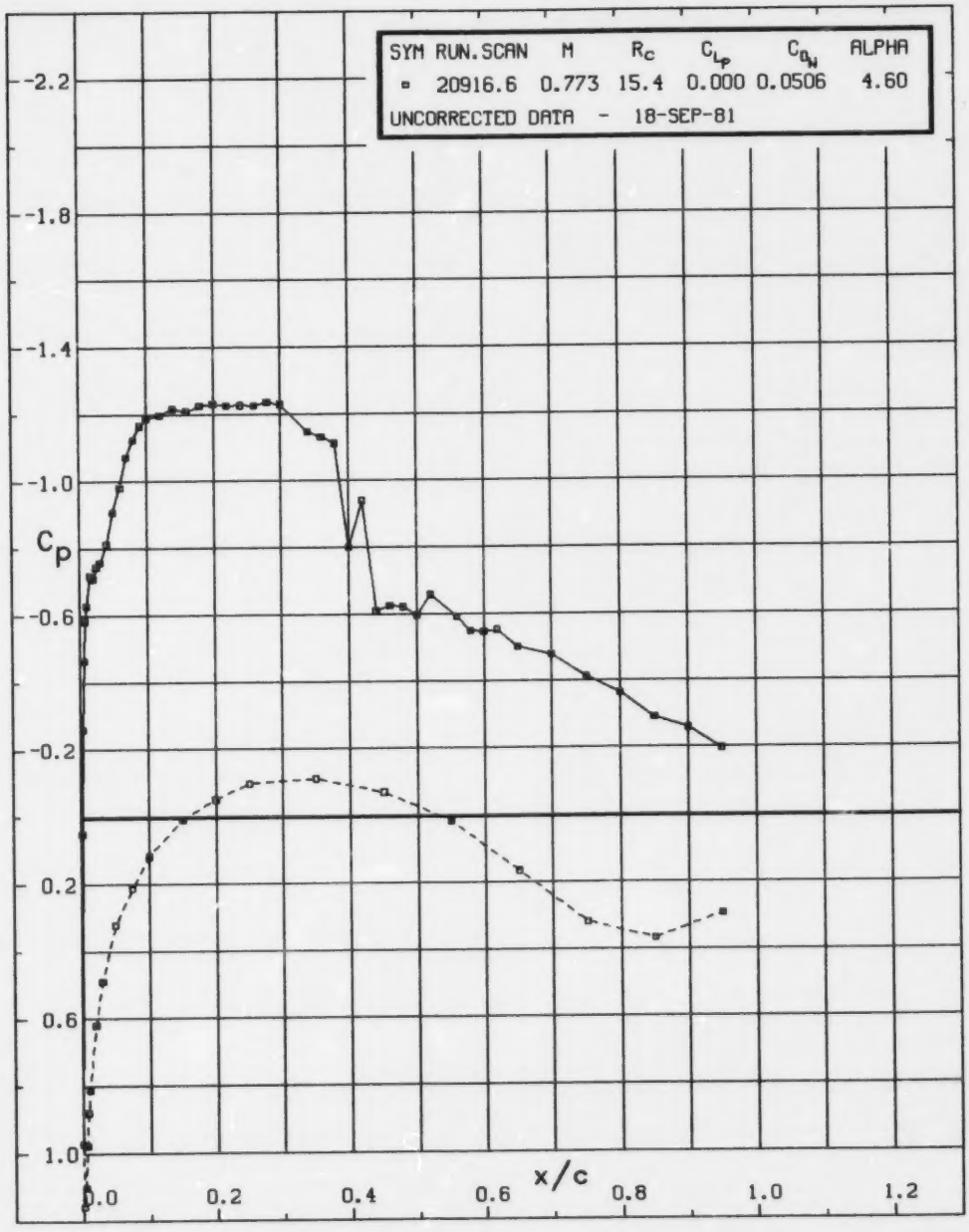

FIG. 11g: STEADY-STATE PRESSURE DISTRIBUTION

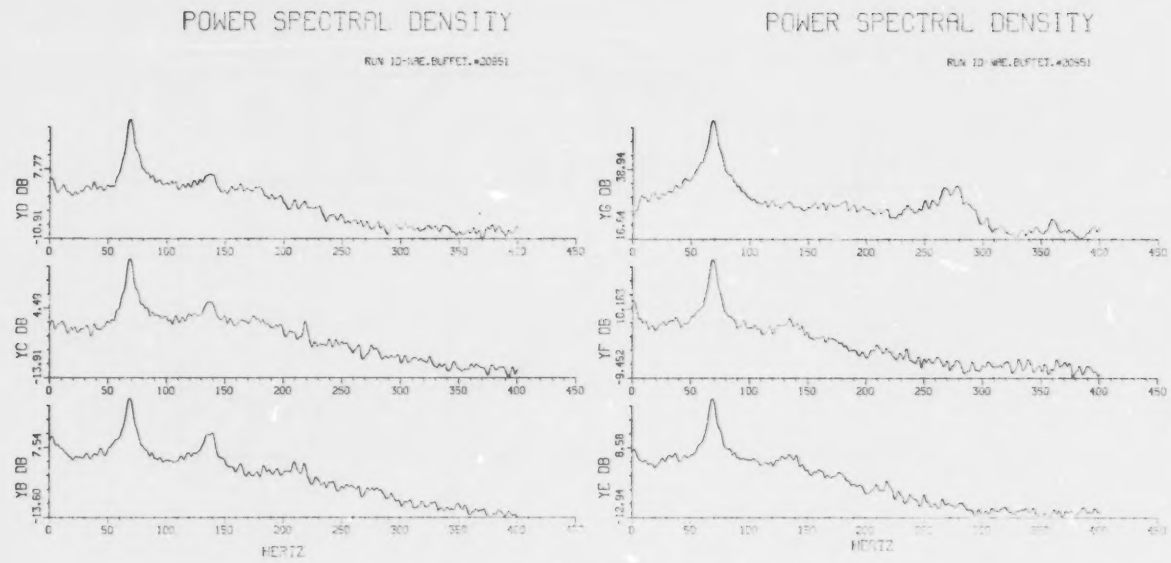

FIG. 12a: POWER SPECTRAL DENSITY FOR M_∞=0.784, C_L = 0.806, Q = 25.1 psi

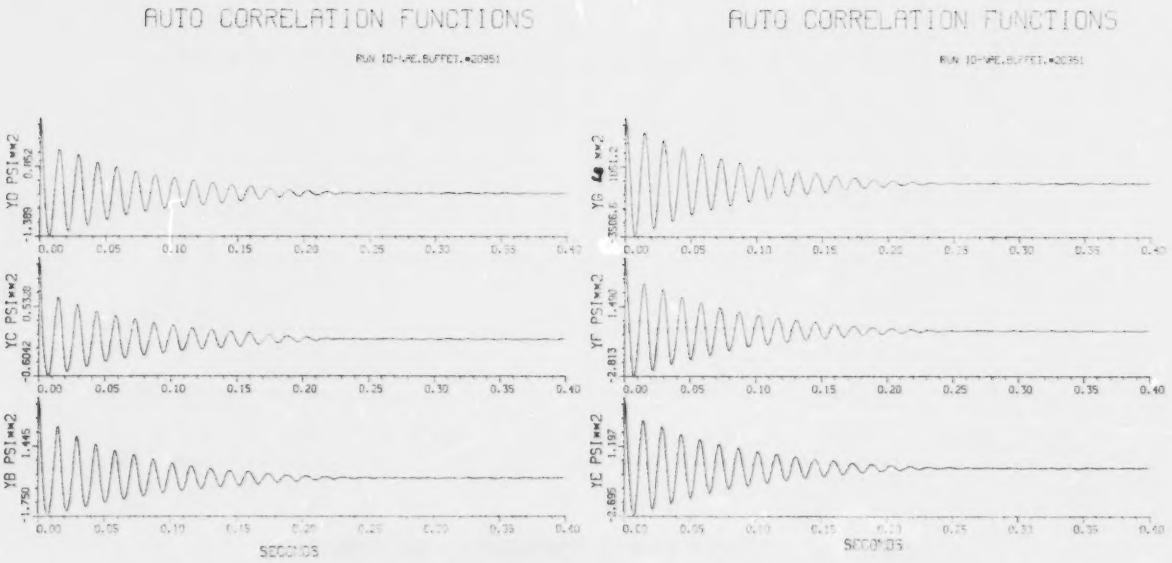

FIG. 12b: AUTO CORRELATION FUNCTIONS FOR M_∞=0.784, C_L = 0.806, Q = 25.1 psi

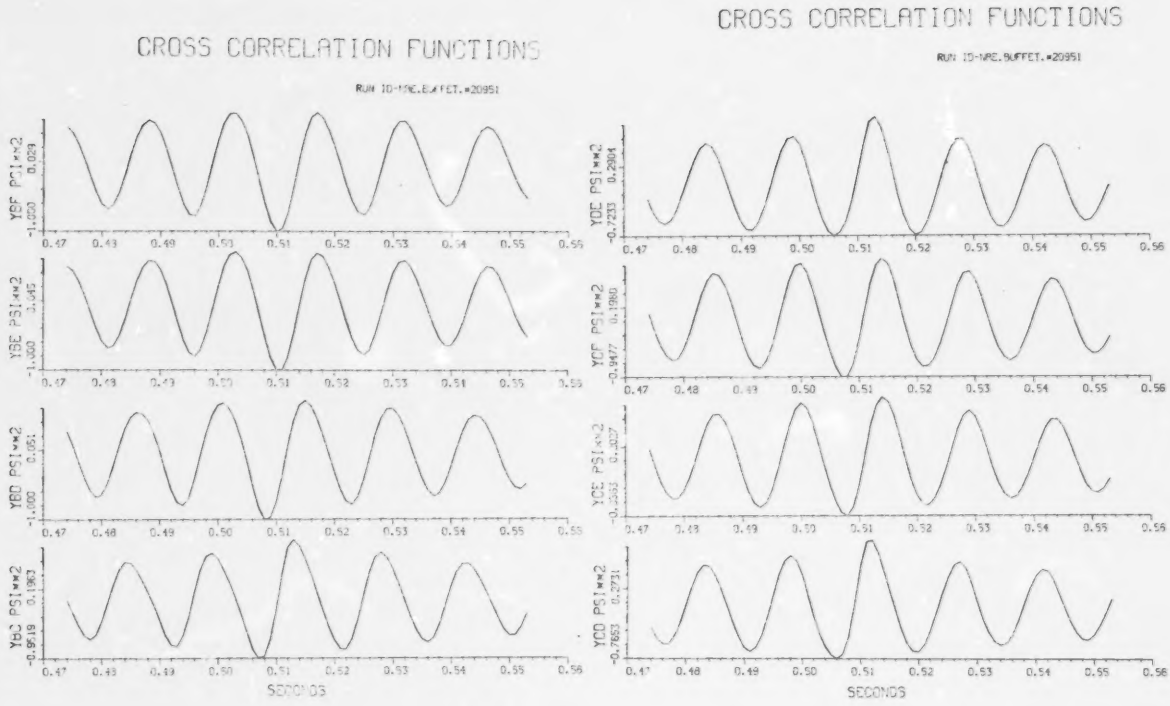

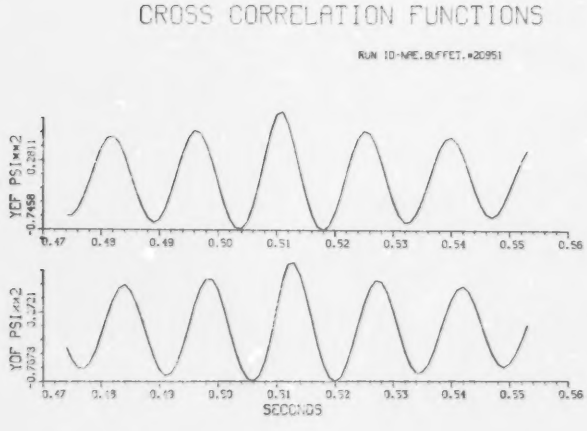

FIG. 12c: CROSS CORRELATION FUNCTIONS FOR M_∞ = 0.784, C_L = 0.806, Q = 25.1 psi

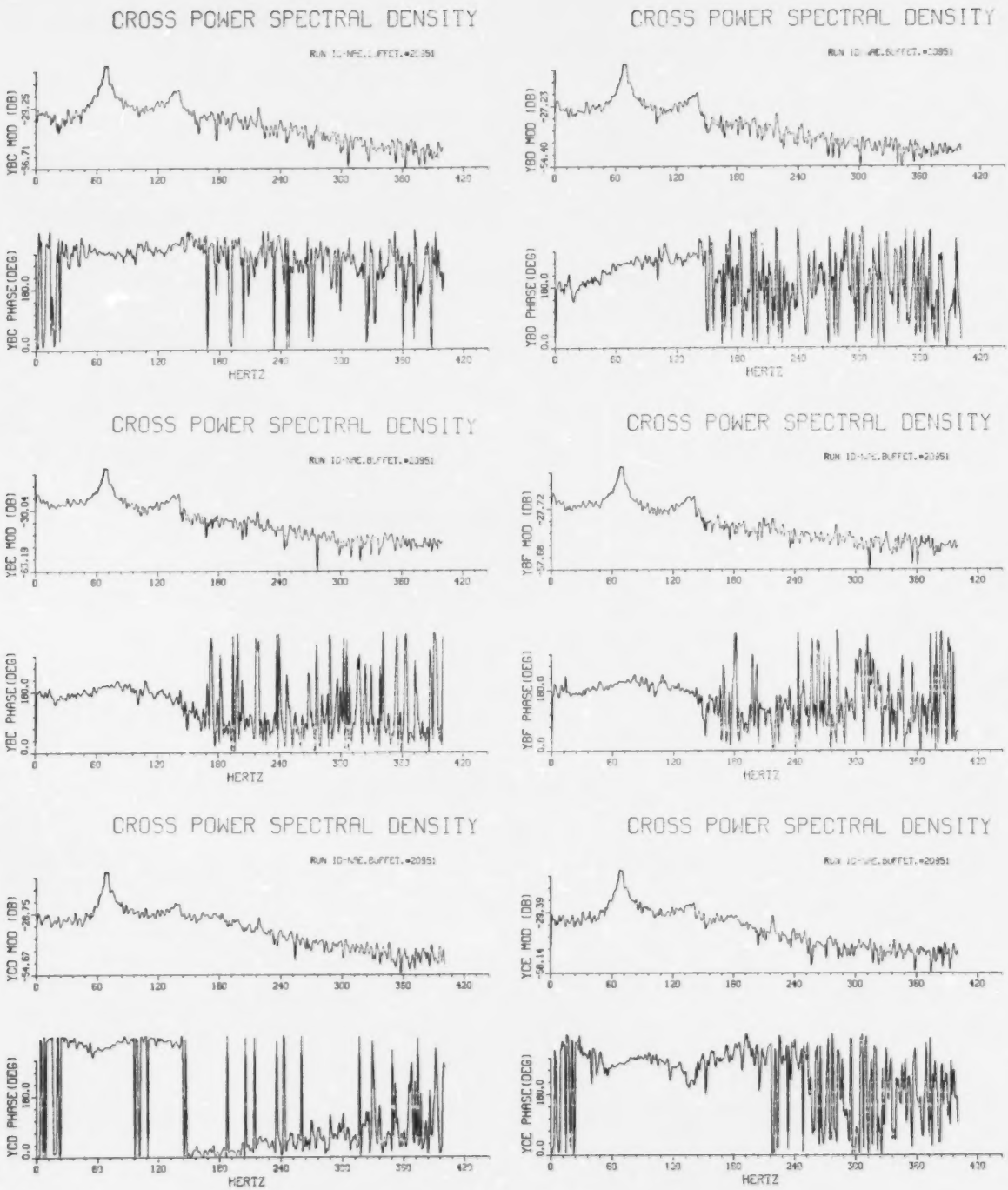

FIG. 12d: CROSS POWER SPECTRAL DENSITY FOR $M_\infty = 0.784$, $C_L = 0.806$, Q = 25.1 psi

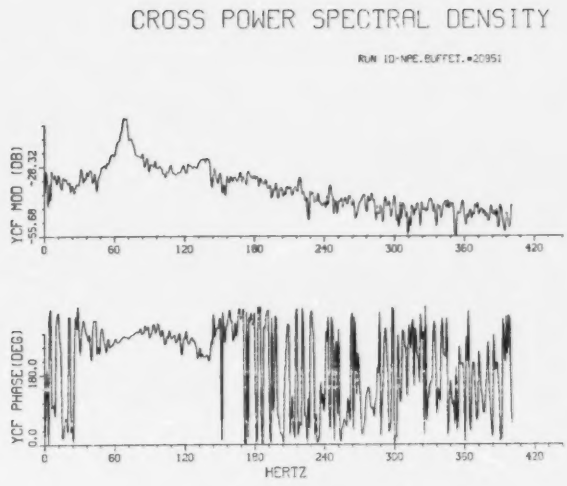

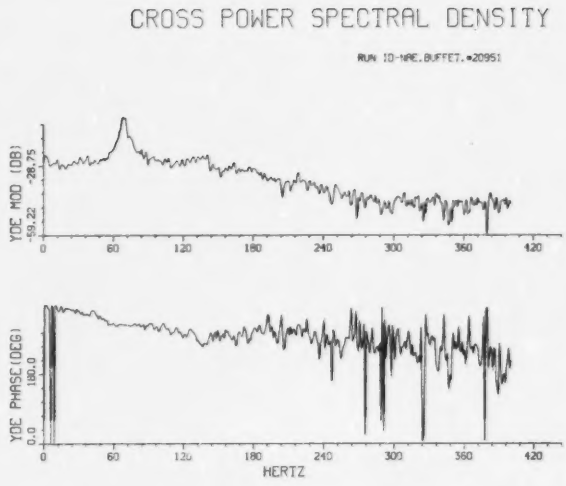

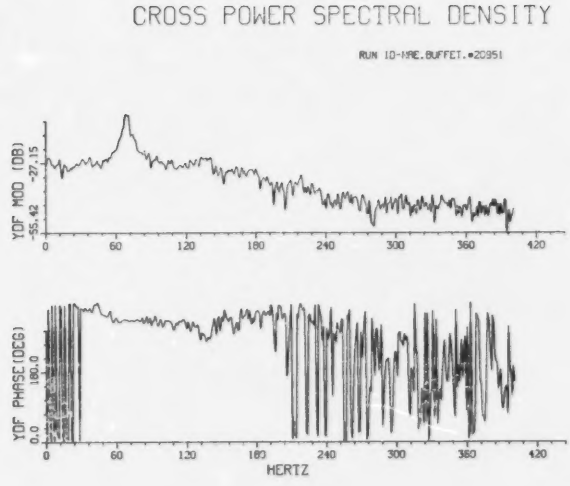

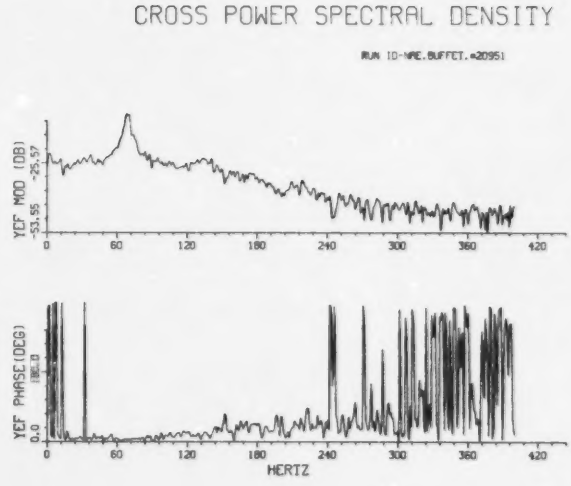

FIG. 12d: CROSS POWER SPECTRAL DENSITY FOR M_{∞} = 0.784, C_L = 0.806, Q = 25.1 psi (Cont'd)

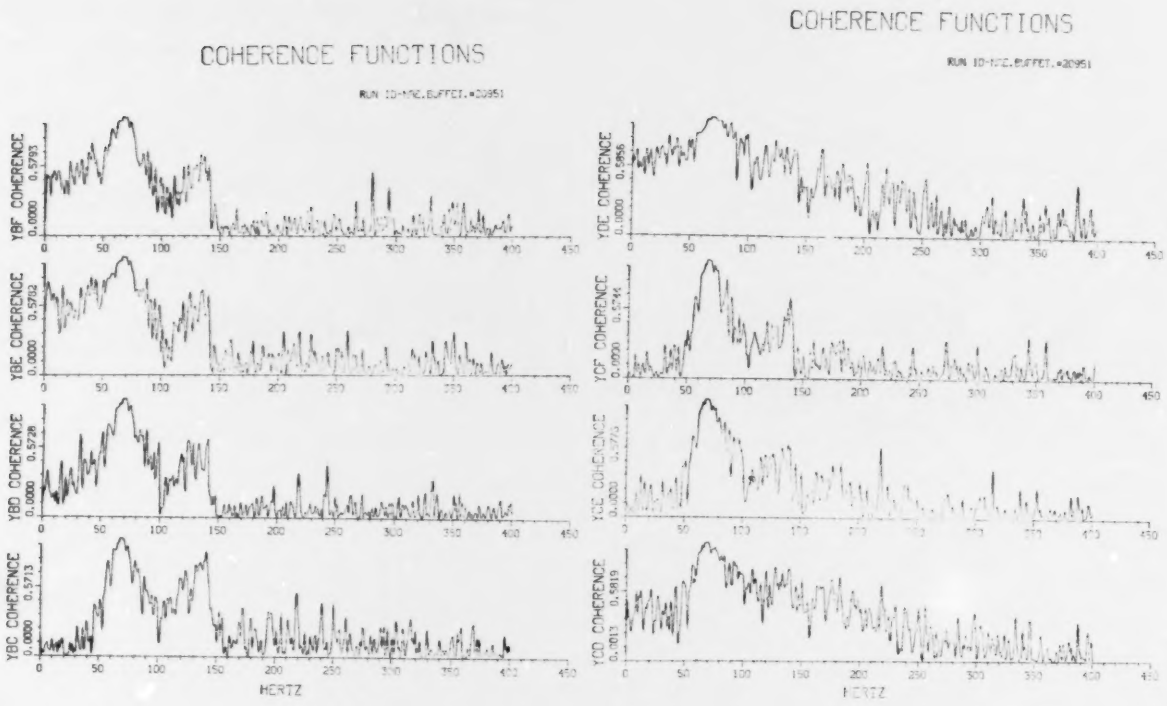

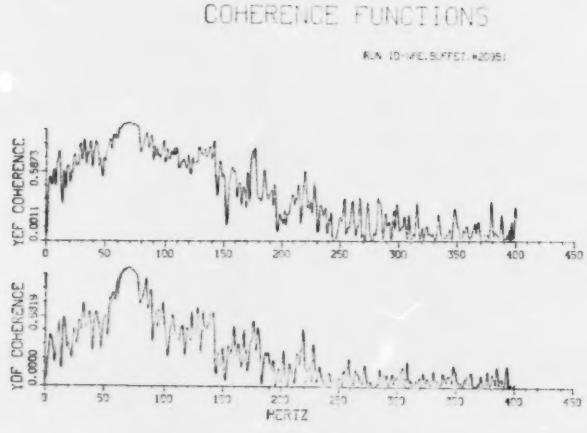

FIG. 12e: COHERENCE FUNCTIONS FOR M_∞=0.784, C_L = 0.806, Q = 25.1 psi

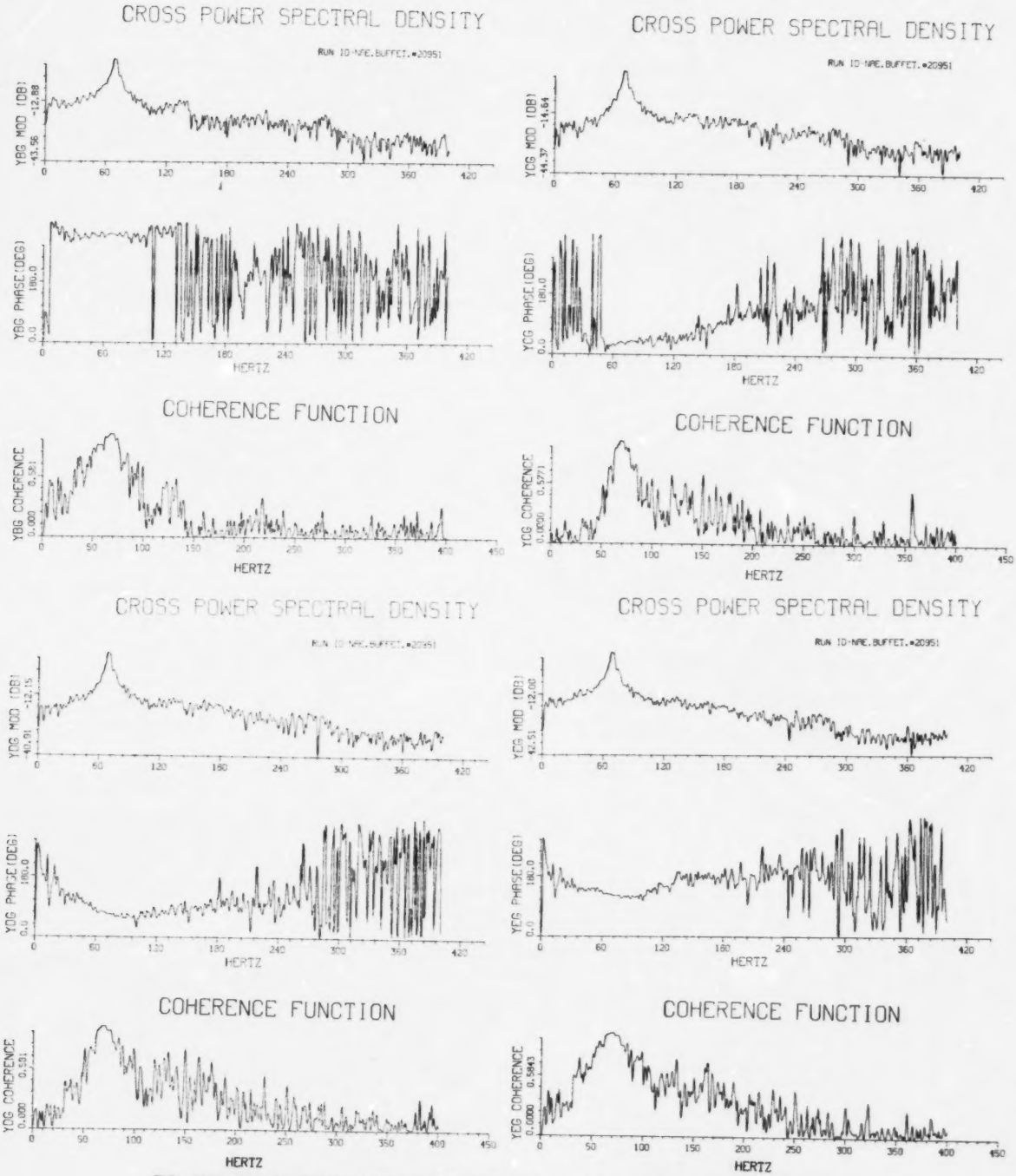

FIG. 12f: CROSS POWER SPECTRAL DENSITY AND COHERENCE FUNCTION BETWEEN PRESSURE AND NORMAL FORCE N_2 FOR M_∞=0.784, C_l = 0.806, Q = 25.1 psi

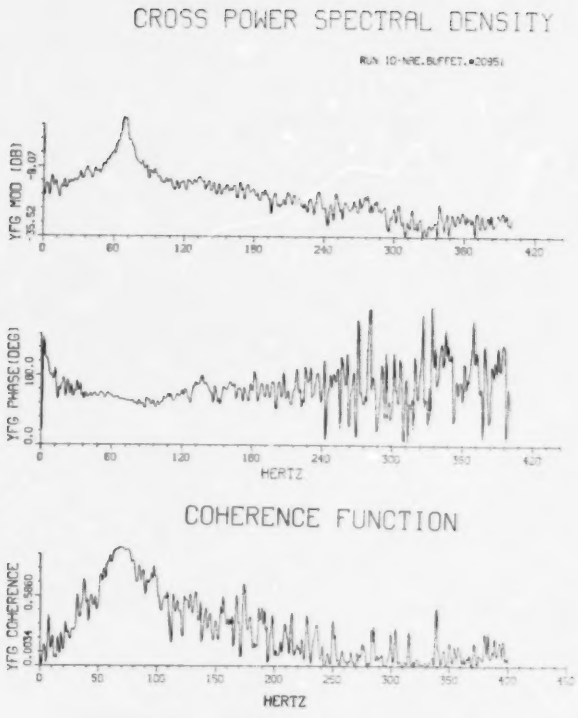

FIG. 12f: CROSS POWER SPECTRAL DENSITY AND COHERENCE FUNCTION BETWEEN PRESSURE AND NORMAL FORCE N_2 FOR M_∞=0.784, C_L = 0.806, Q = 25.1 psi (Cont'd)

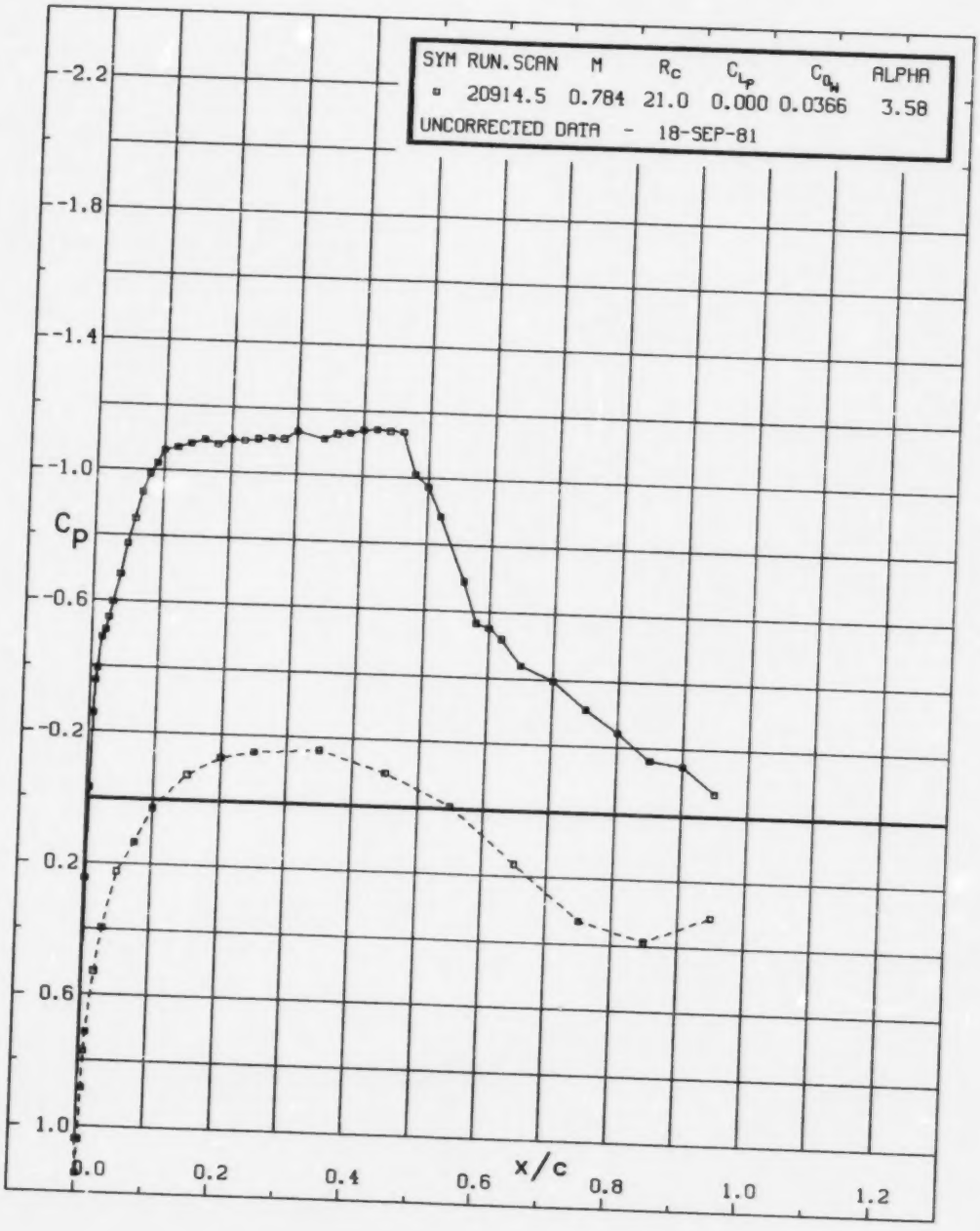

FIG. 12g: STEADY-STATE PRESSURE DISTRIBUTION

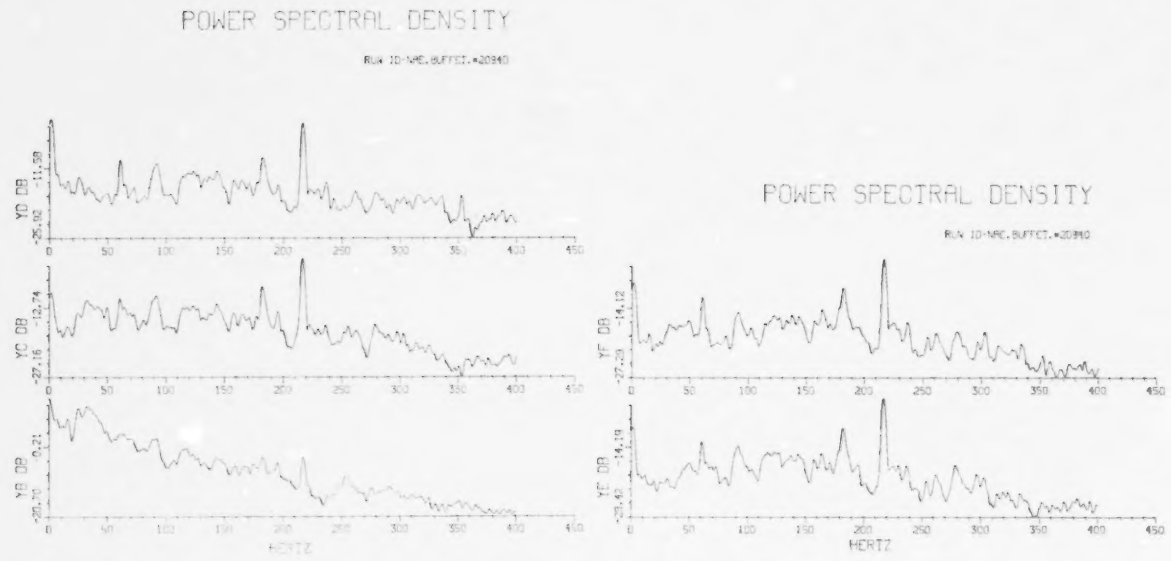

FIG. 13a: POWER SPECTRAL DENSITY FOR $M_\infty = 0.775$, $C_L = 0.762$, Q = 18.3 psi

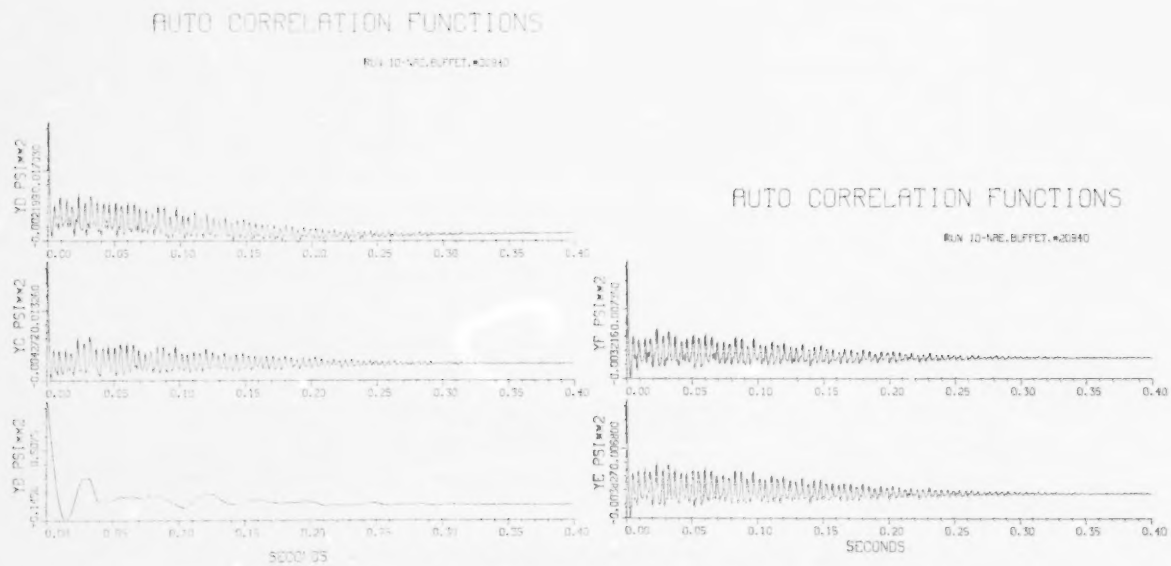

FIG. 13b: AUTO CORRELATION FUNCTIONS FOR $M_\infty = 0.775$, $C_L = 0.762$, Q = 18.3 psi

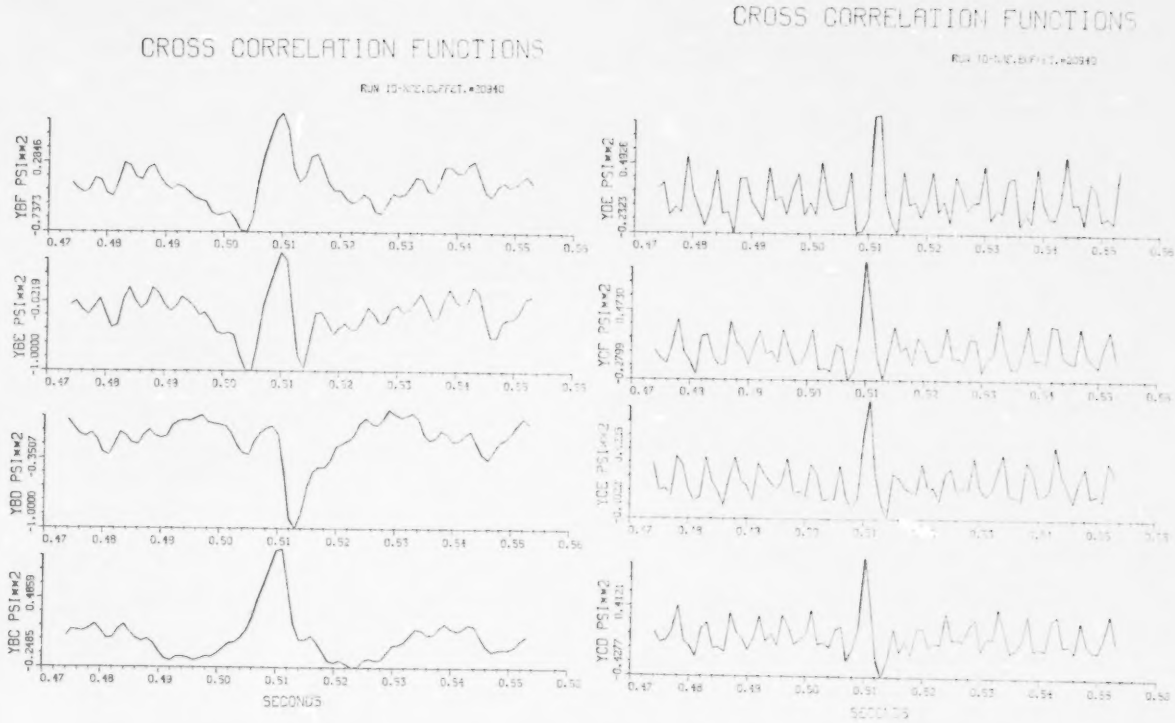

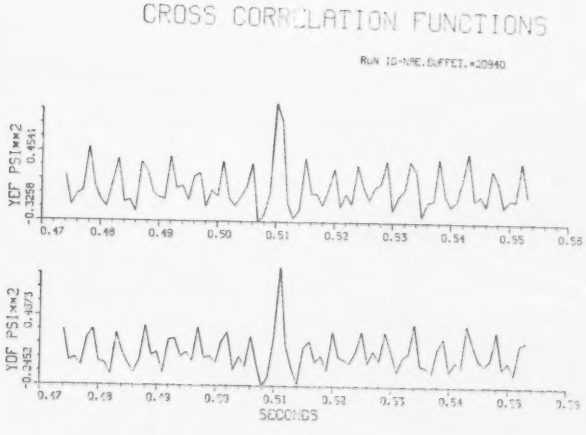

FIG. 13c: CROSS CORRELATION FUNCTIONS FOR M_∞= 0.775, C_L = 0.762, Q = 18.3 psi

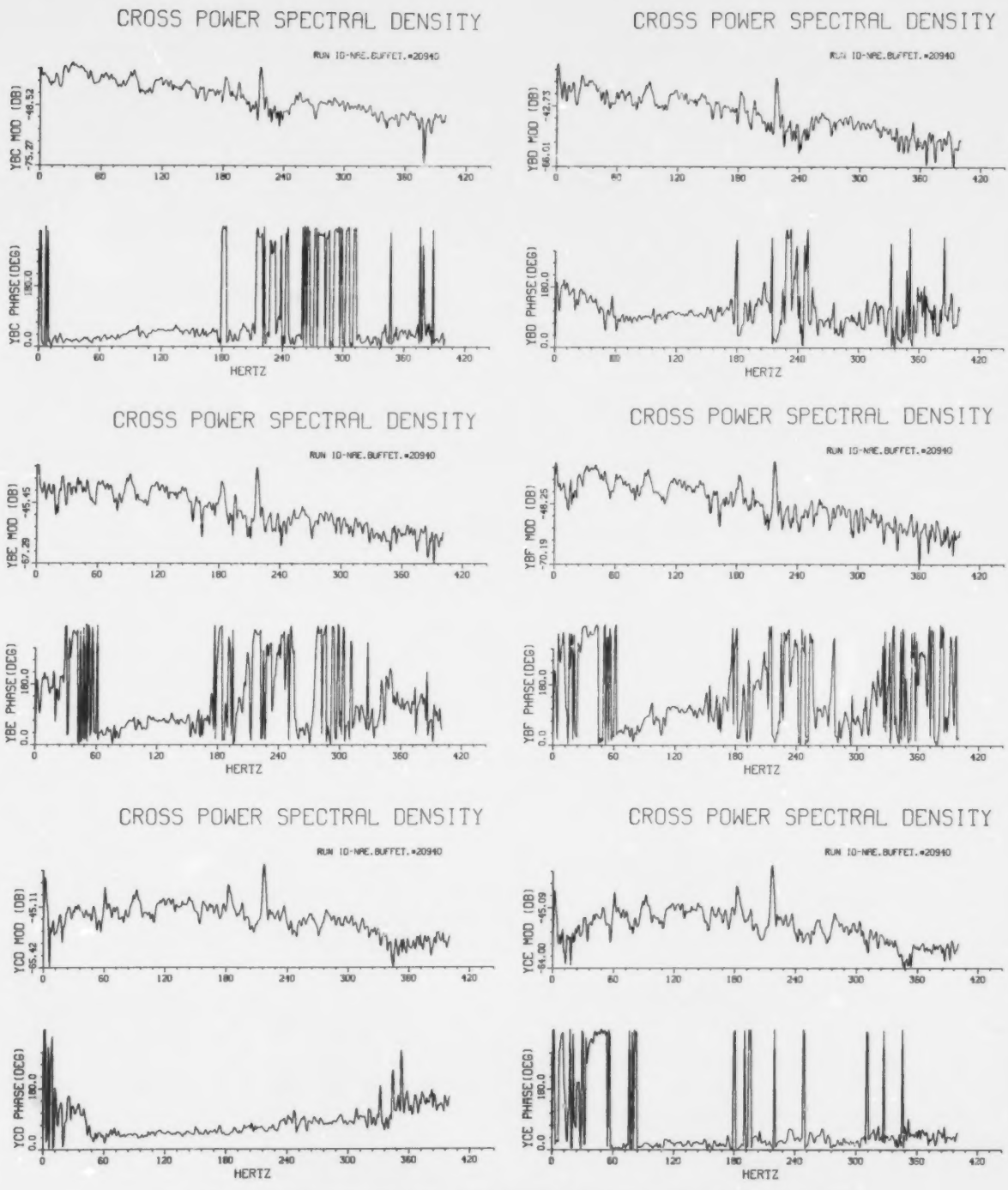

FIG. 13d: CROSS POWER SPECTRAL DENSITY FOR M_∞=0.775, C_L = 0.762, Q = 18.3 psi

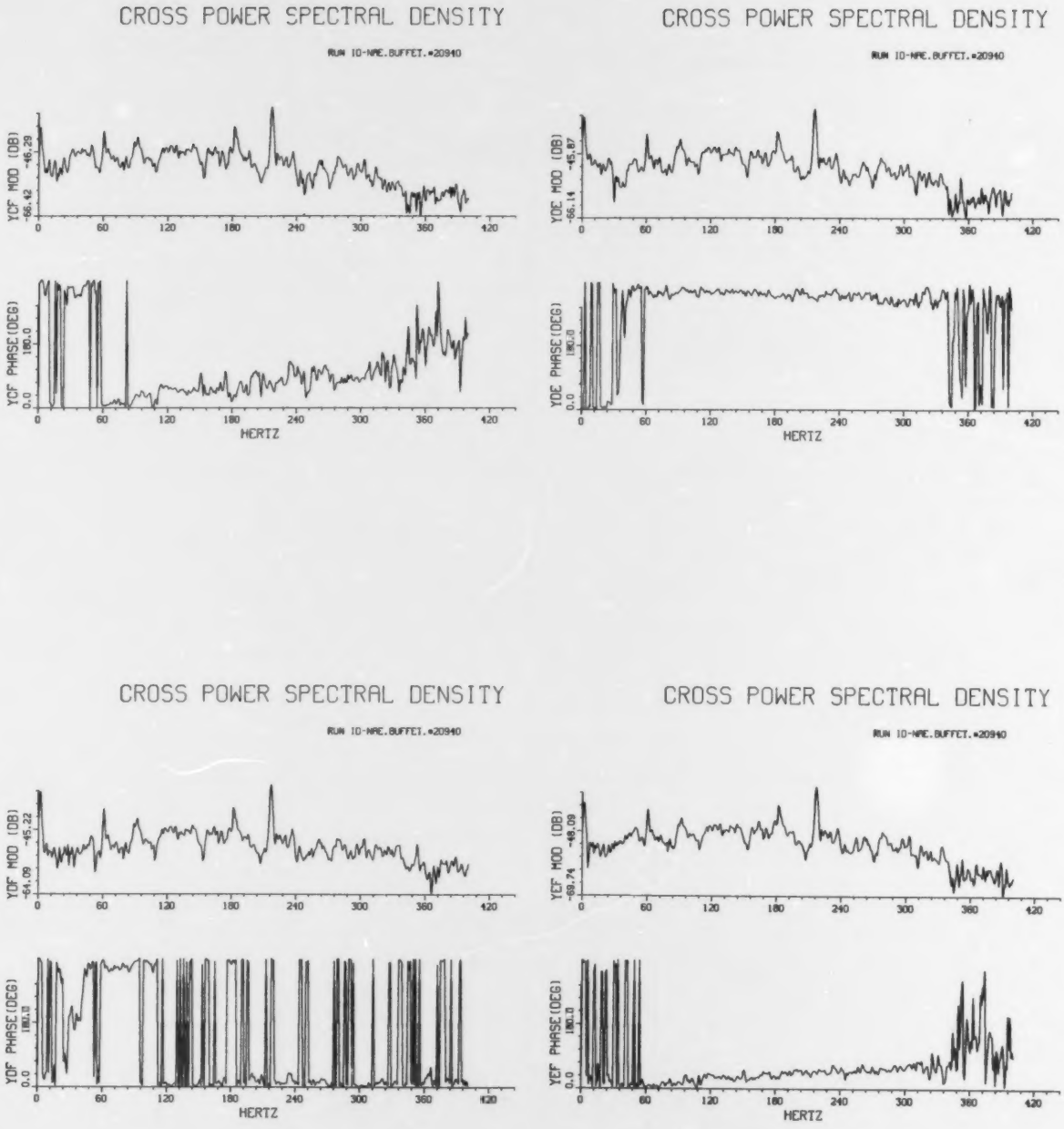

FIG. 13d: CROSS POWER SPECTRAL DENSITY FOR M_∞ = 0.775, C_L = 0.762, Q = 18.3 psi (Cont'd)

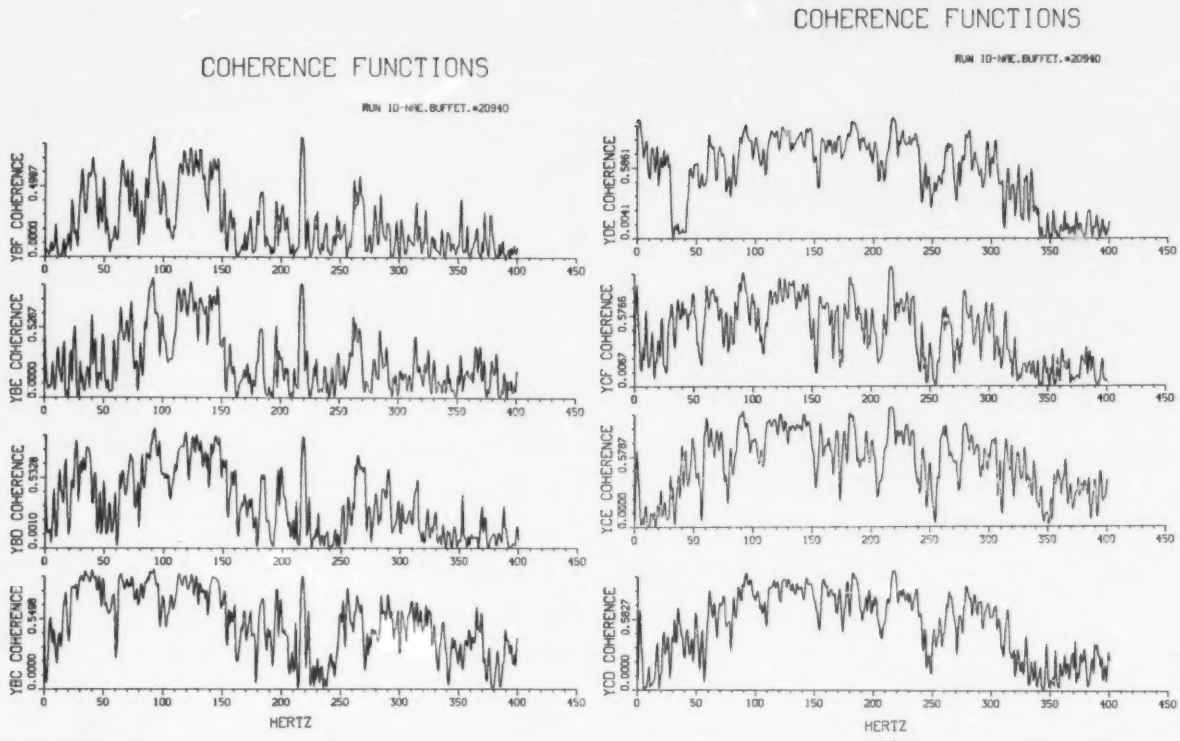

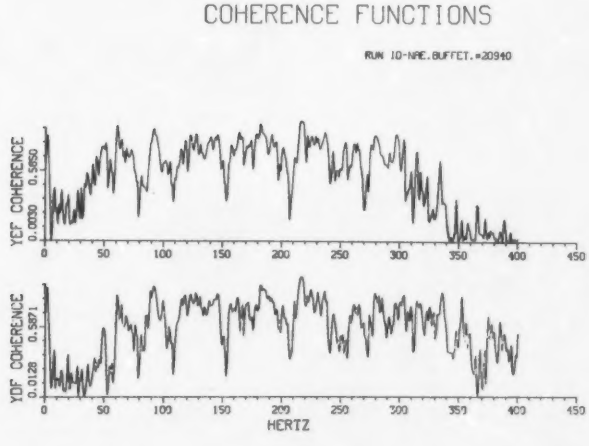

FIG. 13e: COHERENCE FUNCTIONS FOR M_∞=0.775, C_L = 0.762, Q = 18.3 psi

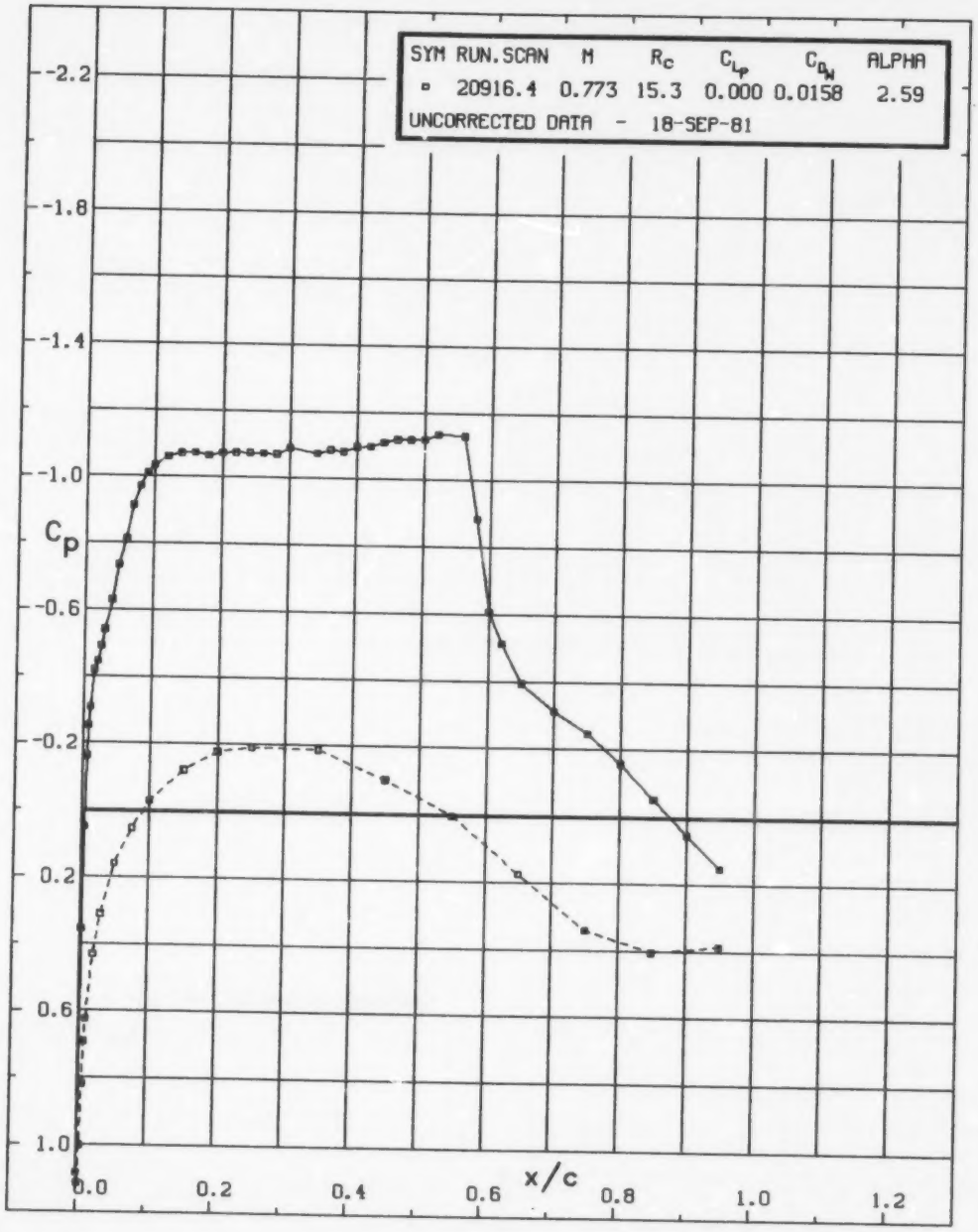

FIG. 13f: STEADY-STATE PRESSURE DISTRIBUTION

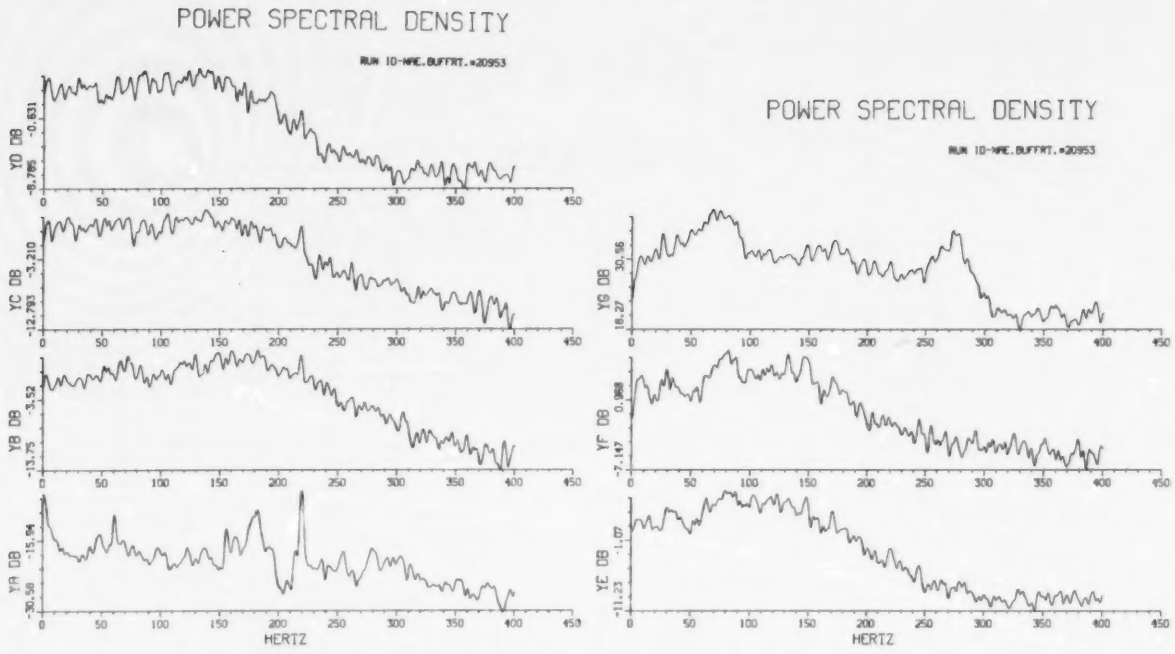

FIG. 14a: POWER SPECTRAL DENSITY FOR M_∞=0.805, C_L =0.727, Q = 25.5 psi

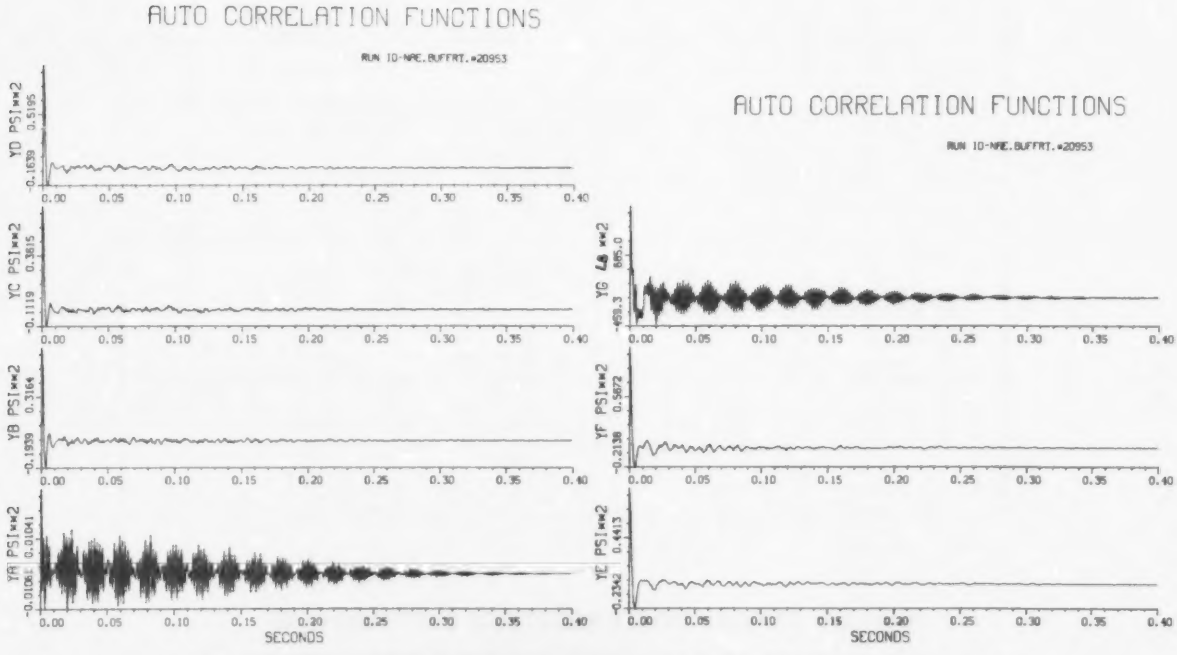

FIG. 14b: AUTO CORRELATION FUNCTIONS FOR M_∞=0.805, C_L = 0.727, Q = 25.5 psi

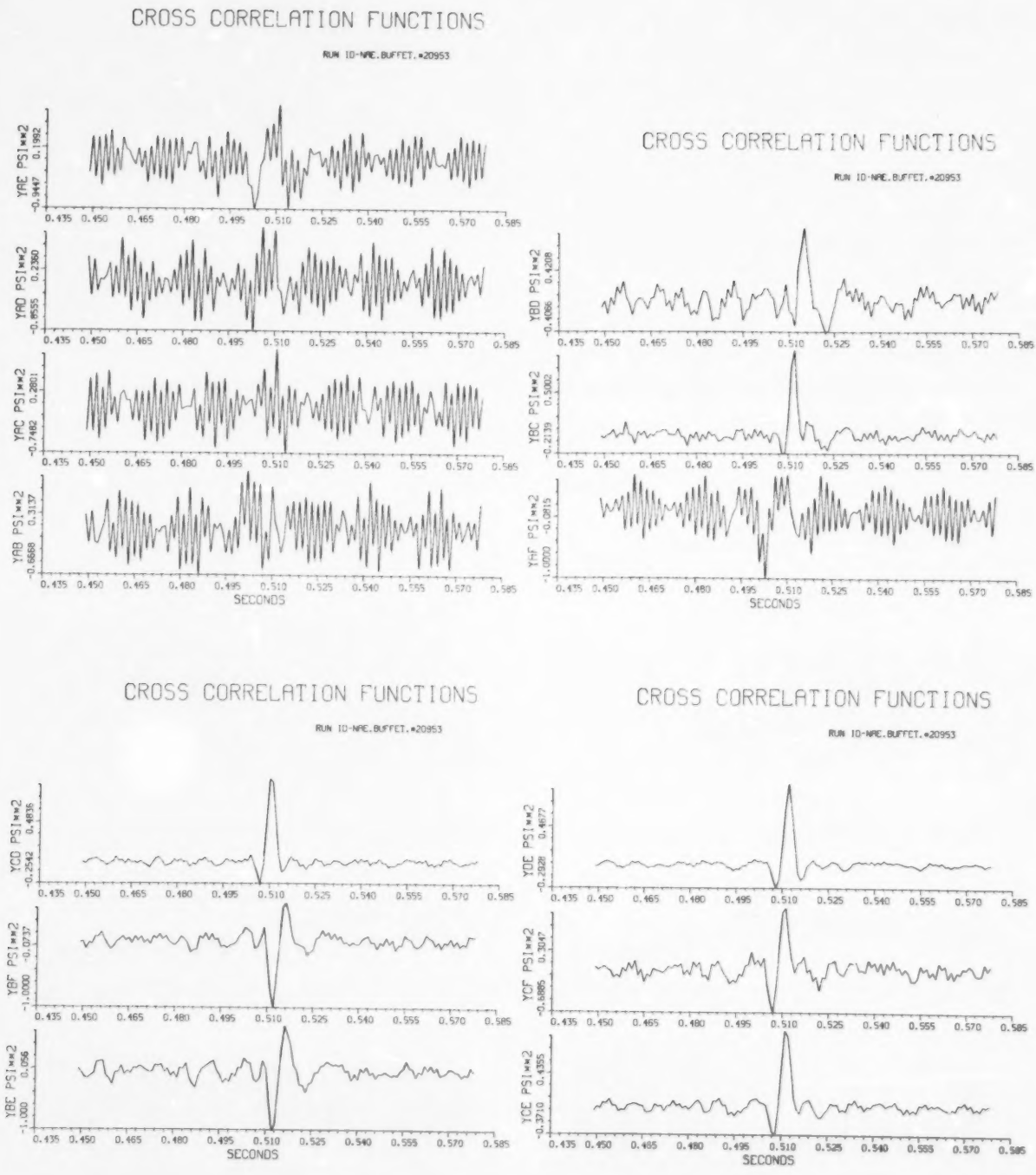

FIG. 14c: CROSS CORRELATION FUNCTIONS FOR M_∞=0.805, C_L =0.727, Q = 25.5 psi

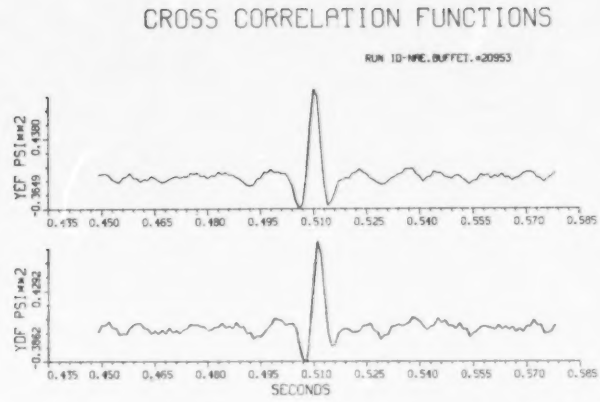

FIG. 14c: CROSS CORRELATION FUNCTIONS FOR M_∞=0.805, C_L = 0.727, Q = 25.5 psi (Cont'd)

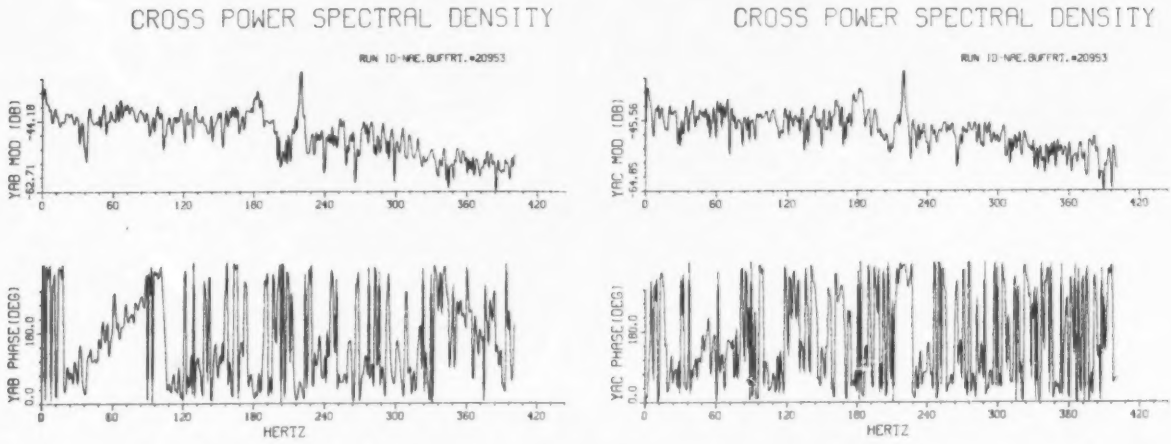

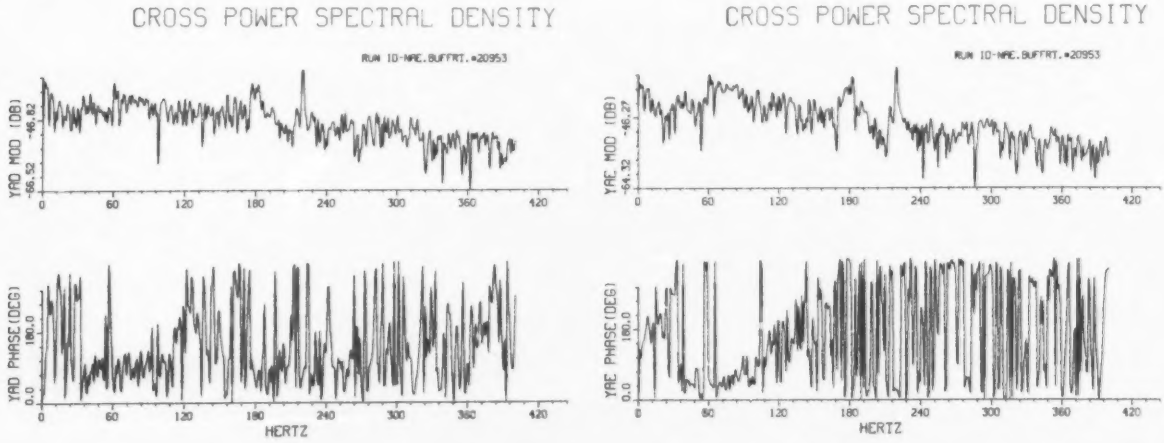

FIG. 14d: CROSS POWER SPECTRAL DENSITY FOR M_∞=0.805, C_L = 0.727, Q = 25.5 psi

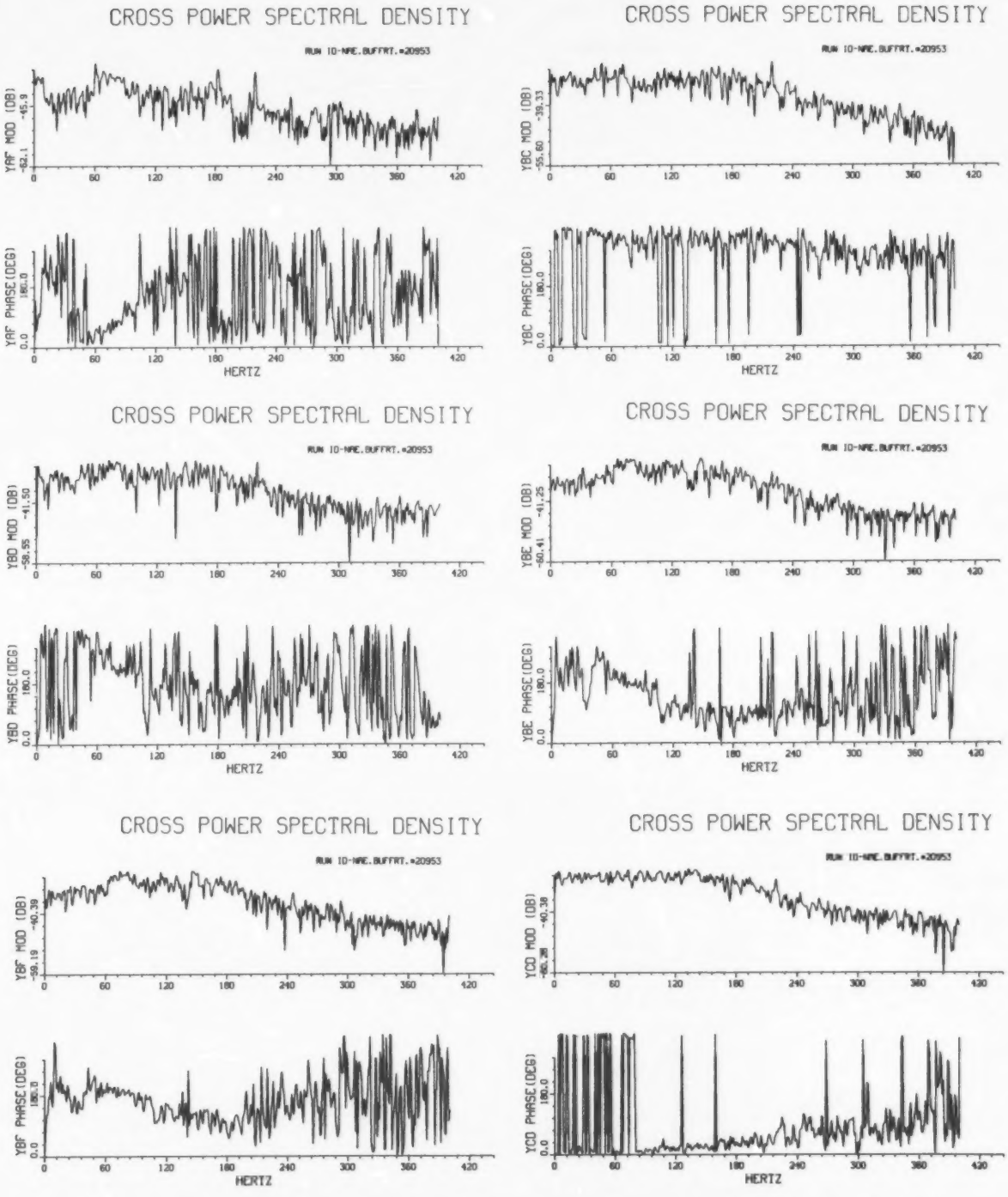

FIG. 14d: CROSS POWER SPECTRAL DENSITY FOR M_∞ = 0.805, C_l = 0.727, Q = 25.5 psi (Cont'd)

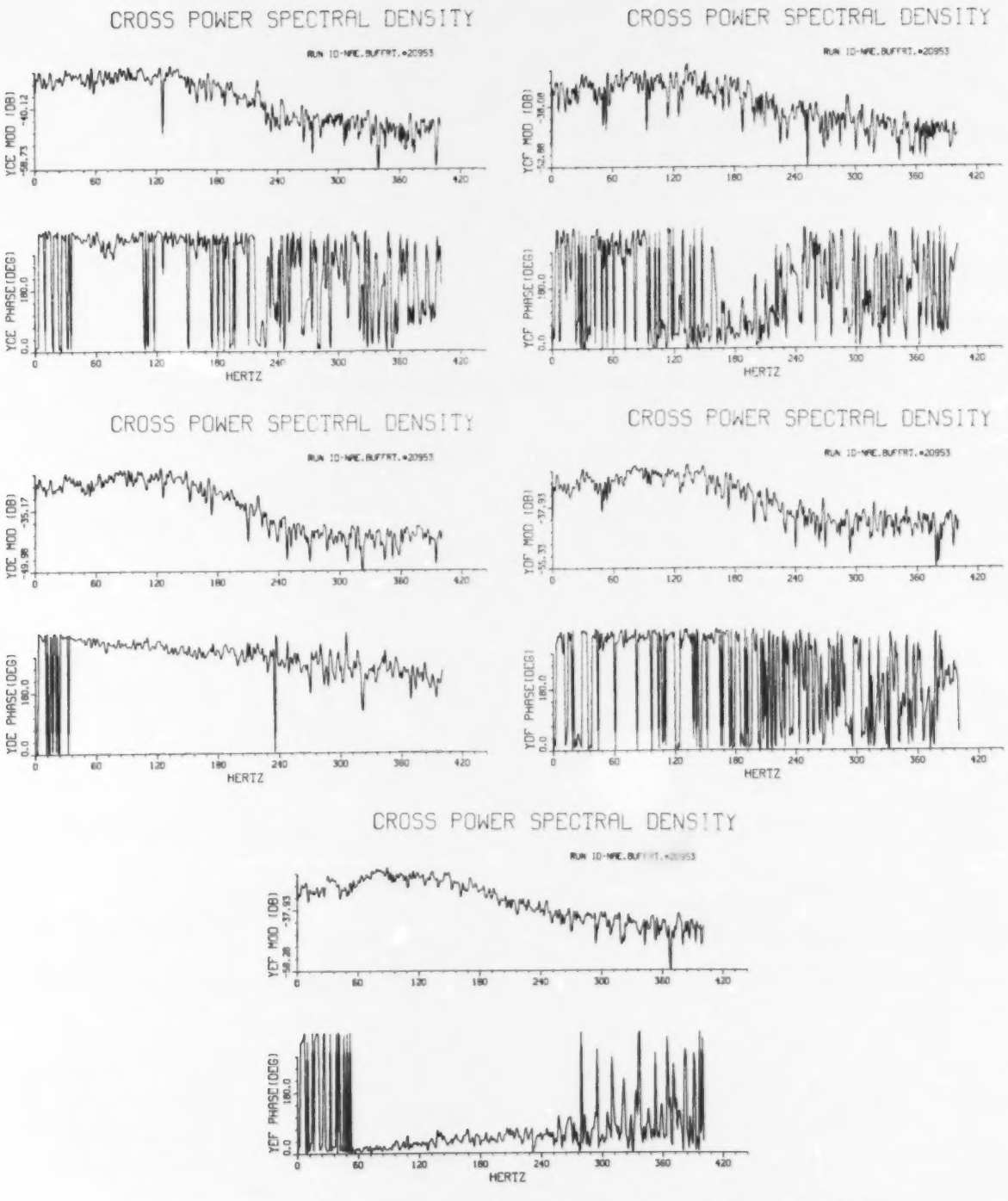

FIG. 14d: CROSS POWER SPECTRAL DENSITY FOR M_∞=0.805, C_L = 0.727, Q = 25.5 psi (Cont'd)

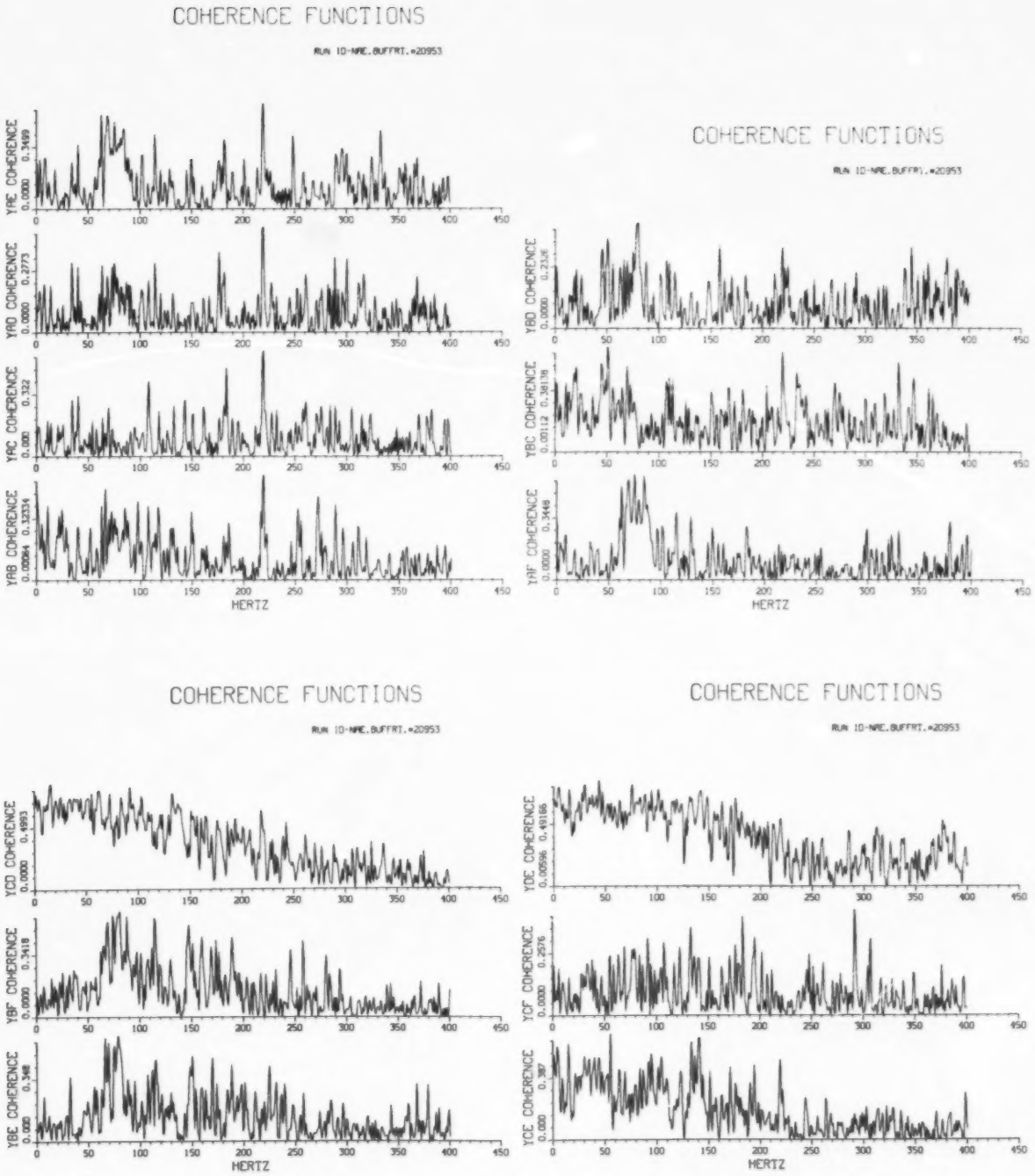

FIG. 14e: COHERENCE FUNCTIONS FOR M_{∞} = 0.805, C_l = 0.727, Q = 25.5 psi

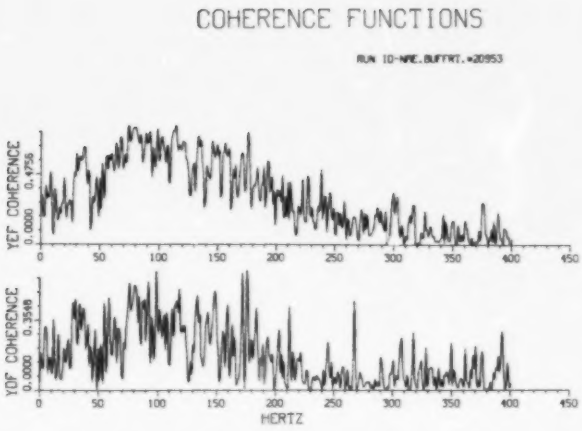

FIG. 14e: COHERENCE FUNCTIONS FOR M_∞=0.805, C_L =0.727, Q = 25.5 psi (Cont'd)

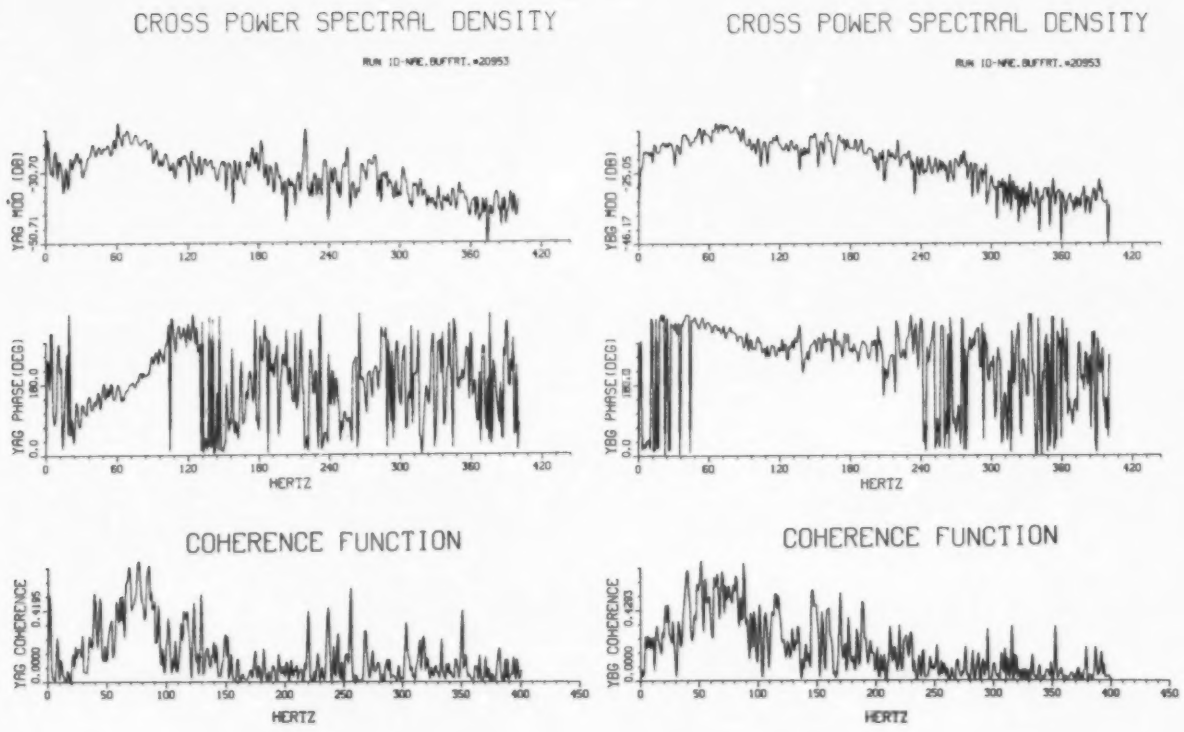

FIG. 14f: CROSS POWER SPECTRAL DENSITY AND COHERENCE FUNCTION BETWEEN PRESSURE AND NORMAL FORCE N_2 FOR M_∞=0.805, C =0.727, Q = 25.5 psi

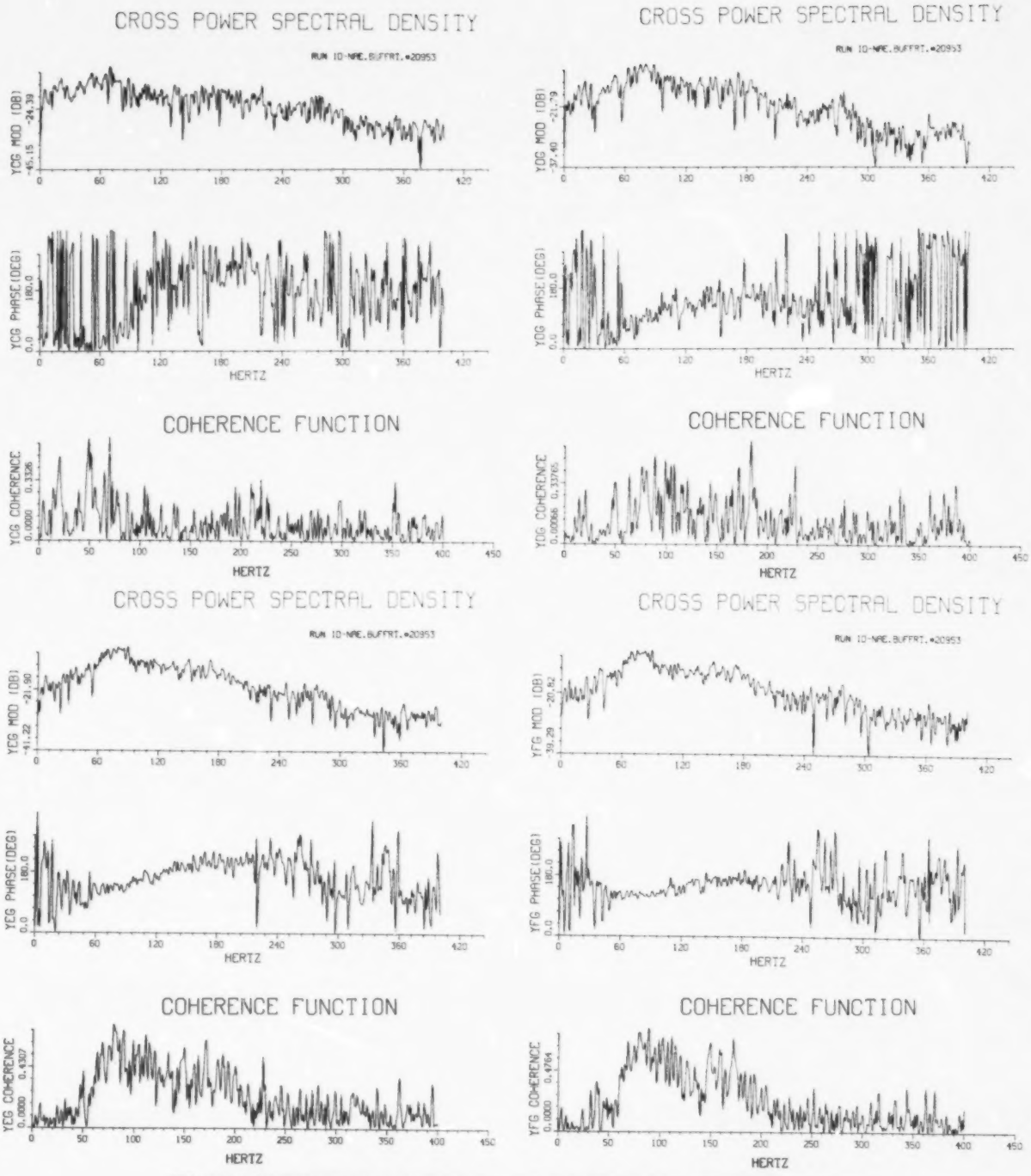

FIG. 14f: CROSS POWER SPECTRAL DENSITY AND COHERENCE FUNCTION BETWEEN PRESSURE AND NORMAL FORCE N_2 FOR M_∞=0.805, C =0.727, Q =25.5 psi (Cont'd)

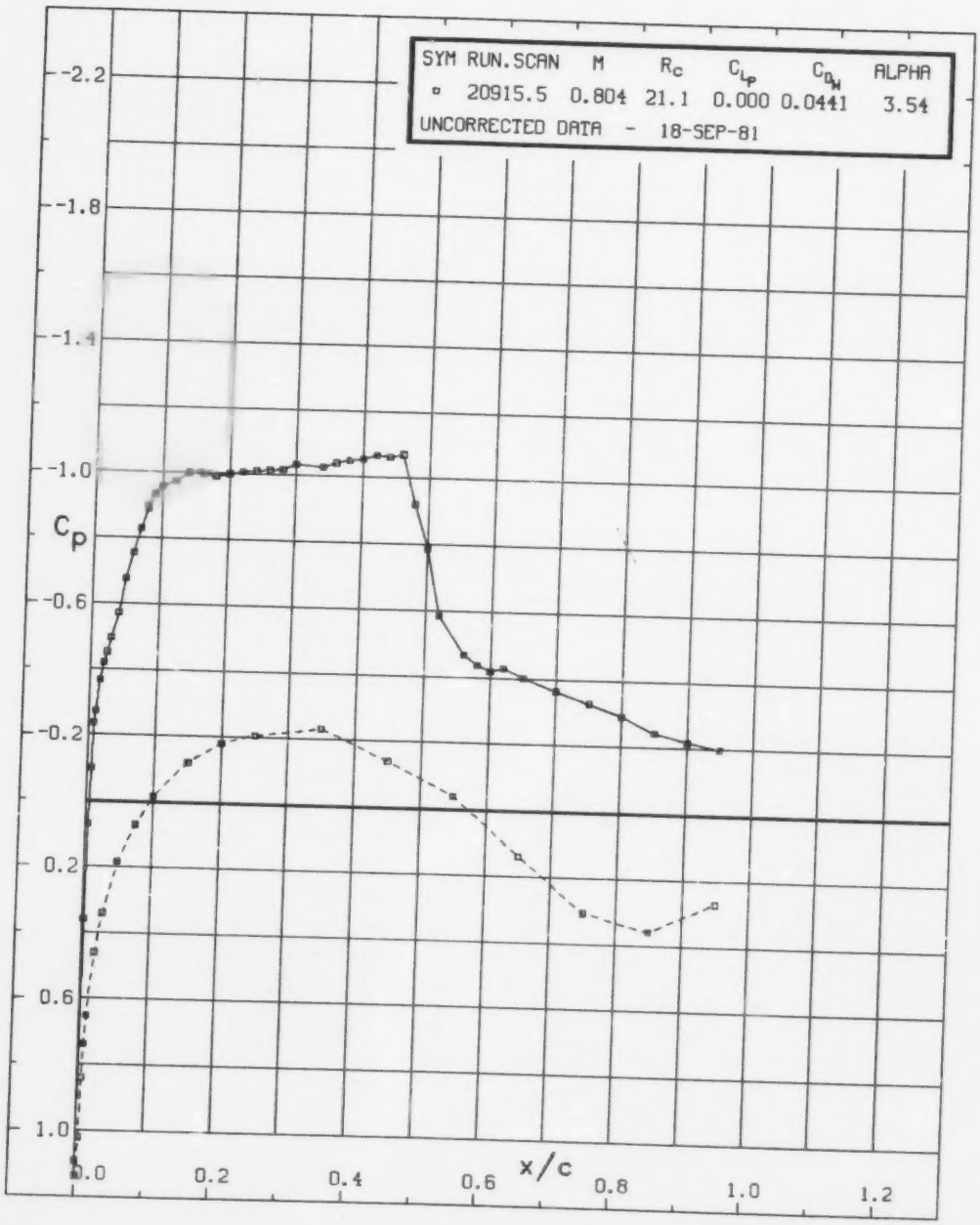

FIG. 14g: STEADY-STATE PRESSURE DISTRIBUTION

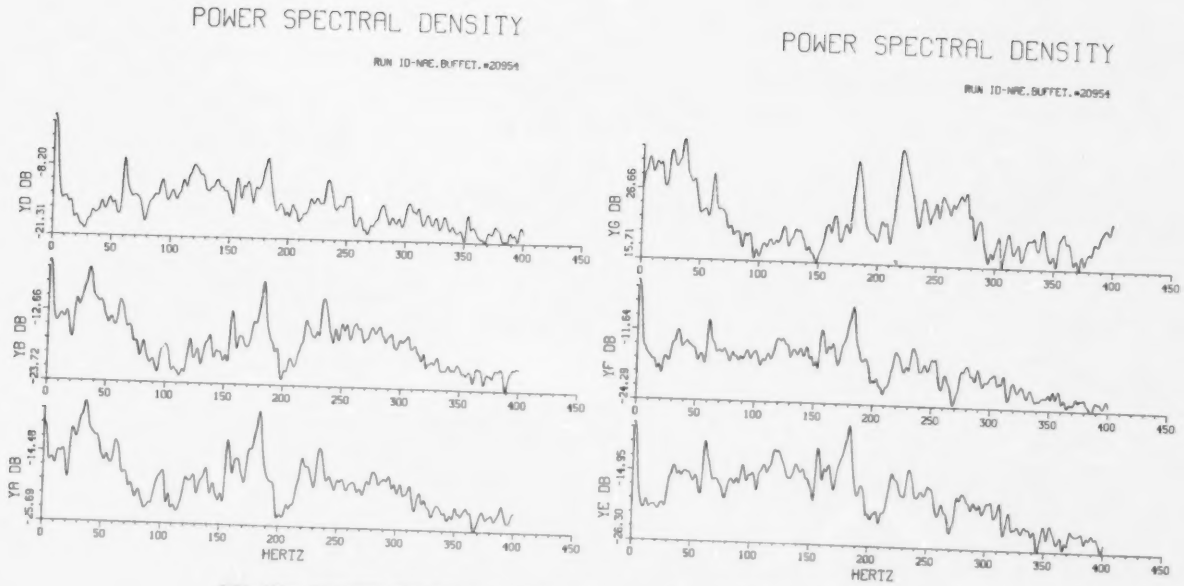

FIG. 15a: POWER SPECTRAL DENSITY FOR M_∞=0.805, C_L = 0.314, Q = 25.5 psi

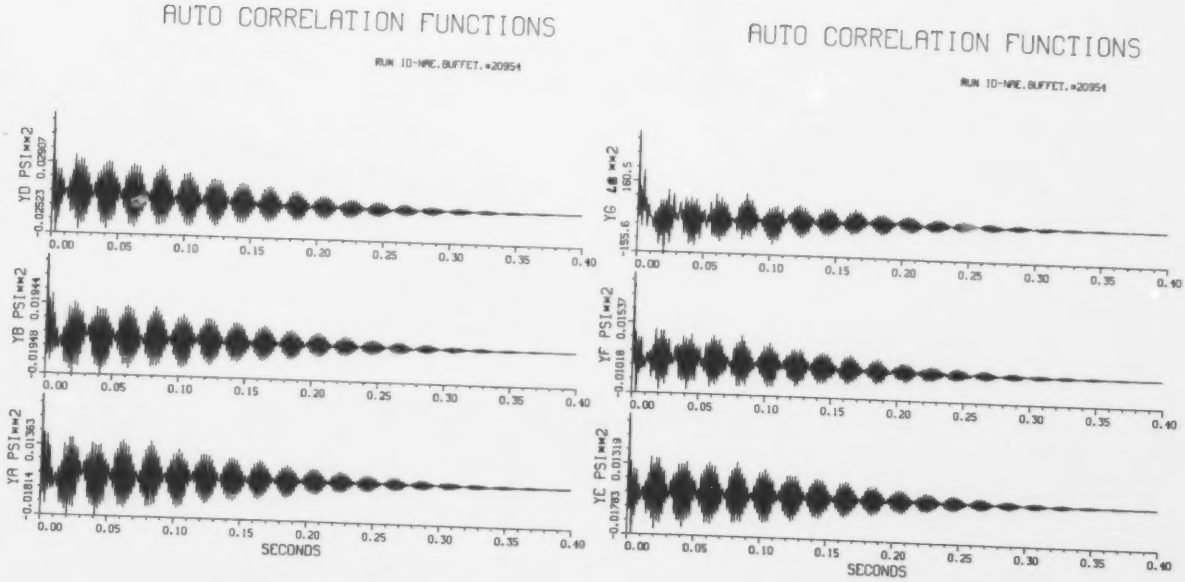

FIG. 15b: AUTO CORRELATION FUNCTIONS FOR M_∞=0.805, C_L = 0.314, Q = 25.5 psi

FIG. 15c: CROSS CORRELATION FUNCTIONS FOR M_∞=0.805, C_L = 0.314, Q = 25.5 psi

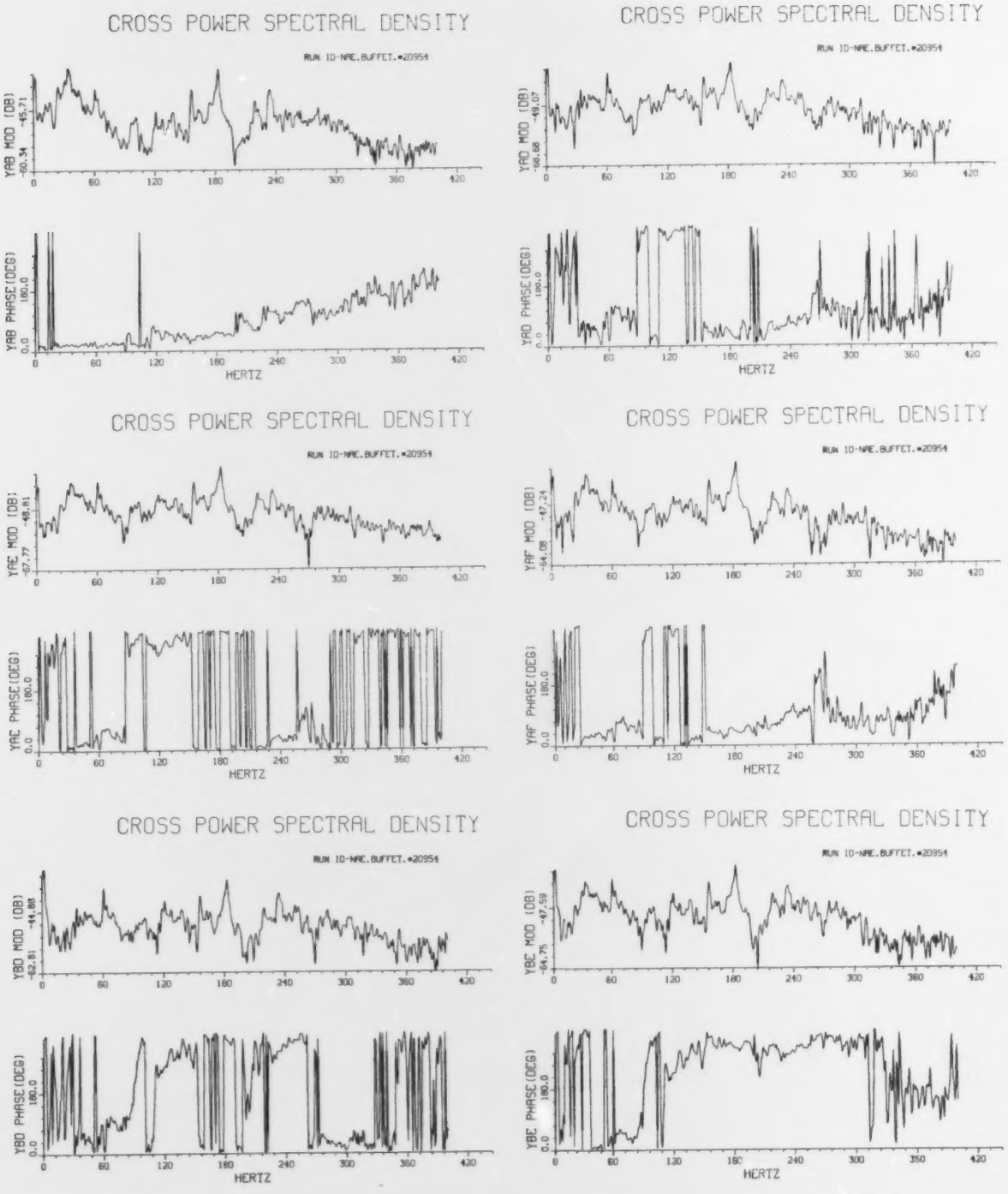

FIG. 15d: CROSS POWER SPECTRAL DENSITY FOR $M_\infty = 0.805$, $C_L = 0.314$, Q = 25.5 psi

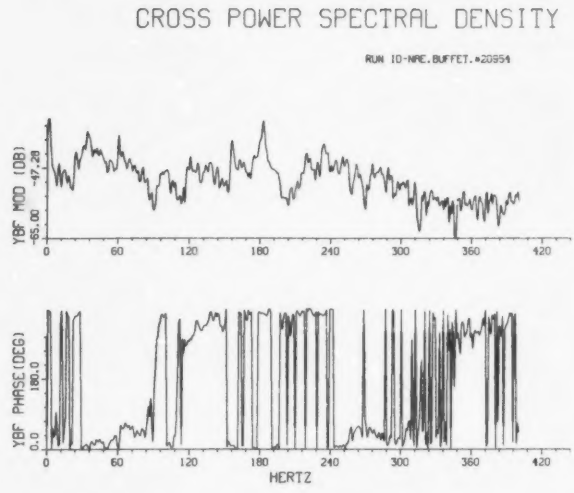

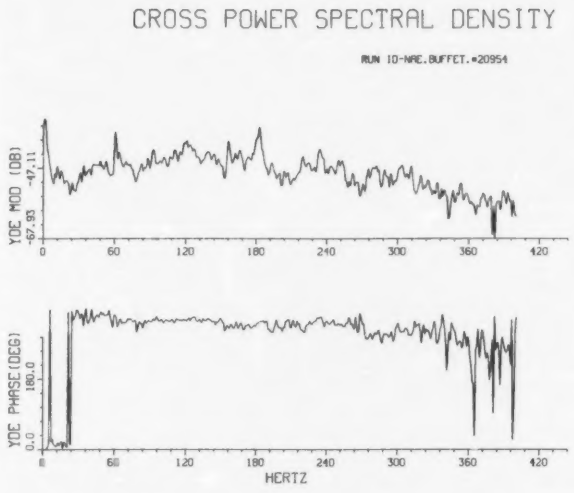

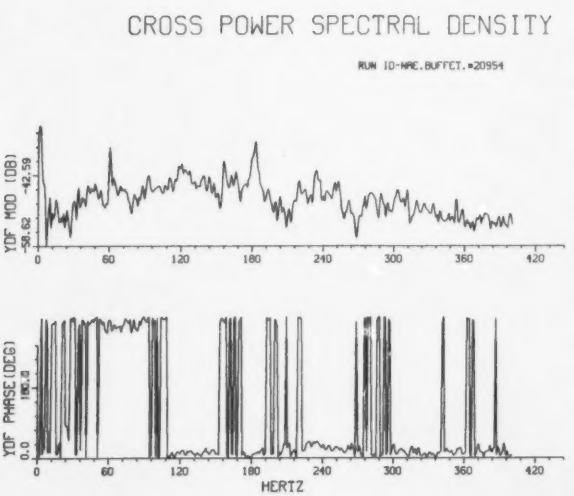

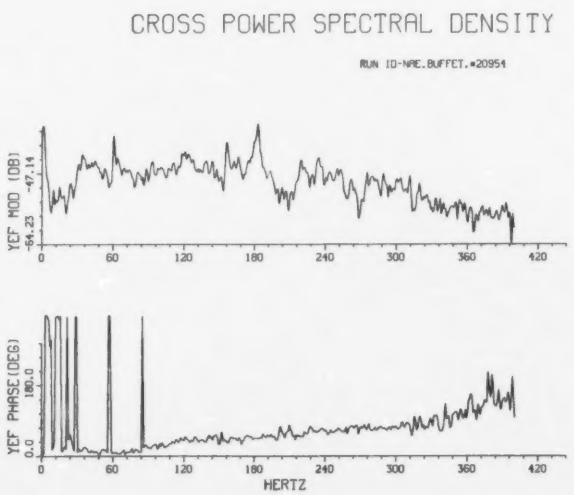

FIG. 15d: CROSS POWER SPECTRAL DENSITY FOR M_∞=0.805, C_L =0.314, Q= 25.5 psi (Cont'd)

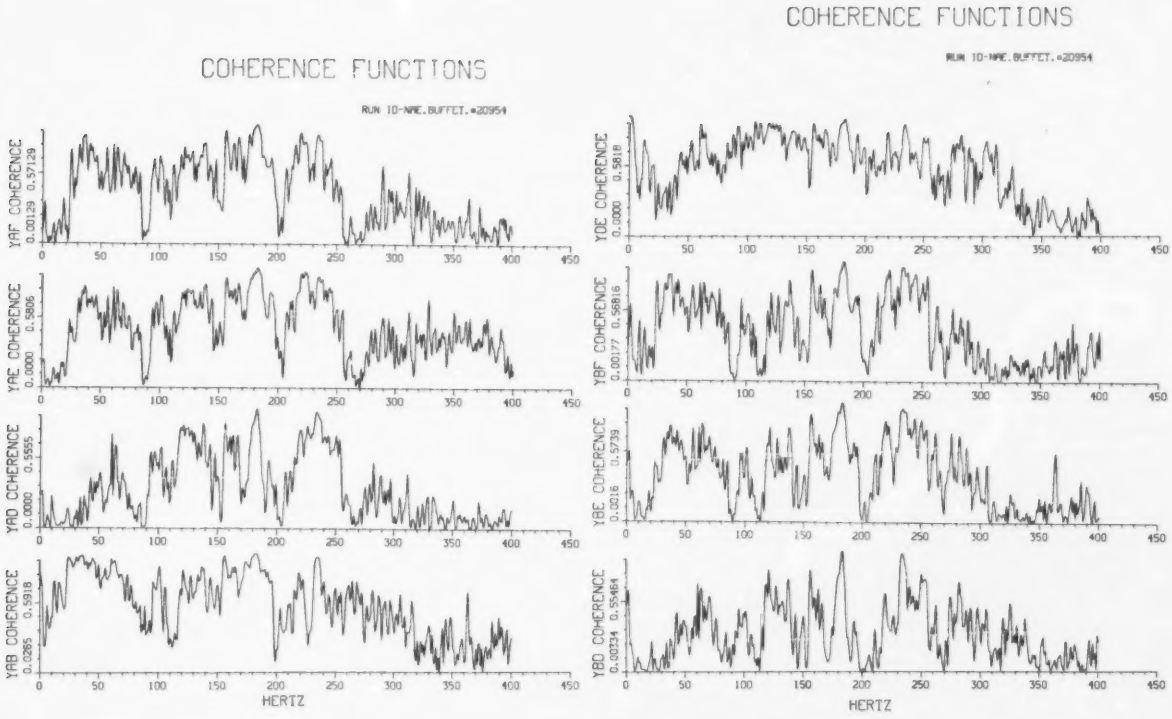

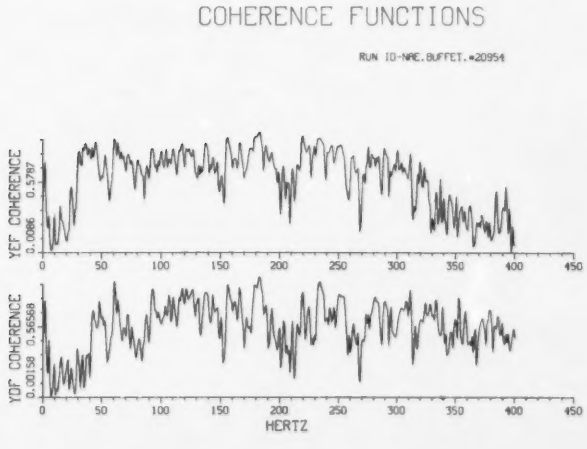

FIG. 15e: COHERENCE FUNCTIONS FOR M_∞=0.805, C_L = 0.314, Q = 25.5 psi

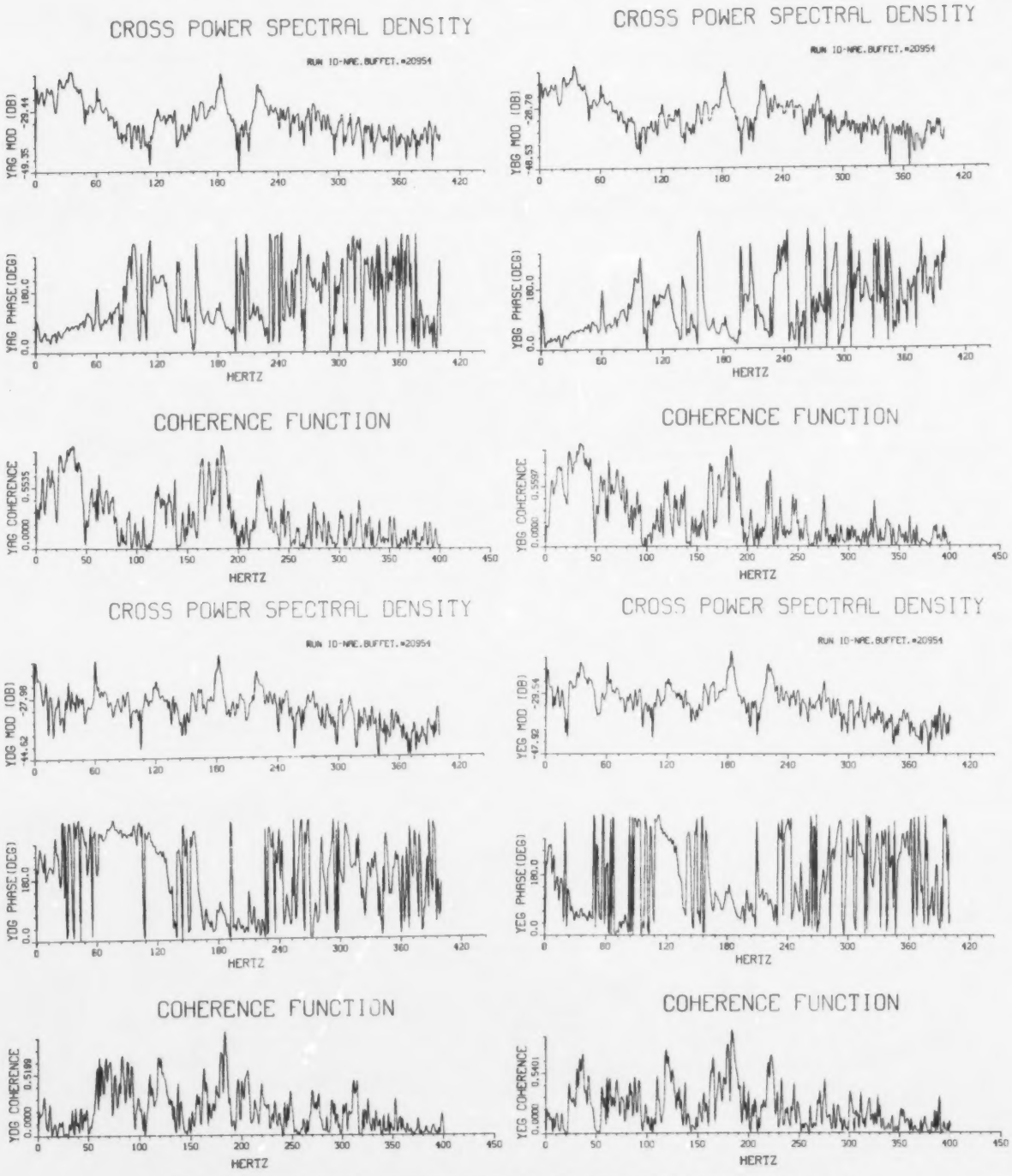

FIG. 15f: CROSS POWER SPECTRAL DENSITY AND COHERENCE FUNCTION BETWEEN PRESSURE AND NORMAL FORCE N_2 FOR M_∞=0.805, C_l = 0.314, Q = 25.5 psi

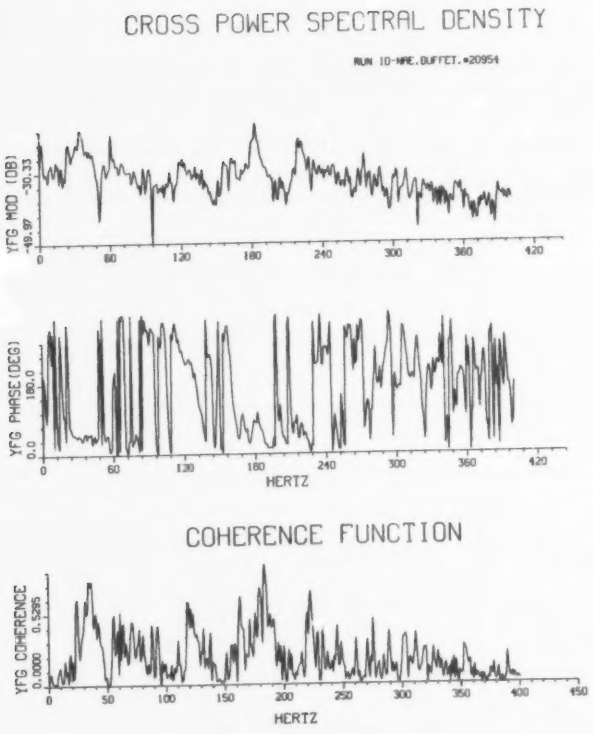

FIG. 15f: CROSS POWER SPECTRAL DENSITY AND COHERENCE FUNCTION BETWEEN PRESSURE AND NORMAL FORCE N_2 FOR $M_\infty = 0.805$, $C_l = 0.314$, $Q = 25.5$ psi (Cont'd)

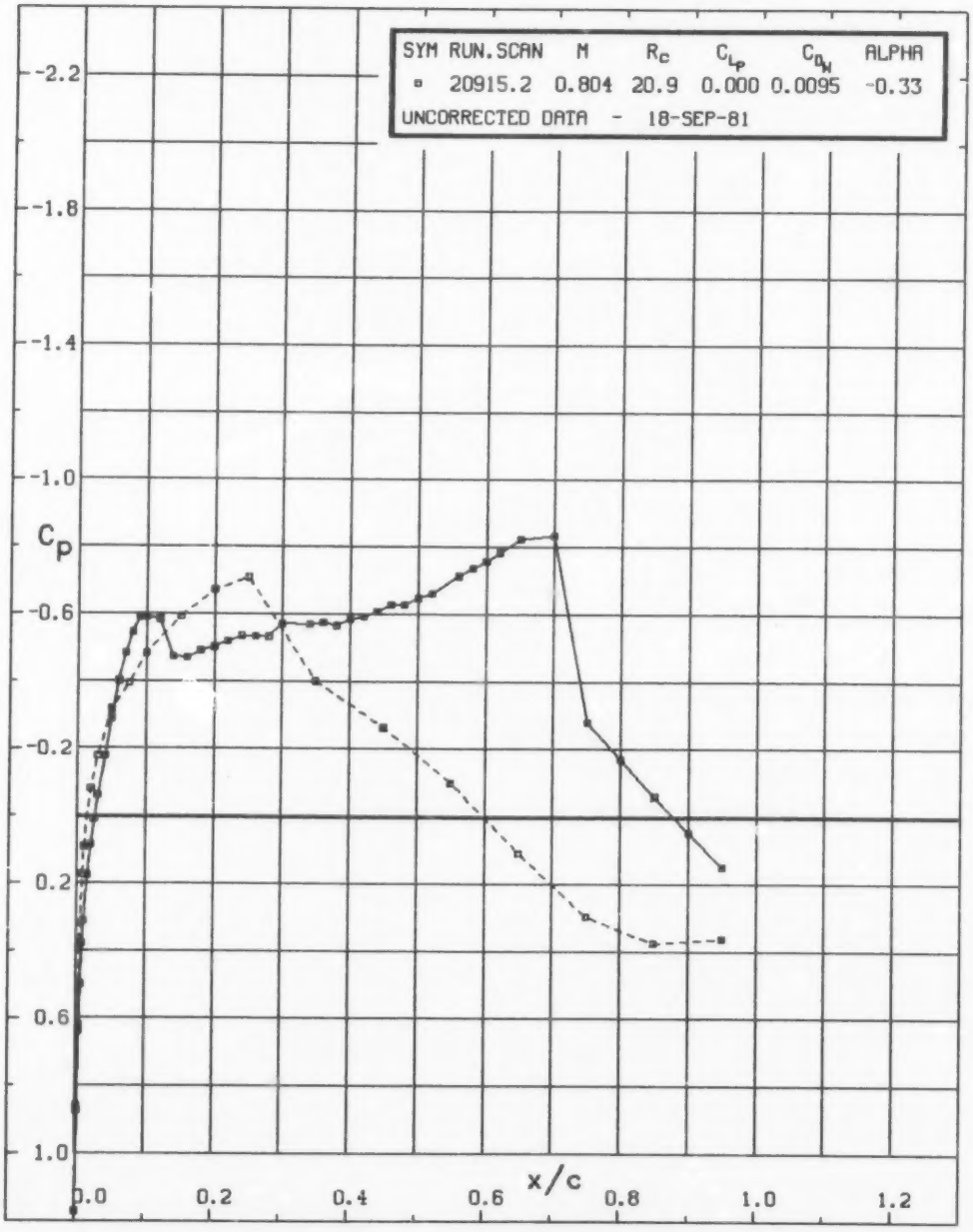

FIG. 15g: STEADY-STATE PRESSURE DISTRIBUTION

REPORT DOCUMENTATION PAGE / PAGE DE DOCUMENTATION DE RAPPORT

REPORT/RAPPORT NAE-AN-14 1a	REPORT/RAPPORT NRC No. 22448 1b
REPORT SECURITY CLASSIFICATION CLASSIFICATION DE SÉCURITÉ DE RAPPORT Unclassified 2	DISTRIBUTION (LIMITATIONS) Unlimited 3

TITLE/SUBTITLE/TITRE/SOUS-TITRE

4 Unsteady Pressure and Force Measurements Associated with Transonic Buffeting of a Two-Dimensional Supercritical Airfoil

AUTHOR(S)/AUTEUR(S)

5 B.H.K. Lee and L.H. Ohman

SERIES/SÉRIE

6 Aeronautical Note

CORPORATE AUTHOR/PERFORMING AGENCY/AUTEUR D'ENTREPRISE/AGENCE D'EXÉCUTION

7 National Research Council Canada
National Aeronautical Establishment — High Speed Aerodynamics Laboratory

SPONSORING AGENCY/AGENCE DE SUBVENTION

8

DATE	FILE/DOSSIER	LAB. ORDER COMMANDE DU LAB.	PAGES	FIGS/DIAGRAMMES
83-06 9	10	11	88 12a	15 12b

NOTES

13

DESCRIPTORS (KEY WORDS)/MOTS-CLÉS

14
1. Aerofoils — aerodynamic characteristics
2. Aerofoils — pressure distribution
3. Buffeting — measurements

SUMMARY/SOMMAIRE

15

Buffet characteristics of the BGK No. 1 shockless airfoil have been investigated. Fluctuating pressure measurements along the airfoil chord and unsteady force balance data have been obtained in various regions inside the buffet regime close to the onset boundary curve. The Mach number range where buffet intensity reaches high values is determined from balance measurements. The rms values of the fluctuating pressure show generally monotonic increase downstream of the shock to the trailing-edge in this speed range. Statistical data from pressure and normal force measurements have been processed and the appearance of distinct frequency peaks in the power spectral density curves has been detected in the speed range $0.7 \leq M_\infty \leq 0.78$. The coherence between pressure signals and pressure and force signals has also been investigated.